

Naht Bindung, ein Neuartiger Mechanismus zur Stabilisierung von Mikrotubuli

Dissertation zur Erlangung des
naturwissenschaftlichen Doktorgrades
der Bayerischen Julius-Maximilians-Universität Würzburg

vorgelegt von

Linda Sandblad

geboren am 8. Mai 1975 in Uppsala, Schweden

Heidelberg 2007

Eingereicht am: 6. Juni 2007

Mitglieder der Promotionskommission:

Vorsitzender: **Prof. Dr. Martin J. Müller, Universität Würzburg**

Gutachter: **Prof. Dr. Georg Krohne, Universität Würzburg**

Gutachter: **Associate Prof. Dr. Andreas Hoenger, University of Colorado at Boulder**

Tag des Promotionskolloquiums: 10. Oktober 2007

Doktorurkunde ausgehändigt am:

Erklärung

Hiermit erkläre ich, dass ich diese Dissertation selbständig angefertigt und keine anderen als die von mir angegebenen Quellen und Hilfsmittel benutzt habe.

Ausserdem erkläre ich, dass diese Dissertation bisher noch in keinem anderen Prüfungsverfahren in gleicher oder ähnlicher Form vorgelegt worden ist.

Auch habe ich bisher noch keinen akademischen Grad erworben oder diesen in einem früheren Verfahren zu erwerben versucht.

Heidelberg, den 6. Juni 2007

Linda Sandblad

Teile dieser Arbeit wurden bereits publiziert:

Sandblad, L., Busch, K. E., Tittmann, P., Gross, H., Brunner, D., and Hoenger, A. (2006). The Schizosaccharomyces pombe EB1 homolog Mal3p binds and stabilizes the microtubule lattice seam. *Cell* 127, 1415-1424.

Die praktische Arbeit wurde im Labor von Associate Prof. Dr. Andreas Hoenger and Dr. Damian Brunner, an Europäischen Laboratorium für Molekular Biologie (EMBL) in Heidelberg ausgeführt. In Rahmen des EMBL PhD Programs.

Zusammenfassung

Mikrotubuli sind eine faszinierende Komponente des Zytoskeletts einer Zelle. Ihre Struktur entspricht der eines Hohlzylinders. Sie sind aus seitlich assoziierten Protofilamenten zusammengesetzt, die aus α - und β -Tubulin Untereinheiten bestehen. Diese Heterodimere sind gerichtet, bedingt durch ihre Kopf-Schwanz Anordnung. Folglich besitzen Mikrotubuli eine definierte Polarität, welche die Basis für die Polarität der Zelle bildet. Die Anordnung der Untereinheiten zu einem so genannten Mikrotubulus Gitter kann in zwei Konformationen vorkommen: In der häufigeren B-Gitter Formation, in welcher die Protofilamente seitlich durch α - zu α - und β - zu β -Tubulin interagieren und in der weniger stabilen A-Gitter Konformation, in der α -Tubulin lateral mit β -Tubulin wechselwirkt. In der Zelle vorkommende Mikrotubuli haben grundsätzlich 13 Protofilamente. Mindestens ein Paar dieser Protofilamente interagiert in der A-Gitter Konformation und bildet die so genannte Gitter-Naht (*lattice seam*). Mikrotubuli Dynamik und Interaktionen sind streng durch Mikrotubuli assoziierte Proteine (MAPs) reguliert.

Die Kombination aus moderner Elektronenmikroskopie (EM) und Bildverarbeitung macht strukturelle Untersuchungen an MAPs und Motorproteinen im Zusammenhang mit Mikrotubuli möglich. Wir haben biochemische und hoch entwickelte EM Techniken benutzt, um die Interaktion zwischen Mikrotubuli und dem Mikrotubuli assoziierten Protein Mal3 *in vitro* zu untersuchen. Mal3p ist ein Homolog des konservierten Ende-Bindungs Protein 1 (EB1) in der Spaltheife *Schizosaccharomyces pombe*. Es wurde bereits gezeigt, dass EB1 die Struktur von Mikrotubuli stabilisiert. Mit Hilfe einer speziellen, hochauflösenden EM Schattierungstechnik haben wir demonstriert, dass Mal3p auf neuartige Weise mit dem Mikrotubulus Gitter interagiert. Dabei besetzt Mal3p Bindungsstellen am Mikrotubulus, die sich von denen der anderen MAPs oder Motorproteinen unterscheiden. Mal3p bevorzugt die Bindung zwischen zwei Protofilamenten, lässt jedoch das übrigen Gitter unbesetzt. In seltenen Fällen wurde Mal3p in zwei nebeneinander angrenzenden Protofilamenten gefunden. An diesen Stellen zeigt sich überraschenderweise eine A-Gitter-Konformation am Mikrotubulus, was auf eine spezifische Naht-Bindung hinweist. Mit Hilfe einer Gitterverstärkung in Form einer Kinesin-Motor-Domäne, die an jede β -Untereinheit bindet, konnte gezeigt werden, dass Mal3p die Naht, den schwächsten Teil eines Mikrotubulus, stabilisiert. Des Weiteren unterstützt die Anwesenheit von Mal3p während der Mikrotubulus Polymerisation die Formierung zur Bildung des Hohlzylinders. Die Untersuchung der monomeren Mikrotubuli-Bindungs-Domäne von Mal3p unter Anwendung von Kryo-EM und anschließender 3-D helikalen Rekonstruktion, führte zur genauen Lokalisierung des Proteins auf dem Mikrotubulus Gerüst. Hierbei bestätigte sich auch die Lokalisation zwischen den Protofilamenten. Des Weiteren konnte gezeigt werden, dass Mal3p die Fähigkeit besitzt, die Konformation des Mikrotubulus Gitters zu beeinflussen.

Zusammenfassend lässt sich sagen, dass das EB1-Homolog nicht nur an das Mikrotubulus Plus Ende, sondern auch an der Naht entlang des ganzen Mikrotubulus bindet. Die Art wie Mal3p mit den Mikrotubuli interagiert, zeigt einen neuen Mechanismus der Mikrotubuli Stabilisierung und eröffnet weitere Sichtweisen, wie Plus End Bindungsproteine die Dynamik von Mikrotubuli beeinflussen. Die Ergebnisse belegen, dass Mikrotubuli zwei definierte Reaktionsplattformen auf ihrer Oberfläche besitzen, die unabhängig mit verschiedenen MAPs und Motorproteinen interagieren.

Till Lea

Seam Binding, a Novel Mechanism for Microtubule Stabilization

**Linda Sandblad
EMBL-Heidelberg**

A part of this work has been published in:

Sandblad, L., Busch, K. E., Tittmann, P., Gross, H., Brunner, D., and Hoenger, A. (2006). The Schizosaccharomyces pombe EB1 homolog Mal3p binds and stabilizes the microtubule lattice seam. *Cell* 127, 1415-1424.

Table of Content

1	SUMMARY	11
2	INTRODUCTION	12
2.1	The origin of polarity	12
2.2	The Cytoskeleton.....	12
2.3	Bacterial cytoskeleton.....	13
2.4	Actin	15
2.5	Intermediate filaments.....	18
2.6	Microtubules.....	19
2.6.1	Cellular microtubule organization	20
2.6.2	Microtubules in the mitotic spindle	23
2.6.3	Microtubule nucleation	24
2.6.4	Molecular structure of the microtubules	26
2.6.4.1	Atomic structure of tubulin in zinc-sheets	27
2.6.4.2	Structure of Stathmin-tubulin crystals	29
2.6.4.3	Structure of frozen hydrated native microtubules.....	29
2.6.4.4	Protofilament number	30
2.6.4.5	A- and B-lattice.....	31
2.6.4.6	The microtubule lattice seam.....	32
2.6.5	Microtubule dynamic instability	33
2.6.5.1	Nucleotide binding and hydrolysis	33
2.7	Drugs affecting microtubule stability.....	35
2.7.1	Destabilizing drugs	35
2.7.2	Stabilizing drugs	35
2.8	Microtubule associated proteins (MAPs).....	35
2.8.1	Microtubule associated motors proteins	36
2.8.1.1	Dynein.....	37
2.8.1.2	Kinesin	37
2.8.2	Microtubule stabilizing proteins	39
2.8.2.1	Tau family.....	39
2.8.2.2	XMAP215 family.....	40
2.8.2.3	Doublecortin	41
2.8.3	Microtubule destabilizing proteins	41
2.8.3.1	Stathmin	41
2.8.3.2	Katanin and Spastin	42
2.8.3.3	Kinesin-13.....	42

2.8.4	Microtubule plus end tracking proteins (+TIPs).....	43
2.8.4.1	Mechanisms of plus end tracking	44
2.8.4.2	+TIPs are not only found at the microtubule plus end.....	46
2.8.4.3	The CLIP-170 protein family.....	47
2.8.4.4	Structure of EB1 family proteins	48
2.8.4.5	Function of EB1 Protein Family members	49
2.8.4.6	Fission yeast Mal3p	50
2.9	Open questions and aim of this thesis	51
3	EXPERIMENTAL METHODS AND INSTRUMENTATIONS	53
3.1	Molecular biology methods	53
3.1.1	Cloning.....	53
3.1.2	Protein expression.....	54
3.1.3	Protein purification	54
3.1.4	SDS-PAGE	55
3.1.5	Microtubule Polymerization	56
3.1.6	Turbidity Measurement.....	56
3.1.7	Co-pelleting assay.....	57
3.1.8	Subtilisin digestion.....	57
3.1.9	Yeast extract preparation	57
3.1.10	Western blot.....	58
3.2	Electron microscopy	59
3.2.1	Negative staining for electron microscopy	59
3.2.2	Freeze-drying and unidirectional shadowing of microtubules for electron microscopy	60
3.2.3	Cryo-electron microscopy.....	61
3.2.4	Image processing and helical three dimensional reconstruction of cryo- electron microscopy images.....	62
3.2.5	Statistical Difference Mapping	65
3.3	Internet based bioinformatic tools	65
4	RESULTS	66
4.1	Expression and purification of Mal3p	66
4.2	Biochemical studies of full-length Mal3p binding to microtubules.....	68
4.2.1	Turbidity measurements.....	68
4.2.2	Co-pelleting Mal3p with microtubules	69
4.2.3	Subtilisin digestion does not affect Mal3p binding	69
4.3	Visualization of Mal3 binding to microtubules by electron microscopy	70
4.3.1	Cryo electron microscopy of microtubules co-polymerized and decorated with Mal3p.....	70

4.3.2	High-resolution shadowing electron microscopy reveal Mal3p binding at the groove between two protofilaments.....	72
4.3.3	Mal3p specifically interacts with the microtubule lattice seam.....	75
4.3.4	Mal3p stabilize the microtubule lattice seam.....	77
4.4	Microtubule polymerization with GMPCPP and the influence of Mal3p.....	78
4.4.1	Microtubule polymerization with GMPCPP under different conditions.....	78
4.4.2	Mal3p stabilizes a closed conformation of GMPCPP microtubules.....	80
4.5	Comparing <i>S. pombe</i> endogenous concentrations of tubulin and Mal3p	81
4.6	Truncated peptides of Mal3p.....	82
4.6.1	Homology, conservation and tertiary structure predictions define the boundaries between protein domains.....	82
4.6.2	Purification of Mal3p truncated peptides.....	85
4.7	Mal3p-N-203 microtubule binding.....	86
4.7.1	Turbidity	87
4.7.2	Cryo-electron microscopy of microtubules co-polymerized and decorated with Mal3p-N-203	87
4.7.3	Helical reconstruction of undecorated, Mal3p-N-203 and <i>Neurospora</i> Kinesin-355 decorated microtubules	88
5	DISCUSSION	95
5.1	Mal3p binds and stabilizes microtubules <i>in vitro</i>.....	96
5.1.1	Turbidity studies reveal polymerization kinetics.....	96
5.1.2	Mal3p binding to taxol-stabilized microtubules	97
5.2	Mal3p microtubule interaction is not detectable using cryo-electron microscopy	98
5.3	Geometry of interaction of dimeric Mal3p with the microtubule lattice seams	99
5.3.1	Mal3p observed by unidirectional shadowing	99
5.3.2	Mal3p matches the geometry of the seam.....	100
5.3.3	Orientation of a dimeric Mal3p along the seam.....	101
5.3.4	Selective binding rather than cooperative binding.....	103
5.4	A Novel mechanism for microtubule stabilization.....	103
5.4.1	Mal3p stabilizes the microtubule lattice seam	104
5.4.2	Mal3p causes a closed microtubule conformation.....	104
5.5	Molecular interactions on the microtubule	105
5.5.1	Mal3p-N-203 binds the entire microtubule wall and no longer shows A-lattice specificity	106
5.5.2	Does Mal3p associate with α - or β -tubulin.....	106

5.5.3	Stabilization of lateral protofilament interactions.....	107
5.5.4	Intramolecular regulation of EB1 family proteins.....	107
5.5.5	The EB1-domain and dimerization are not necessary for microtubule stabilization.....	108
5.5.6	Microtubule nucleation <i>in vitro</i>	108
5.5.7	Mal3p avoids traffic jams	109
5.6	Mal3p influences the microtubule structure	110
5.7	Comparing <i>in vitro</i> results with cellular observations.....	110
5.7.1	Endogenous concentration ratios	111
5.7.2	Influence of taxol	111
5.8	What is going on at the microtubule plus end?	112
5.8.1	MAP network at the growing plus end	114
5.8.2	Depolymerisation.....	114
5.9	The sense of the seam.....	115
5.10	Perspective for Mal3p and the +TIPs	116
5.10.1	The EB1 protein family	116
5.10.2	Microtubule plus end structure	116
5.10.3	Structure and function of truncated Mal3p and microtubules	118
6	SUPPLEMENTARY INFORMATION	119
6.1	Standard curve for HiLoad Superdex 200 prep grade 16/60.....	119
6.2	Monoclonal anti-Mal3p-antibody expression and characterization	120
6.2.1	Hybridoma cell culture	120
6.2.1.1	Defrosting	120
6.2.1.2	Subcloning	120
6.2.1.3	Maintenance and harvest.....	121
6.2.1.4	Freezing cell culture.....	121
6.3.2	ELISA	121
6.3.3	α -Mal3p-Antibody epitope regions on Mal3p	122
6.3	<i>S. pombe</i> endogenous concentrations of tubulin and Mal3p.....	124
7	BIBLIOGRAPHY	126
8	ABBREVIATIONS	149
9	CURRICULUM VITAE.....	150

1 Summary

Microtubules are a fascinating component of the cellular scaffold protein network, the cytoskeleton. These hollow tubular structures are assembled of laterally associated protofilaments containing $\alpha\beta$ -tubulin heterodimers in a head to tail arrangement. Accordingly microtubules have a defined polarity, which sets the base for the polarity of the cell. The microtubule lattice can be arranged in two conformations: In the more abundant B-lattice conformation, where the protofilaments interact laterally through α - to α - and β - to β -tubulin contacts and in the less stable A-lattice conformation, where α -tubulin interacts laterally with β -tubulin. In cells the microtubules generally contain 13 protofilaments of which usually one pair interacts in the A-lattice conformation, forming the so-called lattice seam. Microtubule dynamics and interactions are strongly regulated by microtubule associate proteins (MAPs).

Structural investigations on MAPs and microtubule associated motor proteins in complex with microtubules have become possible in combination with modern electron microscopy (EM) and image processing. We have used biochemistry and different advanced EM techniques to study the interaction between microtubules and the MAP Mal3p *in vitro*. Mal3p is the sole member of the end-binding protein 1 (EB1) protein family in the fission yeast *Schizosaccharomyces pombe*. Previous *in vivo* studies have shown that Mal3p promotes microtubule growth. Our studies with high-resolution unidirectional shadowing EM revealed that Mal3p interacts with the microtubule lattice in a novel way, using binding sites on the microtubule that are different from those reported for other MAPs or motor proteins. Full-length Mal3p preferentially binds between two protofilaments on the microtubule lattice, leaving the rest of the lattice free. A case where Mal3p was found in two adjacent protofilament, revealed an A-lattice conformation on the microtubules, surprisingly indicating specific binding of Mal3p to the microtubule seam. With a lattice enhancer, in form of a β -tubulin binding kinesin motor domain, it was demonstrated that Mal3p stabilizes the seam which is thought to be the weakest part of a microtubule. Further, the presence of Mal3p during microtubule polymerization enhances the closure of protofilament sheets into a tubular organization. Cryo-EM and 3-D helical reconstruction on a monomeric microtubule binding domain of Mal3p, confirm the localization in between the protofilament and result in an accurate localization on the microtubule lattice. The results also indicate Mal3p's capacity to influence the microtubule lattice conformation. Together, studies approached *in vitro* demonstrate that an EB1-family homolog not only interacts with the microtubule plus end, but also with the microtubule lattice. The structure of Mal3p interacting with microtubules reveals a new mechanism for microtubule stabilization and further insight on how plus end binding proteins are able promote microtubule growth. These findings further suggest that microtubules exhibit two distinct reaction platforms on their surface that can independently interact with selected MAPs or motors.

2 Introduction

2.1 The origin of polarity

The cell is a highly structured unit, with organelles and protein complexes organized in a defined and cell type specific way. To facilitate fundamental processes, for example cell division, differentiation and growth or directed motion, the cytoplasm as well as the cell membrane is asymmetrically arranged and exhibits a defined polarity. Bacteria, yeast and multi-cellular organisms may appear as very different systems, but they all use conserved mechanisms to achieve a polarized organization. The polarity is often adapted to specific functions and to the environment of a cell, for example an epithelial cell in the intestine has one side facing the intestinal lumen and another side facing the blood vessels. It is essential that the membranes are functionally different at the opposite sides. An established polarity can be inherited from mother to daughter cells, leaving an initial asymmetric distribution of membrane or cytoplasm, which is maintained or reorganized by the daughter as needed. Other cells divide and grow symmetrically until they are confronted with a polarization determining factor, for example sperm entering into an egg or an external ligand binding to a plasma membrane receptor. Other cells have the capacity of *de novo* polarization, for example bacteria.

Once polarization is triggered in a cell, an intracellular signaling cascade, involving small GTPases and kinases amplifies the signal. A signal can be activated regionally on the cell or the molecules responding to a signal can be regionally localized. Essential targets for a signaling cascade are the cytoskeleton (see section 2.2) and its associated proteins (see section 2.8). The activities of the latter are usually modulated, which results in the rearrangement of the polarized protein polymers comprising most of the cytoskeleton. Finally, the cytoskeleton is proposed to maintain the cells and its own polarity. For example, through molecular feedback loops the cytoskeleton can actively transport and localize the signaling molecules to the region of activation or deactivation in cases where sustained signaling is required.

2.2 The Cytoskeleton

The different cytoskeletal elements form an intracellular scaffold that provides mechanical stability, directs organelle organization and cellular morphology and that creates tracks for the transport of proteins, RNAs and vesicles to different regions of the

cell. The cytoskeleton also plays a fundamental role in motile processes, such as cell growth, chromosome segregation or cell migration, where it is frequently used as a force generator, often in conjunction with motor proteins. For proper functioning, the cytoskeleton also has to be very flexible. Upon signaling the scaffold must respond quickly and be able to efficiently rearrange its organization.

Generally, the cytoskeleton consists of protein subunits that are polymerized into filamentous structures. There are three different types of cytoskeletal filaments in eukaryotic cells: Filamentous actin, intermediate filaments and microtubules (Figure 2.1). Whereas the proteins forming actin filaments and microtubules are evolutionary highly conserved, intermediate filaments are formed by diverse proteins that are difficult to group just based on sequence homology. Intermediate filament subunits are symmetrically arranged into non-polar bundles, whereas actin filaments and microtubules possess intrinsic polarity. The polar arrangement of actin and microtubule subunits is the basis for directed transport, and is used for establishment and maintenance of cell polarity. However the three cytoskeleton components do not act individually. There is considerable crosstalk between them and they also function to directly or indirectly maintain each others structure.

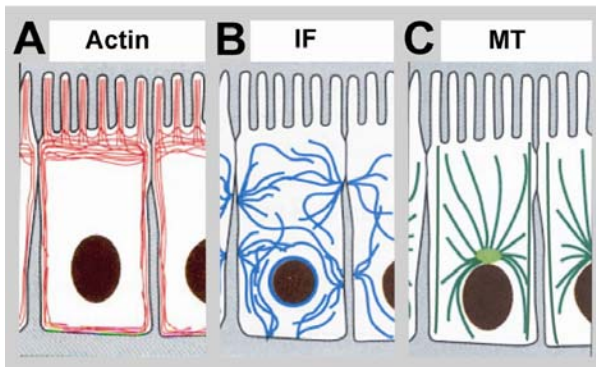


Figure 2.1: Examples of cytoskeleton organization in epithelial cells. (A) Actin arranged around the cortex. (B) Intermediate filaments connecting cell-cell contacts. (C) Microtubules forming an aster from a central centrosome or polarized tracks. Adapted from Alberts *et al.*, 1994.

2.3 Bacterial cytoskeleton

Prokaryotic, bacterial cells are not organized into multiple functional cellular compartments like eukaryotic cells. Nevertheless, bacteria are highly organized and often polarized, and because they do not have membrane compartments, a functional cytoskeleton may be even more important. Consistent with this, homologs of eukaryotic cytoskeletal proteins have been discovered in bacteria and in addition cytoskeletal networks have been described that are not present in eukaryotes. This is currently an exploding field in cell biology (Shih and Rothfield, 2006).

Several actin homologs exist in bacteria, for example MreB and ParM family proteins. MreB can bind and hydrolyze ATP or GTP, polymerize into filaments and form solid cables by arranging into bundles. The bundles form spirals at the cell cortex and are responsible for cell shape determination and coordinating the partitioning of plasmids (Wood *et al.*, 2002; Garner *et al.*, 2004; Esue *et al.*, 2005). ParM filament assembly exhibits the same dynamics at both ends.

FtsZ proteins are tubulin homologs and highly conserved amongst bacteria. The protein folding is very similar to tubulin (Figure 2.2C), although it has only 17% sequence identity to eukaryotic tubulin (Bi and Lutkenhaus, 1991; Lowe and Amos, 1999). It is likely that FtsZ and tubulin evolved from a common ancestor, and that makes it interesting to learn more about similarities and differences between these proteins. FtsZ is a monomer that self-assembles into protofilaments in the presence of ATP (Figure 2.2A and B). The protofilaments bundle into a ring like structure at the cell division site (Figure 2.2D), (Bi and Lutkenhaus, 1991). Ring formation involves at least 10 FtsZ interacting proteins, but very little is known about the assembly process or the structure of this complex. Interestingly, in evolutionary terms, is that a similar, so-called cytokinetic ring that is made of actin and myosin, is fulfilling the task of cell division in animal and yeast cells. (Amos *et al.*, 2004).

Finally, somewhat striking but still controversial is the discovery of the first and so far only intermediate filament homolog, crescentin, found in *Caulobacter crescentus*. This protein is responsible for the characteristic comma like shape of the bacterium (Ausmees *et al.*, 2003)

Additional cytoskeleton-like filamentous structures have been described in bacteria, which do not possess homologues in eukaryotic cells. For example the MinD/ParA protein family members polymerize into filamentous structures in the presence of ATP *in vitro*. MinD is responsible for cell polarity and septum positioning during cell division. MinC and MinE form an oscillating helical structure that coils around the periphery of the cylindrical cell (Figure 2.2D). The proteins are involved in cell polarity and positioning of the FtsZ ring (Shih *et al.*, 2003).

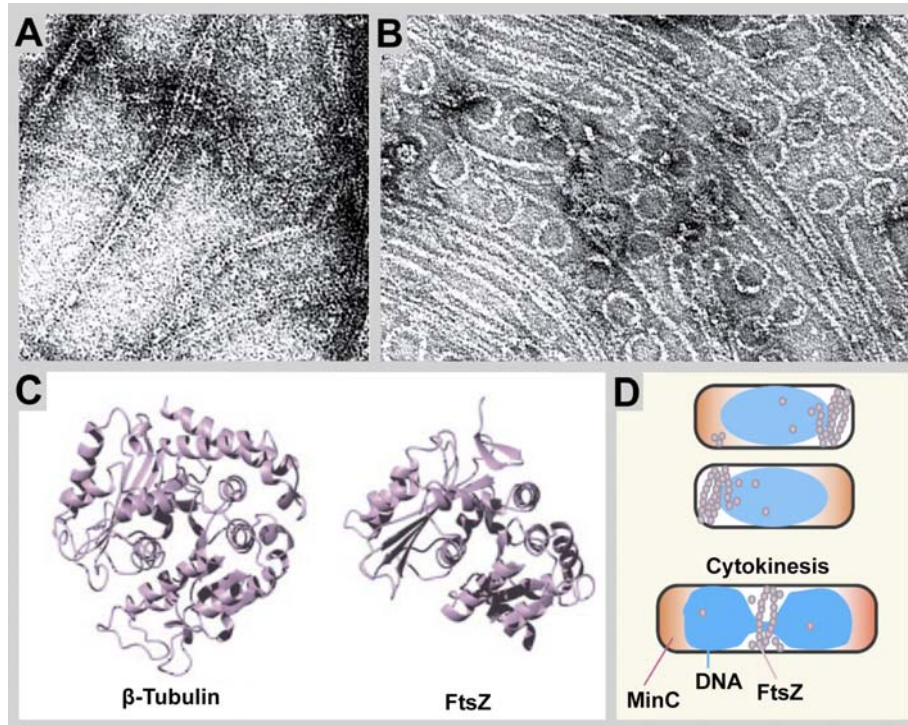


Figure 2.2: Prokaryotic FtsZ is homologous to eukaryotic tubulin. (A) In the presence of GTP, FtsZ polymerizes into straight protofilaments *in vitro*. (B) In the presence of GDP, FtsZ assembles into protofilament rings. Figure (A) and (B) were adapted from Lu *et al.*, 2000. (C) Structure of eukaryotic β -tubulin and prokaryotic FtsZ, adapted from Shih and Rothfield, 2006. (D) In *E. coli* MinC, a negative regulator of FtsZ, oscillates to establish polarity and enable FtsZ ring assembly at the division site; this is essential for bacterial cytokinesis. This model was adapted from Margolin, 2006.

2.4 Actin

Actin assembles into dynamic filaments, also called micro filaments, that are approximately 6 nm in diameter (Steinmetz *et al.*, 1997). Actin is essential for motile processes in all known cell types. A classical example is the role of actin in forming the contractile machinery in muscle cells, the cell type where actin is most abundant (Squire, 1997). But actin is also important for movements in non-muscle cells, for example during cell migration, or cytokinesis (dos Remedios *et al.*, 2003). Furthermore, nuclear actin is involved in RNA transcription (Percipalle and Visa, 2006). For muscle contraction, thin actin filaments interact with thick filaments containing the motor protein myosin. In non-muscle cells filamentous actin interacts with unpolymerized myosin. Myosin uses the free energy from ATP hydrolysis to move along actin filaments, which creates the force needed for muscle contraction or cellular transport (Craig and Woodhead, 2006; Dantzig *et al.*, 2006).

The filamentous F-Actin is the polymerized form of globular G-actin monomers. The asymmetric monomer assembles into a fixed orientation with respect to the filament axis thus forming a polar polymer. This filament can be described as a two-start right-handed helix, where the longitudinal interactions between subunits are stronger than the lateral interactions (Steinmetz *et al.*, 1997). The polarity of F-actin can be visualized by electron microscopy (EM) after stoichiometric decoration with myosin S-1. Thereby, an arrowhead-like pattern appears, where the barbed end polymerizes faster than the pointed end (Figure 2.3A) (Moore *et al.*, 1970). Actin is an ATPase that binds ATP together with a divalent cation, Mg^{2+} , in a cleft in the center of the molecule. In the filament, ATP hydrolysis is fast and P_i dissociation low. Accordingly, ADP- P_i -actin is the major component of the polymerized actin (and turns into ADP after P_i dissociation). Due to trapping of the nucleotide in the polymer, nucleotide exchange is only possible in G-actin (Carrier, 1992). Under physiological conditions the affinity for G-actin assembly at the barbed end is more than 12 times higher than at the pointed end. This results in a dynamic flux through the filaments, referred to as treadmilling: G-actin is preferentially added at the barbed end of filaments, thus driving their polymerization, and it is preferentially removed from the pointed end, driving depolymerization. The freed G-actin is then recycled (Wegner and Isenberg, 1983). *In vitro* the equilibrium between G-actin and F-actin can be manipulated by changing the ionic strength of the buffer. Under low salt conditions the G-actin conformation is favored and at higher salt concentrations (e.g. 100 mM KCl/ 2 mM $MgCl_2$) F-actin is the dominant conformation.

The helical properties of F-actin also made it possible to reconstruct the 3-D structure of filaments from EM images (in principal by the same method that we used for microtubules; see section 3.2.4). The advantages of these studies were that atomic models of actin could be compared with the structure of the cryo fixed native form (Figure 2.3B). Furthermore, the same method could be used to study actin mutations and the interaction between actin and actin binding proteins and drugs (Steinmetz *et al.*, 1997). Eventually, further optimization of 3-D helical reconstruction and molecular docking of atomic structures into electron density maps revealed the power stroke of myosin V on actin filaments (Volkman *et al.*, 2005).

The physiological conditions in the cell constitute a relatively high ionic strength, in which G-actin would be totally polymerized into F-actin. This, however is not the case as equal amounts of G-actin and F-actin co-exist in the cell. Nucleation, polymerization, destabilization and changes in organization of actin are therefore tightly regulated by

actin binding proteins. Actin binding proteins are a variable group of proteins holding the key to different actin functions and organization in different organisms and tissues. Some actin binding proteins, for example membrane proteins or receptor components, directly connect the actin cytoskeleton to extracellular links or to cell-cell adhesions (dos Remedios *et al.*, 2003). At the leading edge of migrating cells, actin filaments treadmill to push membrane protrusions forward; this produces the forces required for movement. The treadmilling of actin filaments is 200 times faster than *in vitro* when regulated by actin stabilizing and destabilizing proteins in a migrating cell (dos Remedios *et al.*, 2003; Pollard and Borisy, 2003). In fission yeast, actin forms patches and cables at the polar growth zones (Figure 2.3C and D), where actin associated proteins and microtubule associated proteins (MAPs) interact, in a tight network to regulate cell polarity (Martin *et al.*, 2005; Martin and Chang, 2006).

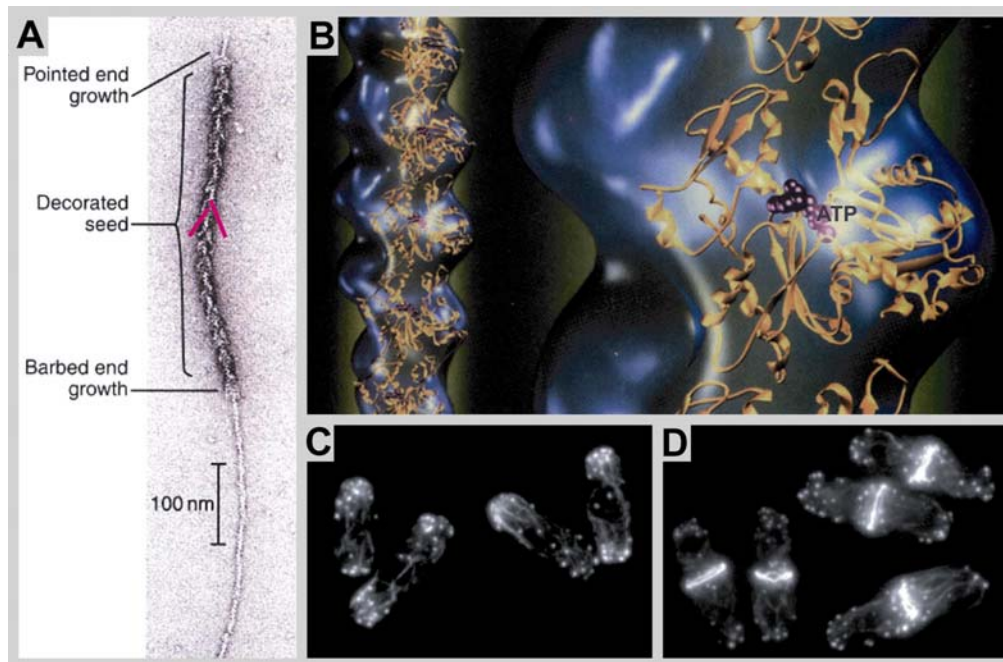


Figure 2.3: Actin. (A) Electron micrograph of negatively stained actin polymerizing from a myosin head domain decorated actin seed, which exhibits an arrow-like pattern (pink lines) The fast growth at the barbed end and slow growth at the pointed end reveal the polarity of F-actin. Adapted from Pollard and Earnshaw, 2002. (B) 3-D reconstruction and model of the atomic structure of helical F-actin. The ATP binding site in the middle cleft of an actin subunit is drawn in purple. Adopted from Pollard and Earnshaw; 2002; Steinmetz et al., 1997. (C) and (D) Fission yeast actin stained with bodipy-phalloidin. (C) During interphase F-actin is localized to the growing cell poles in actin patches and bundles. Actin defines and contributes to polarized growth of the cells. (D) At the onset of mitosis actin cables are redistributed to the cell center to form the cytokinetic ring, fulfilling the same tasks as FtsZ (interestingly, this is the bacterial homolog of tubulin, not actin) in Bacteria. Images of fission yeast were kindly provided by Dietrich Foethke.

2.5 Intermediate filaments

The Intermediate filament protein family is a very diverse group of proteins. So far, more than 70 different genes encoding intermediate filaments have been identified. Their expression is mostly tissue specific. Examples are keratins in epithelia, desmin in muscle or vimentin in mesenchymal cells. An exception to this are the lamins. These nuclear filaments are more ubiquitously expressed in higher eukaryotes. Lamins stabilize the nuclear envelope by forming a network covering the inside of the nuclear membrane. This network also anchors the nuclear pores and is at the same time involved in heterochromatin organization. Cytoplasmic intermediate filaments are believed to serve as a “buffer” that helps to maintain cell shape. Despite these static functions the intermediate filaments are flexible and dynamically turn over. They also extensively cross-talk with the other cytoskeletal components and with the plasma membrane. Through interactions with motor proteins, motile intermediate filaments are organized into a network that is coordinated by actin and microtubules (Helfand *et al.*, 2004; Herrmann and Aebi, 2004).

Common to all intermediate filament proteins is a region of sequence homology at the non-globular N-terminal head and at the globular C-terminal tail. Head and tail are connected by a 45 nm α -helical rod domain forming a coiled-coil that mediates protein dimerization. Different models have been proposed for the symmetric assembly of subunits into 10 nm filaments, with a multi-stranded, left-handed, twisted rope-like structure (Figure 2.4). In contrast to actin filaments and microtubules, the intermediate filaments can self-assemble without nucleotide hydrolysis and the filaments have no intrinsic polarity (Strelkov *et al.*, 2003). Recent EM studies of *in vitro* polymerized intermediate filaments demonstrated different arrangements in filaments and extensive internal filament flexibility (Foeger *et al.*, 2006; Goldie *et al.*, 2006). Accordingly, intermediate filaments are not rigid and do not break upon the application of force or bending (e.g. like microtubules), possibly providing elasticity to the cellular scaffold.

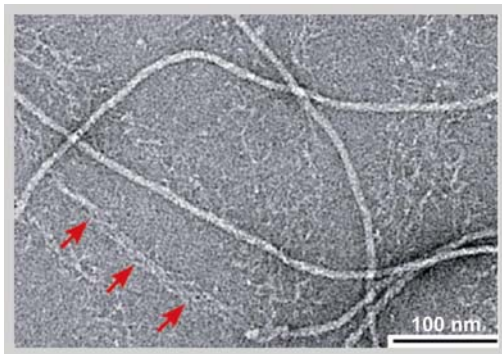


Figure 2.4: EM image of negatively stained vimentin filaments. Vimentin filaments appear as thick compact cables and in a partially unraveled conformation (red arrows). Adapted from Goldie *et al.*, 2006.

Intermediate filaments have greatly diverged in evolution and only structural analysis can reveal homology. For example, intermediate filament like proteins were identified in this way in budding yeast (McConnell and Yaffe, 1993), and most likely, additional intermediate filament related structures will emerge in other species in the coming years.

2.6 Microtubules

Microtubules are essential structures for an increasing number of well-studied cellular events. Their role in chromosome segregation during mitosis, axonal transport to the synapse in neuronal cells and the delivery of vesicles from the Golgi apparatus to other membrane compartments or the plasma membrane are only a few examples.

Microtubules are hollow cylinders, approximately 25 nm in diameter, which makes them more rigid than actin and intermediate filaments. They are assembled from heterodimeric globular α - and β -tubulin subunits that arrange head to tail into linear protofilaments, which in turn associate laterally and in parallel into a cylinder (Figure 2.5A). This arrangement makes microtubules intrinsically polar: β -tubulin is exposed at the plus end and α -tubulin at the minus end. Microtubules generally contain 13 protofilaments, but this number can be more variable for *in vitro* polymerized microtubules (Nogales, 2001; Amos and Schlieper, 2005).

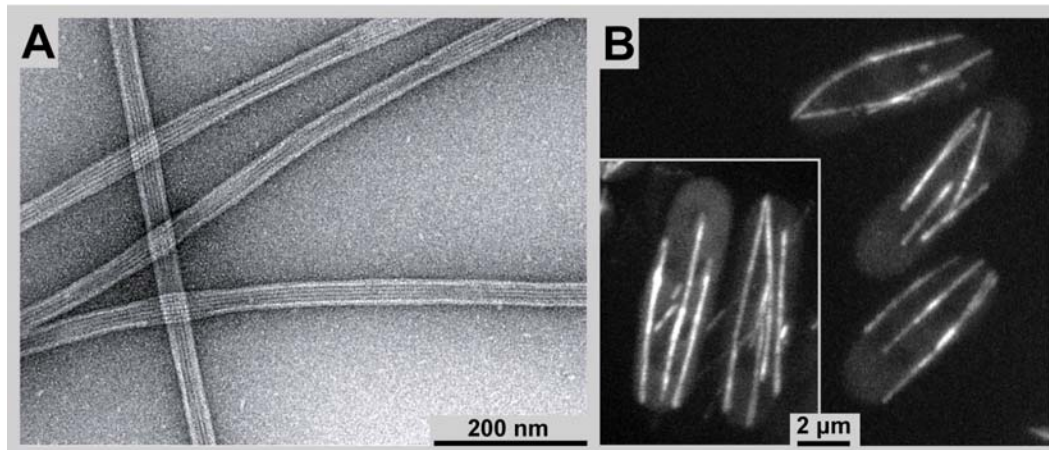


Figure 2.5: Microtubules. (A) Electron micrograph of negatively stained microtubules. The cylindrical structures of laterally associated protofilaments are clearly visible using this method. (B) Microtubule bundles in fission yeast, visualized with GFP-tubulin. In the rod shaped polar cell the bundles are arranged parallel to the cell axis. The microtubules function as tracks for transport of polarity determination factors to the cell poles, and thereby are essential for maintenance of polarity. Images provided by courtesy of Lindsay Murrells.

Microtubule functions are based on their dynamic properties. In the presence of GTP, $\alpha\beta$ -tubulin polymerizes. Similar to actin, polymerization of tubulin is accompanied by nucleotide hydrolysis, which induces depolymerisation and is the basis of dynamic instability (see section 2.6.5), (Mitchison and Kirschner, 1984). If cellular parameters like microtubule polymerization/depolymerization rate or catastrophe/rescue frequency are analyzed in more detail, these events turn out to be manipulated by microtubule associated proteins (MAPs), (Komarova *et al.*, 2002b).

Today many MAPs with microtubule regulating activity are known (see section 2.8). They use different mechanisms to localize to microtubules and to influence their dynamics. MAPs, like Tau and XMAP215, bind along the entire microtubule, stabilizing the polymerized structure. Other MAPs like End-binding protein 1 (EB1) and Cytoplasmic linker protein 170 (CLIP-170), belong to a group of proteins referred to as plus end tracking proteins (+TIPs), (see section 2.8.4). This divergent group of proteins fulfils many important tasks: promotion of microtubule polymerization, prevention of catastrophe, interaction with target structures and deposition of cargo, for example polarity markers to the plasma membrane (Howard and Hyman, 2007; Morrison, 2007). In a simplified system like fission yeast, Mal3p, the homolog of human EB1 is localized to polymerizing microtubule plus ends protecting the plus end from catastrophe. Tip1p, the homolog of CLIP-170, also protects the microtubule from catastrophe and allows the growing plus end to interact with the cortex. It also pauses growth when the microtubule reaches the cell tip (Busch and Brunner, 2004).

As the structure of microtubules and microtubule interacting proteins (MAPs) is the main topic of this thesis, it will be presented and discussed in more detail in the following sections.

2.6.1 Cellular microtubule organization

Microtubule nucleation in all cell types occurs at specific structures called microtubule organizing centers (MTOCs). These are dynamic and transient structures that can catalyse microtubule nucleation and can anchor microtubules by interacting with their plus ends or sides. The structure of MTOCs varies dramatically in different species and tissues, and also within the same cell different types can co-exist, forming different microtubule arrays observed in, for example, yeast, neurons and epithelial cells (Figure 2.6), (Bre *et al.*, 1987; Bartolini and Gundersen, 2006; Luders and Stearns, 2007).

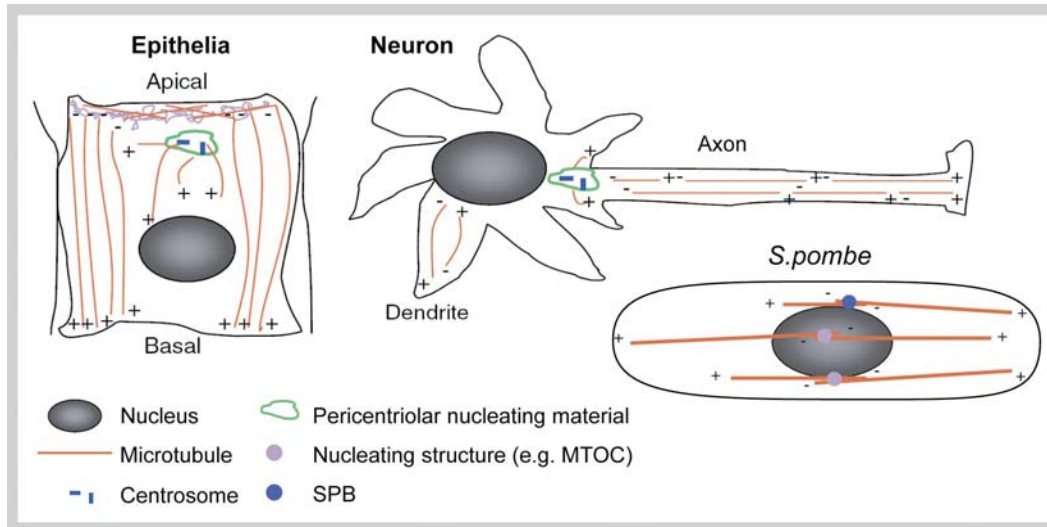


Figure 2.6: Polarized cells with non centrosomal microtubule arrays. In an epithelial cell a population of noncentrosomal microtubules could nucleate from the apical region and interact with their plus end at the basal membrane facilitating directed transport. In neurons noncentrosomal microtubule bundles are arranged parallel in the axons and antiparallel in the dendrites. The fission yeast (*S. pombe*) exhibit strictly regulated polar growth. Microtubule bundles nucleate from several different MTOCs, including the spindle polar body (SPB). The minus ends are arranged in an antiparallel bundle in the cell center, the dynamic plus ends extend throughout cytoplasm and interact with the cortex at the cell tips. Adapted and modified from Bartolini and Gundersen, 2006.

In many animal cells microtubules form a radial array, with the microtubule minus ends trapped in a central centrosome, and the plus ends extending throughout the entire cell (Figure 2.7A). Centrosomes contain two cylinders termed centrioles that are assembled from nine microtubule triplets. The centrioles are embedded in a cloud of pericentriolar material, a proteinaceous material in which the minus ends of the microtubules are captured (Figure 2.7A), (Bornens, 2002). The centrioles are not an essential part of MTOCs. The spindle pole body (SPB) in fungi and the MTOCs in somatic plant cells have no centrioles. Also, after removal of the centrioles in animal cells, microtubules are nucleated and correctly organized, chromosomes separate properly during mitosis, and cells divide normally (Basto *et al.*, 2006). However, centrioles are an essential component of the MTOCs in motile membrane extensions like epithelial cilia and sperm flagella, where they are called basal bodies and are responsible for microtubule organization (Basto *et al.*, 2006). They serve as a template for the nucleation of the characteristic 9+2 microtubule arrangement in axonemes: 9 microtubule doublets arranged in a peripheral ring and 2 single central microtubules (Figure 2.7A), (Dawe *et al.*, 2007).

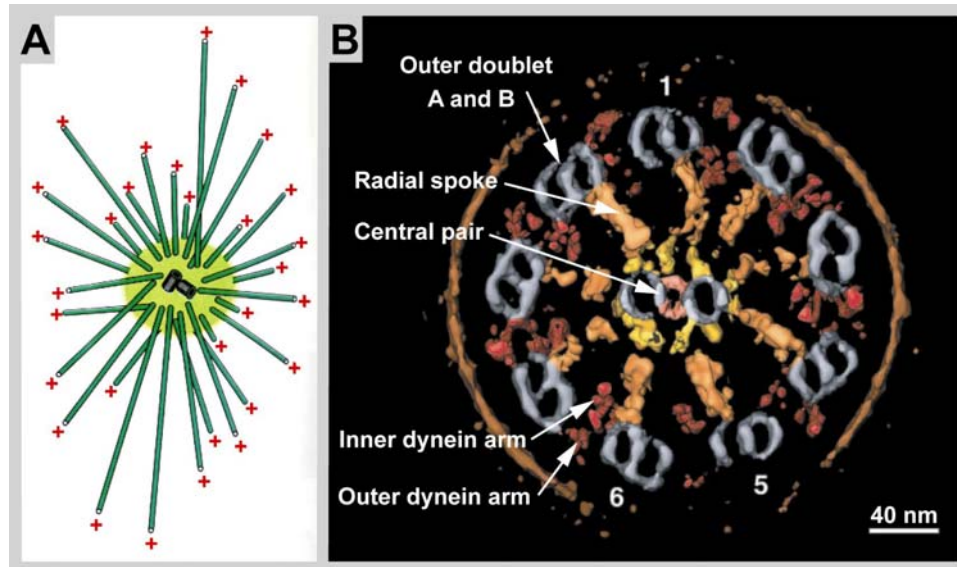


Figure 2.7: (A) A radial array of microtubules. The minus ends of each microtubule are embedded in the centrosome matrix (light green) that surrounds the centriole pair, a microtubule nucleating MTOC. The microtubule plus ends grow in the direction of the cell periphery. Adapted from Alberts *et al.*, 1994. **(B) Electron tomography and 3-D reconstruction of a sea urchin sperm flagellum,** visualizing the characteristic organization of microtubules (grey; 9+2) and the motor protein dynein. Adapted from Nicastro *et al.*, 2005.

The non-centrosomal microtubule arrays in epithelial cells contribute to their cellular polarity. In most epithelial cells microtubules are arranged in bundles close to the lateral cell membrane (Figure 2.6). Usually the microtubule minus ends are located at the apical membrane and the plus ends are growing towards the basal membrane. In this conformation the microtubules are more stable and facilitate directed long-range vesicle transport towards and between the polarized membrane regions. Thereby, the cargo is sorted to different destinations, and the cell polarity is maintained (Musch, 2004).

Neurons have a combination of centrosomal and non-centrosomal MTOCs. In the cell body, short microtubules are nucleated from a centrosome, but in axons they are organized in parallel, and in the dendrites into antiparallel bundles. In axons, stable and long microtubules are arranged with their plus ends facing away from the cell body (Figure 2.6), (Baas *et al.*, 1988; Chen *et al.*, 1992).

The fission yeast *S. pombe*, is a popular model organism for the study of cell polarity. Fission yeast cells have a relatively simple and well studied non-centrosomal and functional symmetrical microtubule arrangement. During interphase, microtubules are nucleated from several different active MTOCs simultaneously (Sawin and Tran, 2006).

Thereby, dynamic microtubules are arranged into 3-6 bundles that extend along the long axis of the cylindrical cell, often spanning the entire cell length (Figure 2.5B and 2.6). A bundle generally contains 1-7 microtubules organized such that the growing plus ends are pointing towards the opposite poles (Drummond and Cross, 2000; Hoog *et al.*, 2007). In the cell center, the minus ends of the antiparallel microtubules are bundled together and mostly associated with the nucleus. When the dynamic microtubules reach the cell poles, polarity determinants are deposited at the membrane of the cell. This is essential for maintaining the direction of growth and cell polarity (Browning *et al.*, 2003).

2.6.2 Microtubules in the mitotic spindle

Centrosomes, basal bodies and SPBs do not form *de novo*. Instead, they are duplicated and are eventually segregated into the two daughter cells. During the onset of mitosis the duplicated centrosomes or SPBs move to opposite sides of the nucleus. When the nuclear envelope breaks down, the centrosomes are induced, by the presence of chromatin, to form two microtubule arrays, which together arrange the mitotic spindle. (In yeast the spindle is nucleated inside the nuclear membrane.) The microtubules in these arrays can be grouped to three categories according to their function (Figure 2.8): (1) Fast growing microtubules capture the kinetochores of each chromosome from both sides with their plus ends. (2) Other microtubules interact in an antiparallel manner with the microtubules from the opposite array. Together the two arrays form a bipolar spindle. (3) The last group of microtubules form an aster, interacting with the cytoplasm and the plasma membrane to positioning the spindle in the cell (Varmark, 2004). This organization is achieved according to the “search and capture” model (Kirschner and Mitchison, 1986). In this model, highly dynamic microtubules explore the whole cell volume and become more stable upon plus end interactions, and are finally captured at the location where they can fulfill their specific task. The family of +TIPs plays an especially important role in the “search and capture” processes. +TIPs regulate microtubule dynamics and facilitate the microtubule plus end interaction with its target (Mimori-Kiyosue and Tsukita, 2003). The kinetochore-attached microtubules pull the chromosomes apart with help from motor proteins and microtubule depolymerization (Westermann *et al.*, 2006). Antiparallel, overlapping spindle microtubules push the spindle apart with help from plus end directed motor proteins (Sawin *et al.*, 1992). Additionally, the separation is balanced by forces on parallel aster microtubules, which pull each pole to its center, with help from minus end directed motor proteins (Sharp *et al.*, 2000). However, centrosomes (or SPBs) are not required for the assembly of a bipolar spindle. *Drosophila* embryos without centrosomes still form bipolar spindles and in every cell mitosis proceeds normally (Basto *et al.*,

2006). In cell extract from *Xenopus* oocytes, the presence of chromatin is sufficient for microtubules to assemble a bipolar spindle (Heald *et al.*, 1996). Accordingly, chromatin itself is also an MTOC.

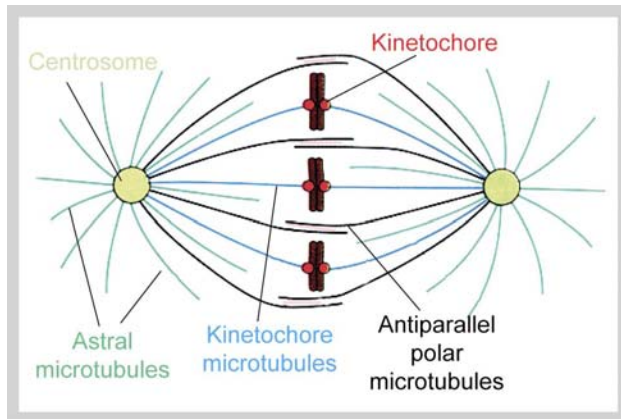


Figure 2.8: Microtubule organization in the mitotic spindle.
Adapted from Alberts *et al.*, 1994.

2.6.3 Microtubule nucleation

The self-assembly of microtubules into complex, flexible and variable functional polymers has puzzled both experimental and theoretical scientists for more than 30 years. The cellular concentration of free tubulin heterodimers is much lower than the critical concentration required for spontaneous nucleation of purified tubulin *in vitro*. The cellular tubulin concentration in fission yeast is estimated to be approximately 5 μM (Loiodice and Tran, personal communication; see also section 6.3). Pure tubulin assemble into microtubules only at a concentration higher than 20 μM in *in vitro* experiments (Gaskin *et al.*, 1974). The cells overcome this dilemma by promoting nucleation at γ -tubulin ring complexes (γ -TuRCs) with help from stabilizing MAPs (Raynaud-Messina and Merdes, 2007). No spontaneous nucleation is allowed because at this concentration of tubulin activation is needed and this is restricted to MTOCs.

In the cell, microtubule assembly is usually seeded from the γ -TuRC, the most essential component of the MTOCs (see section 2.6.1). The major component of this complex is γ -tubulin, which shows homology to α - and β -tubulin. Structural homologs of the γ -TuRC can be found in all eukaryotes. It consists of γ -tubulin and SPC97 and SPC89 or homologous proteins and is assembled as a ring that is “topped” as a cap with other asymmetrical proteins. According to the template model, the circle of γ -tubulin serves as a base for the cylinder of 13 protofilaments, with a diameter of 25 nm (Figure 2.9A). Electron tomography of isolated *Drosophila* γ -TuRCs, in particular γ -TuRC associated with growing microtubules, shows that that this model is consistent with the cellular structure and function (O’Toole *et al.*, 1999; Moritz *et al.*, 2000).

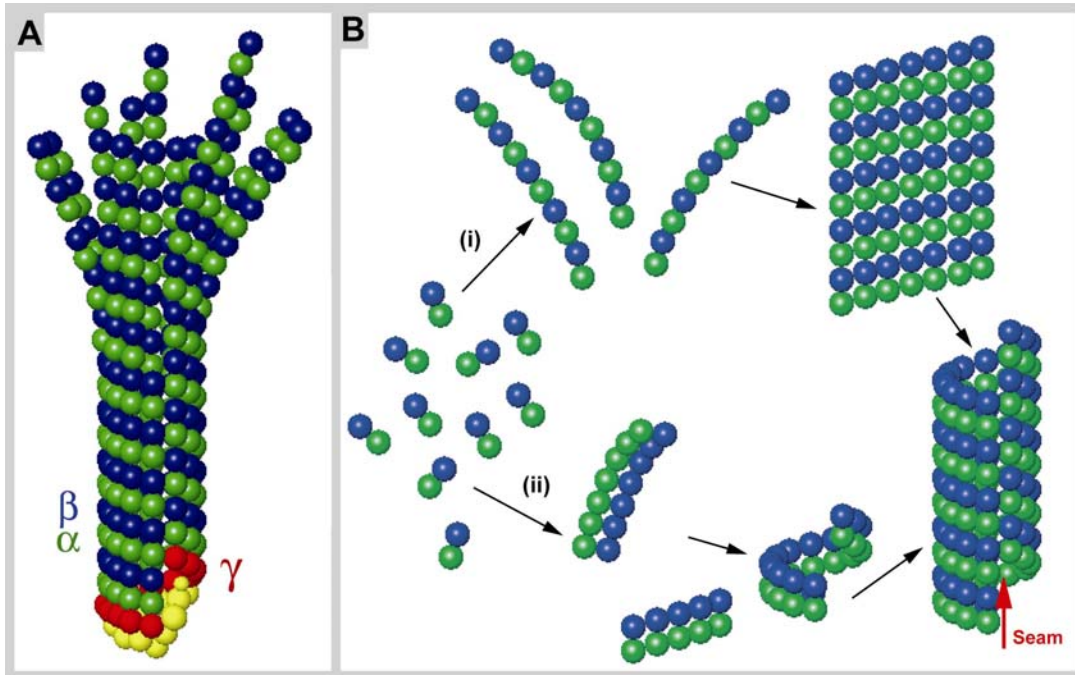


Figure 2.9: Models for microtubule nucleation. (A) *In vivo* the γ -TuRC, a macromolecular complex of γ -tubulin (red) and accessory proteins (yellow), is a template for nucleation and serves as a microtubule minus end protector. (B) Tubulin dimers assemble in to short oligomers either longitudinally (i) or laterally (ii). (i) Short oligomeric protofilaments assemble into a sheet, which is rapidly closed to a tube when the sheet reaches a certain width. (ii) Dimers associate laterally with the ring, which serves as a template for elongation.

In addition to the nucleation event, γ -TuRCs protect the microtubule minus ends from depolymerization while new subunits are added onto the growing plus end (Raynaud-Messina and Merdes, 2007). γ -TuRCs are generally present in the cytoplasm, but are activated through recruitment to MTOCs by other MTOC components, for example Mto1 and Mto2 in fission yeast (Janson *et al.*, 2005; Samejima *et al.*, 2005), and many, often tissue specific, proteins in animal cells (e.g. Pericentrin, Ninin, AKA450 and others) (Raynaud-Messina and Merdes, 2007). Activation probably also involves phosphorylation events (Vogel *et al.*, 2001).

In vitro, microtubules can be self-assembled from pure $\alpha\beta$ -tubulin, GTP and $MgCl_2$ in the absence of a γ -TuRC. The rate of nucleation is dependent on the GTP-tubulin concentration. Interestingly, this reaction never reaches an equilibrium and the rate of nucleation remains constant even after most of the tubulin is inserted into polymers and the amount of free tubulin decreases (Caudron *et al.*, 2000). With time-resolved EM the structures of growing and depolymerizing microtubules have been visualized and also the

existence of short tubulin oligomers before nucleation and after depolymerisation (Mandelkow *et al.*, 1991). Intermediates of nucleation, such as oligomers that are structurally between tubulin heterodimers and sheets, which are able to close into cylinders, have never been isolated and visualized. The actual nucleation mechanism is still a matter of debate. Theoretical studies, based on turbidity measurement results at different tubulin concentrations and mathematical modeling, proposed that nucleation is a multi-stage process with an intermediate containing 15 subunits (Flyvbjerg *et al.*, 1996). Two possible models for *in vitro* nucleation have been proposed (Figure 2.9B), (Job *et al.*, 2003). The first is based on the suggestion that the oligomers visualized by Mandelkow *et al.* are short protofilaments. In this model $\alpha\beta$ -tubulin dimers slowly assemble into a dynamic protofilament that can interact laterally and quickly associate with a sheet, which then finally close to form a short tube (Wang *et al.*, 2005). The second model proposes that the $\alpha\beta$ -tubulin heterodimers associate laterally to form a ring, like the γ -TuRC. This intermediate is the template for further elongation of dimers. Laterally chemically cross-linked tubulin dimers were recovered from depolymerizing microtubules, and to support the second theory it was demonstrated that these cross-linked oligomers are potent nucleators *in vitro* (Caudron *et al.*, 2002).

2.6.4 Molecular structure of the microtubules

The tubulin sequence and structure contains the information required for self-assembly of $\alpha\beta$ -tubulin heterodimers into protofilaments, and of protofilaments into polar and dynamic cylinders. α and β -tubulin are circa 55 kDa molecular weight proteins with 45% sequence homology. However, both α - and β -tubulin are evolutionarily very conserved, with 70 to 80% homology among protozoan, metazoan and fungal homologs.

For microtubule polymerization from $\alpha\beta$ -tubulin heterodimers, the nucleotide GTP is required. Both α - and β -tubulin bind GTP but only GTP bound to the β -tubulin subunit is hydrolysable and exchangeable. Upon polymerization, nucleotide hydrolysis is induced (Nogales, 2001; Amos and Schlieper, 2005) Accordingly, growing microtubules have a short plus end cap of GTP-tubulin, which is subsequently hydrolyzed in the “aged” microtubule lattice (Mandelkow *et al.*, 1991; Chretien *et al.*, 1999).

The asymmetric assembly of $\alpha\beta$ -tubulin dimers constitutes the repetitive basis of the protofilaments. Most commonly, microtubules *in vivo* are composed of 13 protofilaments (Tilney *et al.*, 1973), although nature does exhibit exceptions (Savage *et al.*, 1989; Afzelius *et al.*, 1990). *In vitro* it is possible to form tubulin polymers that contain between

9 and 16 protofilaments. This variation reveals a degree of flexibility and induces a supertwist of the protofilaments in the cylinder (Chretien and Wade, 1991; Chretien *et al.*, 1996). The lateral interactions between the protofilaments are defined by the structure and electrostatic surface of the tubulin heterodimer. Two arrangements are possible: A-lattices exhibit α - α and β - β interactions and B-lattices have alternate α - β interactions (Amos and Klug, 1974). These are visualized as a model in Figures 2.13 and 4.18 and further explained in section 2.6.4.5.

2.6.4.1 Atomic structure of tubulin in zinc-sheets

Purified tubulin normally polymerizes into microtubules. However, in the presence of zinc, tubulin assembles into two-dimensional crystalline sheets. These zinc-sheets were used to obtain electron crystallography data, resulting in the molecular structure of a microtubule protofilament. The 3.5 Å resolution map of tubulin revealed an almost identical structure for: α - and β -tubulin, their nucleotide binding sites, the binding site of the stabilizing drug taxol, and the longitudinal interaction sites in the protofilaments (Figure 2.10A), (Nogales *et al.*, 1998; Lowe *et al.*, 2001). In contrast to normal cylindrical microtubules, the protofilaments are arranged in an antiparallel manner in zinc-sheets. The subunits are packed symmetrically and straight, and the tubulin conformation may therefore not exactly represent the conformation in a microtubule.

The globular monomer is approximately 4 nm in diameter, and the heterodimer is 8 nm high. The N-terminal region of tubulin provides a nucleotide binding pocket, with a high affinity bound magnesium that interacts directly with the nucleotide. In the dimer, GTP bound to α -tubulin is buried in the intra-dimer interface. In this non-changeable (N) site GTP can not be hydrolyzed and stabilizes the heterodimer structure (Figure 2.10A). In contrast, the nucleotide bound to β -tubulin is exposed to the surface of the dimer. At this exchangeable (E) site the GTP is can be hydrolyzed to GDP, which can be released from the free dimer. When GTP, together with magnesium, is bound to β -tubulin, heterodimers polymerize into protofilaments, trapping the nucleotide at the E-site between the dimers. The nucleotides are in fact directly involved in the contact between subunits, both at the intra- and inter-dimer interfaces. The loop T7 (between helix H7 and H8) and helix H8 directly bind to the nucleotide in the adjacent subunit in the protofilament (Figure 2.10A). This implies that the nucleotides are directly involved in the contact between the subunits both at the intra- and inter-dimer interfaces. The hydrolysis of GTP to GDP in a protofilament induces a conformational change at the dimer interface, causing tilting of the interface and curving of the protofilament (Downing and Nogales, 1998).

The C-terminal region of tubulin forms the crest of the protofilaments on the outside of a microtubule. Helix H11 and H12 make up the surface of tubulin and are involved in the interaction with numerous MAPs and motor proteins (Figure 2.10B and 2.14B). The last 13 residues of α -tubulin and 9 residues of β -tubulin are too disordered to be recognized by crystallographic analyses (Nogales, 2001; Amos and Schlieper, 2005). They are assumed to protrude perpendicular to the microtubule axis, giving the microtubule a corona of negative charges (Tuszynski *et al.*, 2005; Tuszynski *et al.*, 2006).

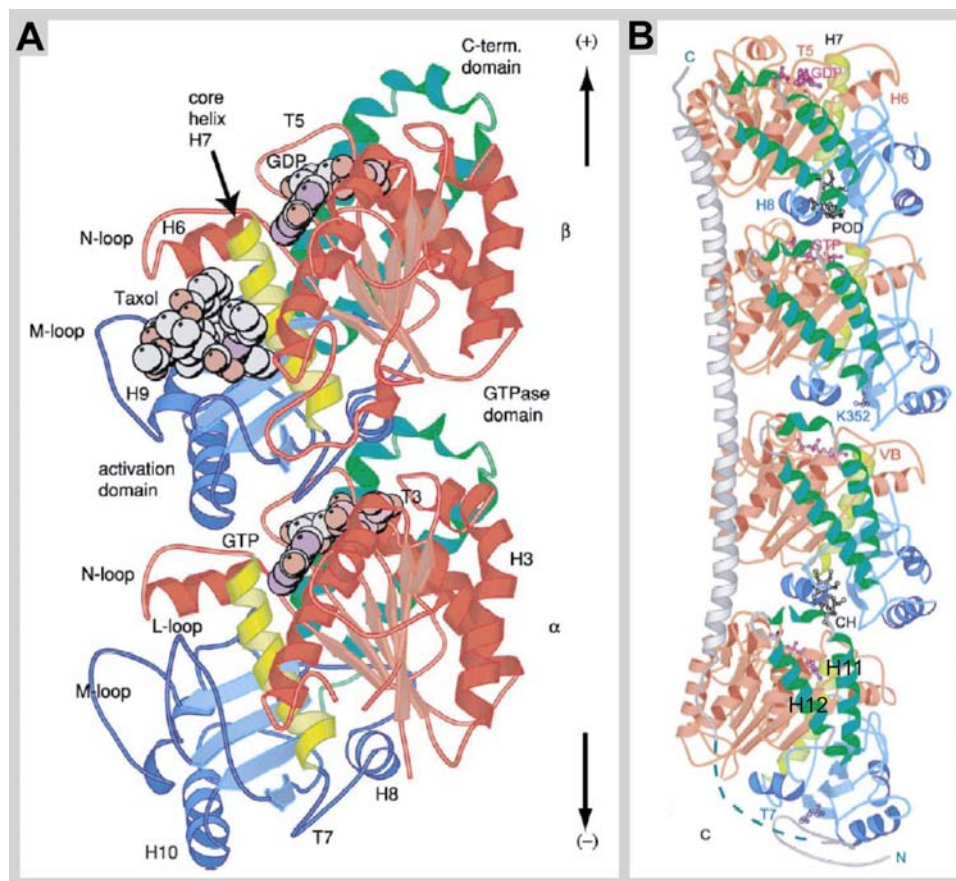


Figure 2.10: Tubulin structure. (A) Ribbon diagram of an $\alpha\beta$ -tubulin heterodimer. The structure solved by electron crystallography using sheets tubulin (Lowe *et al.*, 2001; Nogales *et al.*, 1998), is shown in an orientation corresponding to the inside view of a microtubule. The GTPase domains are colored pink. The C-terminal domain on the surface is green. GTP is sandwiched between the α - and β - tubulin subunits of each heterodimer. Taxol sits in the pocket of β -tubulin on the inside face of microtubules. In α - tubulin, this pocket is occupied by the extended L-loop. (B) Tubulin in the crystal structure of the tubulin-stathmin complex (Ravelli *et al.*, 2004). Stathmin, shown in gray, connects and induces curvature of two tubulin heterodimers. Its N-terminal domain caps one end binding to an α -tubulin subunit. The depolymerizing drugs colchicine (CH) and podophyllotoxin (POD) bind to similar sites on β -tubulin. Vinblastine (VB) binds to the GTPase domain of β - tubulin, to loop T5. The curvature of the stathmin helix indicates the degree of the curvature of this complex, which is likely to be similar for depolymerizing GDP-tubulin. Figures were adapted from Amos and Schlieper, 2005.

2.6.4.2 Structure of Stathmin-tubulin crystals

Several attempts to crystallize tubulin in complex with different destabilizing molecules have produced a view of the flexibility of the tubulin structure. Stathmin is a microtubule depolymerizing MAP (also see section 2.8.3.1), a long α -helical molecule that binds laterally to two tubulin heterodimers (Figure 2.10B). This interaction bends the two dimers into a curved conformation. Longitudinal interactions of this complex form long protofilament spirals. This structure is likely to be close to the structure of depolymerizing GDP-tubulin that can be observed as curved protofilaments by EM. This curvature is accompanied by a conformational change at the heterodimer interface and at the intra-molecular interface. The regions close to the nucleotide binding pocket are most dramatically displaced compared to the straight zinc-sheet conformation (Gigant *et al.*, 2000; Ravelli *et al.*, 2004; Gigant *et al.*, 2005).

2.6.4.3 Structure of frozen hydrated native microtubules

The high-resolution electron crystallography structure of tubulin heterodimers has been of great use for building a microtubule model (Nogales *et al.*, 1999). The structure of frozen hydrated microtubules can be mapped to 8 Å resolution with cryo-EM and 3-D helical reconstruction (similar to Figure 2.11). As it is not possible to gain atomic resolution from intact microtubules, a lot has been learned about tubulin conformation by super-positioning the atomic tubulin structure onto a reconstructed map of frozen hydrated microtubules (Nogales *et al.*, 1999; Li *et al.*, 2002a). GDP-tubulin in the microtubule lattice is trapped in the closed microtubule and adopts an intermediate conformation between the straight zinc-sheet structure and the curled stathmin co-crystallized structure of tubulin (Krebs *et al.*, 2005). Furthermore, computer modeling of atomic structure in the cryo-EM low resolution density map could predict details about the lateral interaction between subunits in the microtubule (Figure 2.11D). The M-loop was not detectable in the stathmin crystals and adopted a slightly different conformation in the low-resolution microtubule map, as compared to the zinc-sheets (it is not detectable in stathmin crystals). The M-loop of one protofilament interacts with loop H1-S2 and helix H3 at the next laterally integrated subunit. Helix H3 follows loop T3, which is involved in binding the nucleotide at the E-site and it was speculated that either the lateral interaction may induce GTP hydrolysis, or that GTP hydrolysis induces a change in the lateral interaction (Nogales *et al.*, 1999). Interestingly, the lateral tubulin interactions are not identical for the α - and β -tubulin subunits (Sept *et al.*, 2003; Drabik *et al.*, 2007). The lateral interactions between protofilaments are considered to be inflexible; not more than a 1 Å shift could be detected in the Moiré pattern of frozen hydrated

microtubules (Chretien *et al.*, 1998). At the same time, all interactions have to be elastic to allow bending of a microtubule (Pampaloni *et al.*, 2006). The complex and flexible structure of tubulin is certainly key to microtubule interactions with MAPs and motor proteins and thus to the control of microtubule dynamics and function.

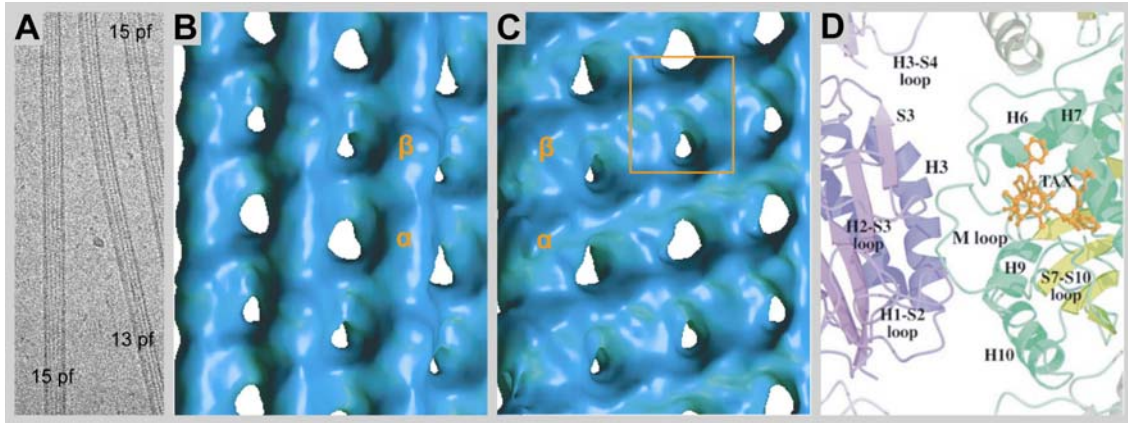


Figure 2.11: (A) Cryo-electron micrograph of vitrified microtubules. *In vitro* polymerization results in a variation in protofilament number (pf). (B) Outside view of a 3-D helical reconstruction rendered Image of the microtubule wall. (C) Inside view of the wall of the same microtubule reconstruction. Orange window is the region of lateral protofilament interaction shown in (D). (B) and (D) were kindly provided by Angelika Krebs. (D) Atomic model of lateral contacts between β -tubulin subunits in two adjacent protofilaments. The main elements forming this interface are the M loop and helix H3 (Nogales *et al.*, 1999), adapted from Nogales, 2001.

2.6.4.4 Protofilament number

When the number of protofilaments in a microtubule is 13, as it generally is in nature (Tilney *et al.*, 1973), the protofilaments are straight (Figure 2.12). *In vitro* polymerized microtubules can exhibit anything between 9 and 16 protofilaments. When the protofilament number is not 13, the lattice has to introduce a slight twist, called a supertwist, to fit all protofilaments with a similar stagger of subunits in the closed cylinder (Figure 2.12), (Wade *et al.*, 1990). This supertwist can be left- or right-handed dependent on protofilament number and is the longest pitched helix in the microtubule geometry. The lateral stagger between the monomers is 0.92 nm, forming a set of helices around the cylinder. In a 13 protofilament microtubule, each subunit helix makes a complete turn over an axial distance of 12 nm. This distance is in fact 1.5 times the tubulin heterodimer length, so this left-handed helix is called a 1.5-start microtubule according to the dimer (Figure 2.12). For smaller or larger number of protofilaments, 1- or 2-start helices (according to the tubulin dimer) might be a more suitable arrangement for the lattice (Wade *et al.*, 1990; Chretien and Wade, 1991). Due to the superposition of the front and the back of the tube, a Moiré pattern occurs in the projection of a microtubule in cryo-

EM. The Moiré pattern has a repeat of the distance of the supertwist turn divided by the protofilament number, and represents one pitch in the supertwist (Mandelkow and Mandelkow, 1985; Mandelkow *et al.*, 1986b). The Moiré pattern for different supertwists and start numbers of microtubules has been characterized. This makes it possible to deduce the polarity of a single microtubule by looking at the Moiré pattern of cryo-EM image (Chretien *et al.*, 1996; Sosa and Chretien, 1998). However, a more reliable way of determining the conformation of a tubulin lattice is to calculate a Fourier transform, which can be visualized as a diffraction pattern of the image. The position of the spots in a diffraction pattern is related to protofilament number, the helix handedness and monomer and dimer arrangements (Amos and Klug, 1974; Song and Mandelkow, 1993).

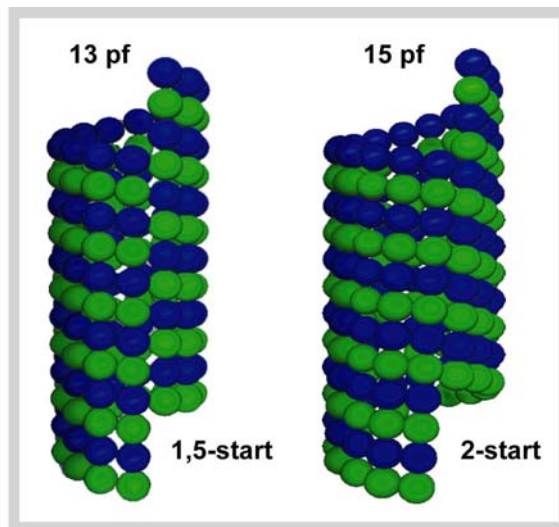


Figure 2.12: Protofilament number in microtubules. When 13 protofilaments (pf) form the cylinder, they run straight, but larger or smaller numbers must wind slowly around the axis if the monomer subunits are to line up correctly at the seam. This supertwist of the protofilaments is most obvious in the 15 protofilament structure. In this lattice, four separate helical lines run through laterally adjacent monomers. For 13 protofilament three shallow helices run in parallel, forming the standard 3-start helix. Perfect helical symmetry (with all lateral interactions alike) is possible for B-lattice microtubules with 15 protofilaments, but a standard 13 protofilament microtubule can only close with a seam in which each α -tubulin monomer makes lateral contact with a β -tubulin subunit (Amos and Schlieper, 2005). Dan Edvardsson contributed to the 3-D model.

The number of protofilaments is to some extent dependent on the polymerization buffer. Of practical importance is that, DMSO increases, high NaCl concentration decreases, and taxol has an influence on the protofilament number in *in vitro* polymerization reactions (Dias and Milligan, 1999; Meurer-Grob *et al.*, 2001).

2.6.4.5 A- and B-lattice

Lateral protofilament interactions occur in two different conformations that are called the A-lattice and B-lattice (Figure 2.13). In an A-lattice, α -tubulin connects laterally to β -tubulin on the neighboring protofilament and theoretically, the A-lattice looks like a malformed chess board. In an B-lattice, α - α and β - β subunits contact laterally, theoretically forming a tilted striped pattern, with a lateral binding angle of approximately 10° (Figure 2.13) (Amos and Klug, 1974). In the same early study by Amos and

Klug, they propose, that the A-tube in the flagellar microtubule doublet exhibits an A-lattice and the B-tube a B-lattice, according to the detected diffraction patterns. However, the difference between α - and β -structure is almost too minute to be detected, but can be enhanced through decoration with kinesin motor domains. The motor domain of a kinesin is globular, easily detectable by EM and binds specifically to the β -tubulin subunits of microtubules. Structural investigations into microtubule-kinesin complexes have revealed a clear dominance of the B-lattice, while A-lattice interactions typically only occur at so-called lattice seams in a single microtubule (Figure 4.8) and at the connections between the A and B tube in a microtubule doublet (Amos and Klug, 1974; Song and Mandelkow, 1993, and 1995).

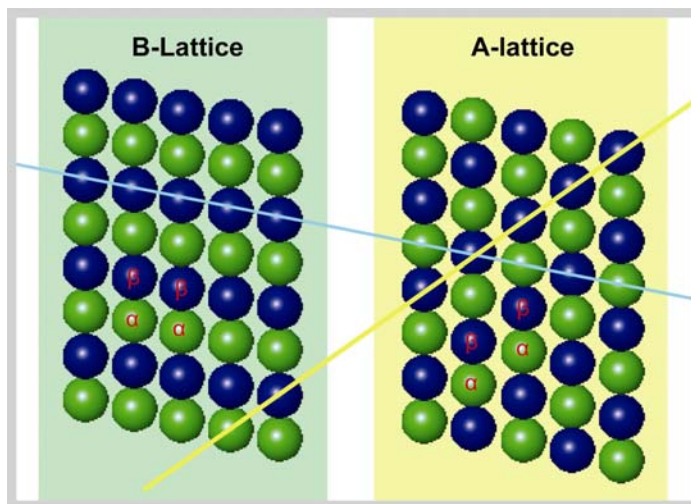


Figure 2.13: A- and B-lattice. In the energetically more stable B-lattice all lateral interactions are between the same subtypes of tubulin. In the A-lattice all lateral interactions are between different subtypes. The lateral stagger between the protofilaments exhibit an inclination of approximately 10° (blue) for a B-lattice and 38° for a A-lattice (yellow).

The M-loop, involved in the lateral subunit interactions between the protofilaments, possesses one of the characteristic structural differences between α - and β -tubulin. In α -tubulin, the M-loop is stabilized by a long S9-S10 loop, which is very small in β -tubulin. This structure leads to an electrostatic difference between the A- and B-lattice. Calculated from molecular models, the lateral bonds in a B-lattice are circa 7 kcal/mol stronger than in an A-lattice, which supports the theory that the B-lattice is the most favorable conformation (Sept *et al.*, 2003; Drabik *et al.*, 2007).

2.6.4.6 The microtubule lattice seam

The B-lattice is the most common arrangement in a microtubule, although A-lattice does occur, and is in fact the conformation of the lattice seam. For microtubules with a certain amount of protofilaments and start number, for example 13 protofilament microtubules, the lattice constraints require a mismatch in order to permit tube formation (Figure 2.12) (Wade *et al.*, 1990; Chretien and Wade, 1991). With freeze-fracture preparations of

microtubule-kinesin complexes, the existence of the seam could be directly visualized (Kikkawa *et al.*, 1994). A back projection approach is also suitable for reconstructing 3-D volumes of microtubule-kinesin complexes. With this method microtubules of different number were reconstructed, showing for example that a 13 protofilament microtubule has one seam or an uneven number of seams (Sosa and Milligan, 1996). Mixed lattices are common, but also B-lattices without a seam are a result of *in vitro* polymerizations, for example a 15 protofilament 2 start microtubule does not have any helical interruptions (Arnal *et al.*, 1996). However, *in vitro*, seams are random and the presence of a seam can never be excluded (Sosa and Milligan, 1996; Dias and Milligan, 1999). It has been suggested that the seam is the last protofilament zipper when the growing plus end sheet is closed to a cylinder (Chretien *et al.*, 1995). The seam must be the weakest part of a microtubule, according to the higher free energy of the A-lattice interaction (Sept *et al.*, 2003). This was further supported by EM images of microtubules with lattice defects in the form of short protofilament openings (Mandelkow *et al.*, 1986a). The microtubule lattice seam is a result of forming a tube with a heterodimeric complex and might be a structural necessity required for proper tube closure. The results of this work will raise new proposals for the significance of the lattice seam.

2.6.5 Microtubule dynamic instability

Microtubules are highly dynamic and can switch stochastically between growth and shrinkage, both *in vivo* and *in vitro*. This non-equilibrium behavior is based on the binding and hydrolysis of GTP, which is functionally linked to microtubule polymerization and depolymerization. The observations of microtubule assembly *in vitro* and *in vivo* resulted in the formulation of the “dynamic instability” model (Mitchison and Kirschner, 1984). This model states that both phases of polymerization and depolymerization are simultaneously persistent, with occasional transitions from one state to the other. The transition from growth to shrinkage is termed a catastrophe and that from shrinking to growth a rescue. Both catastrophe and rescue seem to occur abruptly, infrequently and stochastically.

2.6.5.1 Nucleotide binding and hydrolysis

In a free tubulin dimer the nucleotide binding pocket of β -tubulin, the E-site, is exposed to the surface, allowing for nucleotide exchange. In the presence of GTP, the old GDP is removed, which allows the GTP-tubulin dimers to contribute to polymerization. Tubulin also has a GTPase enzymatic capacity. Subunits that are newly added to the plus end are GTP-bound and form the so called GTP-cap at the plus end (Mitchison and Kirschner,

1984). The GTPase activity of tubulin is enhanced upon binding to a microtubule, so that all subunits except the newly added ones have GDP bound in the E-site. GDP-tubulin accommodates a slightly bent inter-dimer interaction. According to the GTP-cap model, the straight conformation of the plus end subunits is sufficient to prevent bending of the protofilaments (Chretien *et al.*, 1999). If GMPCPP, a non-hydrolysable analog of GTP, is used for *in vitro* polymerization, tubulin still assembles into what looks like normal microtubules, but they are not dynamic. This implies that hydrolysis is not needed for assembly, but rather for the depolymerization of microtubules (Hyman *et al.*, 1992). This led to the hypothesis that microtubules containing GDP-tubulin are intrinsically unstable and that microtubules are protected from catastrophe by the GTP-cap. More recent structural analysis of the structure of tubulin in different nucleotide states showed that hydrolysis affects the conformation of the entire dimer. In helical tubes formed from salt-induced GDP protofilaments, the inter-dimer interface and also the intra-dimer interface bent more than they are in the zink-sheet structure. GDP is proposed to effect T-loop on the opposite side of β -tubulin, which then also alters the inter-dimer interphase (Wang and Nogales, 2005). GDP protofilaments bend with a 12° angle between the subunits but protofilaments in GMPCPP-stabilized sheets bend only 5° . The bending of GMPCPP-stabilized sheets is the same as the bending of GTP-tubulin at polymerizing plus ends. This was it observed *in vitro* with cryo-EM (Chretien *et al.*, 1995; Chretien *et al.*, 1999).

Catastrophe thus occurs at the plus end when nucleotide hydrolysis catches up with polymerization and the microtubule loses its GTP-cap. Consistent with this view, EM pictures of depolymerizing microtubules in frozen hydrated samples showed individual protofilaments curling away from the cylinder, forming circular GDP-rings (Mandelkow and Mandelkow, 1985; Mandelkow *et al.*, 1991; Chretien *et al.*, 1995). *In vitro* the free minus end is also dynamic and at high tubulin concentrations it can polymerize more slowly than the plus end. Interestingly, the minus end does not depolymerize as fast as an un-capped plus end. The explanation could be that a GTP is bound to the N-site (non-hydrolyzable) at the intra-dimer interface. This makes the last subunit straight, with a strong interaction between the terminal α -subunits (Tran *et al.*, 1997).

Taken together, the current model suggests that microtubules consume energy from GTP hydrolysis to maintain a state of dynamic instability.

2.7 Drugs affecting microtubule stability

The role of microtubules for chromosome segregation of the duplicated genome before cell division makes microtubules a perfect target for anti-mitotic drugs. Microtubules are especially dynamic during mitosis, and mitosis is uncontrolled and fast in tumor growth. Microtubule affecting drugs are important in cancer treatments. The number of discovered microtubule influencing drugs is increasing. In general, there are two classes of natural toxins affecting microtubules: stabilizing and destabilizing. Here we only present classical and drug “tools” useful in molecular biology, principally representing the mechanisms used by various drugs.

2.7.1 Destabilizing drugs

Microtubule destabilizing drugs usually bind tubulin in a curved conformation, inhibiting the longitudinal association into straight protofilaments and thus into tubes. The drug colchicine from meadow saffron, for example, binds β -tubulin close to the intra-dimer interface. In this location colchicine induces a bending distortion to the heterodimer, preventing it from establishing lateral contacts in the microtubule lattice (Ravelli *et al.*, 2004). In contrast, vinblastine binds to a region that forms the longitudinal contact between the tubulin dimers. This forces the protofilament into a tightly wound spiral and induces depolymerization (Gigant *et al.*, 2005). These drugs were co-crystallized with a tubulin-stathmin complex, visualized in figure 2.10B.

2.7.2 Stabilizing drugs

A second class of toxins promotes polymerization (Schiff *et al.*, 1979) and inhibits microtubule dynamics through stabilization. Taxol was discovered in the bark of the Pacific yew tree (Wani *et al.*, 1971). The drug binds to the inside of the microtubules (Figure 2.10A) and is thought to strengthen lateral contacts between subunits, thereby helping to maintain a straight, tubular conformation. Taxol provides structural stability to the M-loop, which tightens contact to the H1-S2 loop on the neighboring subunit. In addition, taxol has a strong allosteric effect on α -tubulin, causing slight lateral compression and longitudinal straightening (Andreu *et al.*, 1994; Xiao *et al.*, 2006). Taxol is a frequently used stabilizer in our *in vitro* studies, allowing work on microtubule structure in a polymerized state at low tubulin concentrations.

2.8 Microtubule associated proteins (MAPs)

The dynamic properties of a microtubule are central to its functions. In a cell approximately 50% of the cellular tubulin is polymerized and 50% is in an unpolymerized

dimeric form. Once a microtubule is nucleated this balance is mainly controlled by MAPs. They alter the rates of subunit polymerization and catastrophe, and mediate interactions with other cellular components. They can act globally, e.g. in response to regulatory signals during the cell cycle or locally to alter microtubule dynamics at specific locations inside the cell. MAPs are the actors carrying out the orders directed from protein signaling cascades, in other words, rearranging the cytoskeleton according to the cellular needs. This family of proteins has no common structure or mechanism, the only thing MAPs have in common is their interaction with microtubules, somewhere on the polymer. MAPs control microtubule dynamics through stabilization and destabilization, promoting polymerization or depolymerization and acting along the lattice or only at one or both ends (Cassimeris, 1999; Howard and Hyman, 2007).

2.8.1 Microtubule associated motors proteins

Molecular motors use the energy gained from hydrolysis of ATP to carry out mechanical work, generally in the form of movement along microtubules. Their cellular obligations can be divided into three major categories. Primarily, they transport cargoes like organelles, vesicles, proteins or mRNA along microtubules to specific locations inside the cell (Figure 2.14A), (Vale, 2003). Secondly, they move and organize microtubules relative to each other or relative to other organelles (Bartolini and Gundersen, 2006). The sliding of microtubules along each other furthermore generates the movements of flagella and cilia (Gibbons, 1981). The third function of motors is to destabilize microtubule plus ends (Moores and Milligan, 2006). In some cases destabilizing motors are also thought to generate movements, for example, during the segregation of chromosomes in the mitotic spindle (Westermann *et al.*, 2006).

On the polar microtubules, different types of motors move in different directions along the lattice (Figure 2.14A), facilitating directional cargo delivery. There are two major classes of microtubule associated motors, kinesins and dyneins (Vale, 2003). The architecture of the two motor proteins is completely different. However, the kinesin motor domain and the dynein stalk head both bind in a stoichiometry of one protein head per tubulin dimer. This means in an 8 nm repeat in the axial direction (Song and Mandelkow, 1993; Mizuno *et al.*, 2004). Cryo-EM and 3-D helical reconstruction of microtubule motor/dynein stalk head complexes show that both proteins interact with the C-terminal surface of β -tubulin, mainly with α -helix H12 (Mizuno *et al.*, 2004). This implies that the different motors compete for the same binding site, but whether this has a cellular consequence is unknown.

2.8.1.1 Dynein

Dyneins occur either in the cytoplasm, were together with dynactin they generally mediates minus end directed transport along microtubules (Pfister *et al.*, 2005); or within the integral structure of axonemes (Figure 2.7B), were they generate the forces that drive flagellar beating (Gibbons, 1981; Nicastro *et al.*, 2005). The 1.2 MDa large cytoplasmic dynein forms homodimers and is exists in a dimeric form, generally moving with 8 nm steps (Reck-Peterson *et al.*, 2006). The globular microtubule binding domain is connected via a stalk, an intramolecular coiled-coil, to the ring shaped motor domain, as observed by electron microscopy (Samso *et al.*, 1998; Burgess *et al.*, 2003). An N-terminal stem is responsible for dimerization and cargo binding. The ring shaped motor domain contains six AAA domains (ATPase associated with various cellular activities). Only the first AAA domain exhibits measurable ATPase activity; the next three AAA domains are thought to regulate dynein activity. ATP hydrolysis in the AAA domain ring induces a conformational change, which involves a change in the angle of the stalk compared to the stem. This may represent the mechanism of dyneins power stroke (Burgess *et al.*, 2003).

The cytoplasmatic dyneins interact with several tightly linked subunits, called intermediate chains. The intermediate chains link dynein to p150^{Glued}, a subunit of the dynactin complex. The dynein/dynactin complex functions as a microtubule +TIPs (see section 2.8.4). At the microtubule plus end it acts as a cross-linker for other MAPs, but also to membranes (Vale, 2003). Membrane-bound dynein/dynactin can trap microtubule plus ends at specific membrane regions, and so optimize directed vesicle transport (Shaw *et al.*, 2007). Another proposed mechanism is that membrane attachments provide an anchor to allow generation of pulling forces on astral microtubules, driven by dynein minus end directed motor activity (Yeh *et al.*, 2000). This is important for spindle positioning during mitosis for example.

2.8.1.2 Kinesin

The kinesin superfamily is a large and heterogeneous group of motor proteins. A new systematic nomenclature divided them in to 14 different families of kinesis (Lawrence *et al.*, 2004; Miki *et al.*, 2005). Kinesins have a conserved globular motor domain, normally 35 kDa large, generally followed by a flexible neck region, a coiled-coil involved in oligomerisation and ending with a tail region, involved in cargo binding. Kinesins appear as monomers, homo- or hetrodimers or tetramers. However, according to their structure and the intramolecular localization of the catalytic motor domain, kinesins can be divided in three main groups (Marx *et al.*, 2005). N-type kinesins, including the so called

conventional kinesins, have an N-terminal motor domain, and have plus end directed motility. C-type kinesins contain their motor domain at the C-terminus and move towards the minus end of microtubules. The last group is kinesins with a central motor domain, which are named M-type or Kin I, some but not all of which are shown to function as depolymerizing machines (see section 2.8.3.3).

Conventional kinesin is shown to bind to microtubules at a stoichiometry of one kinesin head per tubulin dimer, along the direction of the protofilament (Hoenger *et al.*, 1998; Thormahlen *et al.*, 1998; Skiniotis *et al.*, 2003). Chemical cross-linking and 3-D helical reconstructions of microtubule motor complexes show that the motor head interacts mainly with β -tubulin (Song and Mandelkow, 1993; Thormahlen *et al.*, 1998). The interaction between microtubules and a kinesin motor domain involves two-way communication. The microtubule-kinesin interaction induces a conformational change in the kinesin's nucleotide binding pocket, which stimulates the ATPase activity of the motor domain (Gilbert *et al.*, 1995). In turn, hydrolysis of ATP causes further conformational changes in the microtubule binding region so that kinesin has an altered binding affinity in the presence of ADP (Woehlke *et al.*, 1997). 3-D helical reconstruction comparing un-decorated and kinesin decorated microtubules show that the conformation of tubulin also changes upon interaction with kinesin (Krebs *et al.*, 2004). Taken together these conformational changes contribute to kinesins power stroke.

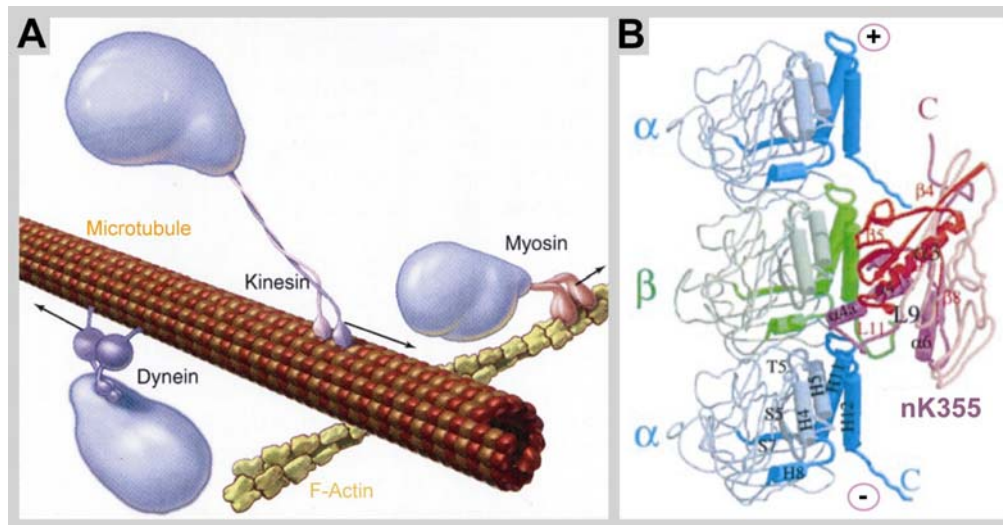


Figure 2.14: Motor proteins use the cytoskeleton among other functions for intracellular transport of vesicles. (A) Dynein is a minus end directed motor and kinesin is generally a plus end directed motor; both walk along microtubules. Myosin interacts with actin. The figure is adapted from Pollard and Earnshaw, 2002. (B) Kinesin motor domains use the C-terminal helices H11 and H12 and the acidic flexible tail of β -tubulin (green) to interact with the outside surface of microtubules. Atomic structure adapted from Song *et al.*, 2001.

Some kinesins move processively along microtubules in a hand-over-hand mechanism (Hoenger *et al.*, 2000b; Yildiz and Selvin, 2005), while others are thought to undergo one-dimensional diffusion along the microtubule lattice (Helenius *et al.*, 2006). As mentioned above, they can move directionally towards either end of a microtubule to transport cargoes or to organize microtubules, or they influence microtubule dynamics by destabilizing their plus ends. Several types of kinesins play an important role in the establishment of the mitotic spindle. Plus end directed tetrameric and bipolar motors like Kinesin 5 contain four motor domains and were proposed to cross-link antiparallel microtubules and use their processivity to push the spindle microtubules apart. (Sawin *et al.*, 1992; Kapitein *et al.*, 2005). This drives the organizational changes during mitosis.

The fission yeast kinesin Tea2p, is a M-type kinesin and was shown to be a plus end directed motor. However, it is also involved in the regulation of microtubule dynamics, since cells lacking Tea2p exhibit short microtubules and altered cell polarity (Browning *et al.*, 2003). The +TIP Mal3p regulates microtubule binding and stimulates the ATPase activity of Tea2p (Busch *et al.*, 2004; Browning and Hackney, 2005). In return, Tea2p transports Mal3p and other plus end binding MAPs along polymerizing microtubule plus ends (Busch *et al.*, 2004). Hence motor proteins and MAPs are interacting in a microtubule plus end network, where all components profit from each other.

2.8.2 Microtubule stabilizing proteins

In interphase microtubules are long and stable. The stability is provided by MAPs without the need for abandoning microtubule dynamics. The classical stabilizing MAPs tend to have repeating domains, which allow each molecule to associate with more than one tubulin heterodimer. With this mechanism they control microtubules in two ways; first their binding to tubulin stabilizes the straight conformation of dimer subunits, second they cross-link straight dimers and trap the subunits in the polymer lattice. The binding of the structurally stabilizing MAPs is in turn regulated by phosphorylation, in many cases regional located kinases and phosphatases control MAPs locally (Amos and Schlieper, 2005). This is a large family of MAPs; many MAPs are expressed cell specifically, here we only present a selected repertoire of well characterized classical MAPs, representing different stabilizing mechanisms.

2.8.2.1 Tau family

Tau family proteins stabilize the straight conformation of the protofilaments. One molecule can cross-link four or more dimers and the N-terminal region extends from the

microtubule surface and repels neighboring microtubules, thus defining the distance between microtubules in a bundle. Tau and MAP2 are found in neurons, where MAP2 specifically stabilizes microtubules in dendrites but Tau is active only in the axon. In non-neural cells a larger homolog MAP4 stabilizes microtubules in a similar way (Drewes *et al.*, 1998; Garcia and Cleveland, 2001). Phosphorylation of Tau family proteins induces dissociation from microtubules (Ebner *et al.*, 1999). However, hyperphosphorylation and specific mutations of Tau can promote its aggregation into helical amyloid filaments which are thought to be involved in neurodegenerative diseases such as Alzheimer's disease (Crowther and Goedert, 2000; von Bergen *et al.*, 2006).

Tau and its homologs are heat stable and lack detectable secondary structure, however the complex of microtubule bound Tau/MAP2 structure and the microtubule binding properties has been extensively studied with cryo-EM and 3-D helical reconstruction and high-resolution shadowing EM (Al-Bassam *et al.*, 2002; Santarella *et al.*, 2004). The N-terminus is acidic and extends far out from the microtubule surface and cannot be detected in a structure average. A central proline rich central region and four conserved C-terminal repeats bind tightly to the microtubule. The Tau repeats and also the inter-repeats bind along or cross-link the protofilaments and associates with the tubulin surface at α - and β -tubulin C-terminal helices H11 and H12, with the strongest 8 nm repeating density on α -tubulin. On the microtubule surface Tau competes for binding to microtubules with kinesin. Overexpression of Tau consequently inhibits the trafficking along microtubules (Ebner *et al.*, 1998).

2.8.2.2 XMAP215 family

XMAP215-family proteins are microtubule stabilizers because these proteins shift the equilibrium to a polymerized tubulin conformation, but at the same time they are dynamic enhancers. Close homologs of this protein family are found in many organisms, for example XMAP215 in *Xenopus*, TOGp in humans, and the two paralogs Alp14p and Dis1p in fission yeast. XMAP215 enhances microtubule plus end growth rate and increases the total microtubule length. Through the cell cycle its activity is strictly regulated by phosphorylation, allowing the microtubules to undergo catastrophe and to build up the mitotic spindle. EM data showed that XMAP215 is an elongated flexible molecule. In the cold, one XMAP215 can associate with 8 tubulin dimers (Cassimeris *et al.*, 2001). The structure is built up of HEAT repeats. Each HEAT motif is a curved row of α -helices. It has been proposed that XMAP215 enhances the addition and removal

of tubulin subunits at the microtubule plus end through cross-linking the subunits in short oligomers (Kerssemakers *et al.*, 2006).

2.8.2.3 Doublecortin

Doublecortin (DCX) is essential for neural migration during development, and according to its name, mutations leads to disorders in human cerebral cortex formation. Like many MAPs, DCX is a tubulin stabilizer and bundler (Horesh *et al.*, 1999). *In vitro* DCX works as a nucleator, decreasing the critical concentration for nucleation. The molecular structure is not an extended filament like Tau and XMAP215, the organization is more similar to the +TIP subfamily of MAPs (see section 2.8.4). DCX exhibits two repeated globular domains, of these only the N-terminal domain bind to microtubules (Kim *et al.*, 2003). DCX is one of few MAPs analyzed by cryo-EM and 3-D helical reconstruction. The reconstruction reveals a binding site for the N-terminal globular domain in between the protofilaments, cross-linking the protofilaments with an 8 nm repeating pattern. However, DCX binds preferentially to microtubules with 13 protofilaments, and weakly to 14 protofilaments (Moore *et al.*, 2004), this reveals another mechanism for regulation of the protofilament number in microtubules.

2.8.3 Microtubule destabilizing proteins

At the transition from interphase to mitosis, the catastrophe rate increases globally. This change is regulated through dissociation of stabilizing MAPs from the microtubules, often mediated by phosphorylation, this results in activation of destabilizing MAPs. Also, during mitosis microtubules are more dynamic and the mitotic processes are regulated through activation and deactivation of stabilizers and destabilizers. For example, during late anaphase microtubules are more sensitive to destabilizers; this is crucial for chromosome segregation. One of the processes going on in the spindle at this phase is depolymerization of the kinetochore-attached microtubules. Through regulated depolymerization chromosomes are pulled apart towards the spindle poles.

2.8.3.1 Stathmin

The microtubule destabilizer stathmin is also called Op18, for oncoprotein 18. The name Op18 reflects the association of this MAP with several types of cancer. One stathmin molecule forms a complex with two tubulin dimers in a curved conformation (see section 2.6.4.2; Figure 2.10B). (Gigant *et al.*, 2000; Ravelli *et al.*, 2004). Two different mechanisms for stathmin destabilization of microtubules have been identified *in vitro*. It either sequesters subunits or stimulates microtubule catastrophes. Sequestering of

subunits results in a decrease of the free tubulin concentration and therefore has a dual effect on microtubule dynamics; it slows down growth and increases the catastrophe rate at both ends (Cassimeris, 2002). The microtubule affinity of stathmin is reduced by phosphorylation of four serine residues. This deactivation is necessary to build up the mitotic spindle or to locally extend microtubules in the leading edge of a migrating cell (Wittmann *et al.*, 2004). Dephosphorylation leads to reactivation and is essential for entry into mitosis and continuation the cell cycle (Marklund *et al.*, 1996).

2.8.3.2 Katanin and Spastin

Katanin and Spastin belong to the AAA protein superfamily (like dynein, section 2.8.1.1) and are specialized in microtubule severing in the middle of the lattice. The effect is quick formation of new ends and creation new microtubules without involving γ -tubulin in this process. The hexameric ring complex binds ATP and recognizes the C-terminal tail of β -tubulin by the central pore. Another domain of the complex is proposed to exert a force on tubulin, leading to a conformational change in the tubulin heterodimer, which ends with release of tubulin from the microtubule (White *et al.*, 2007). Electron tomography studies reveal that that the meiotic spindle in *C. elegans* requires microtubule severing by Katanin around the chromatin. Short microtubule fragment are stabilized and can elongate to form a bipolar spindle (Lu *et al.*, 2004).

2.8.3.3 Kinesin-13

Members of the kinesin-13 (or Kin1) subfamily of the kinesins (see section 2.8.1.2) do not move along the microtubules, instead, they use energy in the form of ATP to depolymerize microtubules at their ends. Kinesin-13 members participate in many mitotic processes, for example Kin1 has been intensively studied with EM. 3-D helical reconstruction of a Kin1-microtubule complex in different nucleotide conformations tells us more about the destabilizing mechanism. Kin1 uses ATP to bend the tubulin heterodimers, forcing the bound heterodimer to dissociate from the polymer. The ATPase activity is enhanced first when Kin1 binds strongly to a bent tubulin dimer, since Kin1 exhibits a more curved tubulin binding surface than conventional kinesins do (Moores *et al.*, 2003).

Other depolymerizing kinesins like *Drosophila* KLP10A and KLP95C affect interphase microtubule plus ends. These destabilizers are dependent upon the +TIP EB1 to associate with microtubules and become active only after EB1 is removed from the microtubule plus end (Mennella *et al.*, 2005). The crystal structure of the kinesin-13 family member

KIF2C demonstrated that the N-terminal of the protein is large, ridged and inhibits binding to the microtubule lattice. At the depolymerizing ends of the microtubule, protofilaments flare apart and allow KIF2C binding, which enhances depolymerization (Ogawa *et al.*, 2004). Further, it has been shown that the linker and N-terminal domain is involved in oligomerization into rings and spirals of kinesins in complex with curled tubulin protofilaments (Moore *et al.*, 2006; Tan *et al.*, 2006), this traps many destabilizing subunits at the microtubule ends and makes depolymerization a cooperative process.

2.8.4 Microtubule plus end tracking proteins (+TIPs)

A special class of MAPs accumulate specifically at microtubule plus ends and for that reason are termed +TIPs (Schuyler and Pellman, 2001). In general, +TIPs are involved in a diverse set of functions which include the targeting and anchoring of specific cellular structures by microtubules, the recruiting of protein complexes to microtubule plus ends and their delivery to the cell periphery, and most importantly, the regulation of plus end dynamics (Carvalho *et al.*, 2003; Akhmanova and Hoogenraad, 2005; Vaughan, 2005).

The first +TIP discovered was the cytoplasmic linker protein 170 (CLIP-170), found as a linker of endocytic vesicles to microtubules (Rickard and Kreis, 1990). It was later shown to localize to growing microtubule plus ends with a stabilizing effect (Perez *et al.*, 1999) and to contribute to the microtubule plus end interactions with the kinetochores in the mitotic spindle (Dujardin *et al.*, 1998). Apart from regulating microtubule dynamics, CLIPs are involved in many processes mediated by their interaction with other MAPs. The most important are the CLASPs, p150^{Glued} as a part of the dynactin complex and the protein LIS1 (Akhmanova and Hoogenraad, 2005; Galjart, 2005). CLASPs (CLIP associated proteins) were identified through their interaction with CLIP-170 family members (Akhmanova *et al.*, 2001). In contrast to CLIP-170, which is found on all microtubule plus ends CLASPs are thought to be specialized regulators of microtubule dynamics and +TIPs interactions for certain tissues or regions in the cell, for example at the leading edge of motile cells (Galjart, 2005). Through activation of CLASP in axons, microtubule assembly is suppressed (Lee *et al.*, 2004). The protein p150^{Glued}, also called the dynactin complex heavy chain, facilitates CLIP-170 binding to the motor protein dynein and its associated cargoes vesicles to the plus ends, but it also guides microtubules to specific membrane connections (Vaughan *et al.*, 1999; Wittmann and Desai, 2005). +TIPs are often involved in the “search and capture” processes (also described for microtubule capture of kinetochores). For example, the +TIP p150^{Glued} physically

interacts with membrane proteins, like N-cadherin and β -catenin to facilitate a direct delivery of membrane proteins needed in adherens junctions (Shaw *et al.*, 2007).

At the same time many different proteins seems to be present at a microtubule plus end and observations that +TIPs interact with each other are extensive. One core component at the plus end is EB1, which directly or indirectly interacts with almost all other described +TIPs (Morrison, 2007). In Humans the EB1 family has 3 paralogs, EB1, EB2 also called RP1, and EB3 (Juwana *et al.*, 1999; Su and Qi, 2001). Homologs of this conserved family are present in all eukaryotes, for example Mal3p in fission yeast (Beinhauer *et al.*, 1997). The members of the EB1 protein family were described to promote microtubule growth (Tirnauer *et al.*, 2002b; Busch and Brunner, 2004) and are also responsible for recruitment of other protein complexes, both MAPs and motor proteins, to the plus ends (Busch *et al.*, 2004; Mennella *et al.*, 2005; Slep *et al.*, 2005).

EB1 was initially identified in a yeast-2-hybrid screen for proteins that interact with adenomatous polyposis coli (APC) (Su *et al.*, 1995). APC is a +TIP originally shown to be a human tumor suppressor protein (Smits *et al.*, 1999; Green and Kaplan, 2003). It is an important adapter from cell signaling to the organization of the cytoskeleton. APC microtubule interaction and activity as a plus end stabilizer is regulated by EB1 and motor proteins (Askham *et al.*, 2000; Mimori-Kiyosue *et al.*, 2000; Jimbo *et al.*, 2002). Nevertheless, APC also interacts independently with microtubules and actin (Langford *et al.*, 2006).

The list of +TIPs is even more extensive, see recent reviews for a more comprehensive list (Carvalho *et al.*, 2003; Akhmanova and Hoogenraad, 2005). Of all the above presented proteins the EB1 family, CLIPs and p150^{Glued} are found on all growing microtubules and have the best claim to be the core component of +TIP complexes.

2.8.4.1 Mechanisms of plus end tracking

The plus end tracking of +TIPs is observed as comets of staining moving along the microtubule plus end when the proteins are fluorescently labeled, e.g. with GFP (Perez *et al.*, 1999). Remarkably, the mechanism underlying plus end tracking is still poorly defined. Three major models describing and explaining this process have been proposed: treadmilling together with microtubule polymerization, hitchhiking on other microtubule binding proteins and transport by plus end directed motor proteins (Carvalho *et al.*, 2003; Morrison, 2007). Treadmilling of +TIPs involves the recognition of specific features of

growing microtubule plus ends and subsequent release from older parts of the filaments. As long as the microtubule is polymerizing, new or recycled +TIPs are constantly recruited, thereby forming the typical comet-like structure. The plus end tracking comet is, according to this model, an optical illusion, although individual +TIPs bind in a stationary manner to tubulin, the population of proteins appears to “surf” on a growing plus end (Galjart and Perez, 2003). In theory this model is very realistic, but the specific feature that enhances the affinity at the plus end is a critical point, and might vary for different +TIPs.

One possibility is that +TIPs possess a high affinity for the specific conformation of GTP-tubulin that is the straight conformation of the plus end cap. When tubulin hydrolyzes GTP to GDP, +TIPs might dissociate. Budding yeast kinetochores prefer to bind to GMPCPP (Severin *et al.*, 1997), a GTP homolog, microtubules *in vitro*, but no +TIPs have been shown to bind along an entire lattice of GMPCPP microtubules (for example not Mal3p, our unpublished data) and CLIP-170 and p150^{Glued} did not appear to have enhanced affinity for GTP-bound tubulin relative to GDP, arguing against a GTP-cap interaction (Diamantopoulos *et al.*, 1999; Vaughan *et al.*, 2002). Selective plus end accumulation can also be due to the protein binding to free tubulin subunits and subsequent co-polymerization. Indeed, sedimentation velocity experiments suggest that CLIP-170 binds to unpolymerized tubulin and promotes the formation of tubulin oligomers (Diamantopoulos *et al.*, 1999). EM of *in vitro* polymerizing microtubules show that CLIP-170 binds to short tubulin protofilaments and co-assembles with microtubules, enhancing the polymerization rate (Arnal *et al.*, 2004). However, co-polymerization would only produce selectively plus end accumulation if it was coupled to the rapid release from the microtubule wall. Early studies suggest that phosphorylation might be an important mechanism to generate rapid dissociation of CLIP-170, and phosphorylation by the kinase mTOR diminishes CLIP-170 binding to the microtubules (Choi *et al.*, 2002). CLIP-170 has the flexibility to change between an open microtubule binding structure and a close self-inhibiting conformation (Lansbergen *et al.*, 2004). There is however, no experimental evidence that phosphorylation and self-inhibition are intermediates in the treadmilling cycle.

EB1 treadmills with the growing plus ends without binding to free tubulin dimers before polymerization (Tirnauer *et al.*, 2002b; Gache *et al.*, 2005). A second, not obviously treadmilling, population of EB1 binds along microtubule walls. Fluorescence recovery after photobleaching (FRAP) of EB1 and the fission yeast homolog Mal3p show

that the association and disassociation rates are similar along the microtubule wall and on the microtubule ends (Tirnauer *et al.*, 2002b; Busch *et al.*, 2004). These observations point towards the same binding mechanism for both binding patterns, but it does not explain why the affinity is higher for tubulin at the microtubule plus end.

The other two mechanisms are hitchhiking for proteins that bind to the microtubule via other +TIPs like for example CLASP, and the transport of +TIPs by plus ends directed motor proteins. Often, these mechanisms cannot clearly be separated, for example in the case of Tip1p, the fission yeast homolog of CLIP-170, which is transported towards microtubule plus ends via the motor Tea2p, but can also bind to microtubules via the EB1 homolog Mal3p. A deletion of Mal3p also removes Tip1 from the plus ends (Busch and Brunner, 2004). Hitchhiking was proposed for APC, because the EB1-binding domain of APC is sufficient for functional plus end tacking. Without the EB1-binding domain APC binds via the microtubule binding domain along the entire microtubule (Askham *et al.*, 2000). In a different approach APC plus end localization is ATP dependent and transport driven by KIF3 kinesin along the growing plus end was suggested as an alternative mechanism (Jimbo *et al.*, 2002).

So far, most of our knowledge about plus end tracking comes from cellular observations and extract experiments. Most likely +TIPs associate with the microtubule plus end by multiple mechanisms. *In vivo* the separate mechanisms are difficult to elucidate, because most +TIPs have several interaction partners. One *in vitro* approach, based on recombinant protein and taxol-stabilized microtubules, could confirm that CLIP-170 associates with microtubules via co-polymerization. EB1 does not co-polymerize and rather binds randomly to microtubules after polymerization. However, if both CLIP-170 and EB1 co-polymerize with microtubules, these two proteins bind at the plus end together. In this experiment only the double CAP-Gly domain (N-terminal domains) of CLIP-170 was used (Ligon *et al.*, 2006). More *in vitro* studies are necessary to explain these mechanisms satisfactorily.

2.8.4.2 +TIPs are not only found at the microtubule plus end

+TIPs often exhibit multiple microtubule binding patterns. EB1 shows a high affinity for the plus end and at the same time a low, but detectable binding affinity for the entire microtubule (Mimori-Kiyosue *et al.*, 2000; Tirnauer *et al.*, 2002b; Busch *et al.*, 2004). In over-expression experiments the same intensity of +TIPs are found along the entire microtubule (Schwartz *et al.*, 1997; Ligon *et al.*, 2003) and CLIP-170 bundles cellular

microtubules (Pierre *et al.*, 1992). In yeast, over-expression causes abnormal cell morphology and inhibits cell growth (Beinhauer *et al.*, 1997). At MTOCs, where the minus ends of the microtubules are trapped, some +TIPs also accumulate, for example EB1, APC and p150^{Glued} are involved in microtubule nucleation and anchoring at the centrosome (Chen *et al.*, 2000; Askham *et al.*, 2002; Tirnauer *et al.*, 2002a; Louie *et al.*, 2004). In contrast, other studies show that +TIP localization at MTOCs is independent of microtubules, since it was not abolished by treatment with microtubule depolymerizing drugs (Rehberg and Graf, 2002).

2.8.4.3 The CLIP-170 protein family

As described above, CLIP-170 was first identified as a microtubule associated protein with a molecular weight of 170 kDa (Rickard and Kreis, 1990). The protein consists of two similar N-terminal CAP-Gly motifs and two metal binding motifs at the C-terminus. The central region of the protein forms a coiled-coil, which allows CLIP-170 to form a homodimeric molecule. The CAP-Gly domains are responsible for microtubule binding (Pierre *et al.*, 1992; Pierre *et al.*, 1994), while the metal binding motifs are used to bind other proteins like p150^{Glued} or LIS1. Studies using atomic force microscopy and FRET (fluorescence resonance energy transfer) furthermore indicated that the CAP-Gly associates with the first metal binding motif of the CLIP-170 C-terminus, thereby folding the protein back on itself (Lansbergen *et al.*, 2004). This intramolecular interaction is thought to interfere with the binding of CLIP-170 to microtubule tips, as well as to p150^{Glued} and LIS1, and its regulation might allow the cell to locally activate or inactivate CLIP-170 function.

An equal CAP-Gly domain folding, for which the crystal structure is characterized (Li *et al.*, 2002b), makes up a functional region of p150^{Glued} and the neural CLIP-115, but only in a single copy per peptide. Puzzling in the +TIP interaction networks is that the CAP-Gly domain has the capacity to interact with microtubules as well as other +TIPs. The CAP-Gly domains constitute the major connection motifs among the +TIPs (Hayashi *et al.*, 2005; Honnappa *et al.*, 2006).

The budding and fission yeast CLIP-170 homologs, Bik1 and Tip1p respectively, also have only one CAP-Gly domain and one metal binding region per monomer (Brunner and Nurse, 2000). Tip1p specifically prevents catastrophes of microtubules that touch the cortex in central regions of the cell, and allows them to reach the cell poles, where Tip1p is an important linker molecule in the establishment of cell polarity (Brunner and Nurse,

2000). Deletion of Tip1p results in premature catastrophes of microtubules that touch the central cortex. Careful analysis in living yeast cells revealed that Bik1 and Tip1p are transported towards the plus ends by the kinesins Kip2 and Tea2p respectively (Busch *et al.*, 2004; Carvalho *et al.*, 2004). Interestingly, the accumulation of Tip1p at the microtubule plus ends in *S. pombe* furthermore depends on its binding to Mal3p, the fission yeast homolog of EB1. Deletion of Mal3p also removes Tip1p from the plus ends (Busch and Brunner, 2004), while the presence of Bik1 at the microtubule plus end in budding yeast does not require the EB1 homolog Bim1.

2.8.4.4 Structure of EB1 family proteins

Members of the EB1 protein family are highly conserved in eukaryotes and have a common domain structure in a homodimeric complex. The protein contains an N-terminal calponin homology domain (CH-domain) that is linked via a flexible stretch of approximately 50 amino acid residues to the so called EB1 domain, which mediates homodimerization via a coiled-coil interaction. The last residues of the C-terminal consist of another flexible stretch of amino acids with an overall negative charge (Figure 5.1). The globular N-terminal domain, for which a crystal structure is known, interacts with microtubules (Bu and Su, 2003; Hayashi and Ikura, 2003). CH-domains were identified in a variety of proteins ranging from actin cross-linkers to signaling proteins (Gimona *et al.*, 2002). The CH-domain of EB1 contains a highly basic area between amino acid 55 and 102, which is predicted to form the interface with the acidic surface of the microtubules. N-terminal residues on the opposite side of the globular domain are predicted to be phosphorylated and might regulate EB1 activity in a cell cycle dependent manner (Hayashi *et al.*, 2005). The analysis of the crystal structure of the C-terminal EB1-domain indicated that EB1 family proteins form a stable dimer with a four helix bundled coiled-coil, and that dimerization is essential for the formation of the C-terminal EB1 domain (Honnappa *et al.*, 2005; Slep *et al.*, 2005). The EB1-domain is responsible for the binding of several interacting proteins such as APC and p150^{Glued} (Bu and Su, 2003; Honnappa *et al.*, 2005). The corresponding domain of fission yeast Mal3p is responsible for the interaction with Tip1p and Tea2p (Busch and Brunner, 2004; Busch *et al.*, 2004). Although the very C-terminal amino acid stretch of EB1 is unfolded and flexible, a structural analysis was possible in a complex with the CAP-Gly domain of p150^{Glued}, because the interaction stabilizes the acidic tail. The C-terminal α -helices interact with the β 2- β 3 loop of the CAP-Gly domain, trapping the conserved EEY/F-COO⁻ sequence of EB1 (Hayashi *et al.*, 2005; Honnappa *et al.*, 2006). These findings suggest that the CAP-Gly domain serves as a recognition domain for the EEY/F-COO⁻

motif, which is a characteristic sequence in EB1, CLIP-170 and α -tubulin. The C-terminus thus represents an important link for the +TIP network (Honnappa *et al.*, 2006).

EB1 activity might be regulated through a self-inhibition mechanism, involving the C-terminus, which might be relaxed by CAP-Gly domain binding. Evidence for this comes from the finding that the weak microtubule growth promoting activity of recombinant EB1 is considerably enhanced in the presence of p150^{Glued}. Also consistent with this, a C-terminally truncated recombinant EB1 that is unable to bind p150^{Glued}, exhibits an even stronger polymerizing effect on microtubules *in vitro* (Hayashi *et al.*, 2005).

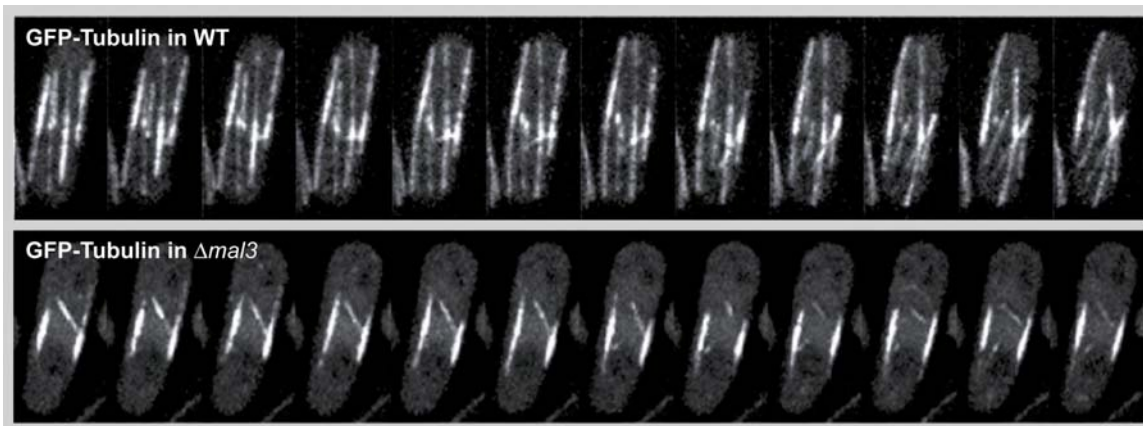


Figure 2.15: Fission yeast *in vivo* microtubule dynamics. Movie sequences of cells expressing GFP-tubulin. In a Wild type (WT) cell the microtubule grow and become arranged parallel to the cell axis until they reach the cell poles. After a period of pausing, the microtubules depolymerize and the polar cortex interactions are taken over by new microtubules. In a *mal3* deleted cell microtubules undergo catastrophe in the cytoplasm and are never able to interact with the cortex at the cell poles, which is a fundamental process for fission yeast polarization. Images adapted from Busch and Brunner, 2004.

2.8.4.5 Function of EB1 Protein Family members

EB1 proteins are found to associate with microtubules through all stages of the cell cycle (Morrison *et al.*, 1998). While some EB1 binds along the whole length of a microtubule, it is mostly concentrated in comet like structures at the tips of growing microtubule plus ends. However, differences in binding exist between different cell types. In budding yeast the EB1 homolog Bim1 decorates the entire microtubule cytoskeleton when the protein is over-expressed (Schwartz *et al.*, 1997). At endogenous levels however, it was only detectable at microtubule plus ends and at the SPB (Tirnauer *et al.*, 1999). Similar results were obtained in human cells (Morrison *et al.*, 1998) and fission yeast (Busch and Brunner, 2004). A cell cycle variation was observed in *Xenopus* egg extracts. In

interphasic extracts EB1 was present all along the microtubule lattice even at low expression levels, while it formed comets at the microtubule plus ends in mitotic extracts. Live imaging of individual microtubules revealed that addition of EB1 did not affect polymerization rates in mitotic extracts, whereas in interphase they were increased (Tirnauer *et al.*, 2002b). Similar results were obtained for the EB1 homolog Bim1 in budding yeast, where the effect of Bim1 deletion is especially prominent in G1 phase. In Bim1 deleted cells, microtubules were shorter overall and less dynamic due to reduced growth and shrinkage velocities and lower catastrophe and rescue rates (Tirnauer *et al.*, 1999). In fission yeast, the deletion of *Mal3* reduced microtubule growth and shrinkage only little, while the catastrophe rate was greatly increased (Figure 2.15), (Busch and Brunner, 2004). Interestingly, human EB1 which shares about 40% percent sequence homology with Mal3p can substitute for Mal3p function in fission yeast, suggesting that basic EB1 functions are evolutionarily conserved, at least to some extent. (Beinhauer *et al.*, 1997; Browning *et al.*, 2003). Consistent also with this view is that Mal3p can mimic the interaction of EB1 with APC *in vitro*, even though there is no APC homolog in fission yeast (Nakamura *et al.*, 2001).

2.8.4.6 Fission yeast Mal3p

The regulation of microtubule dynamics has been extensively studied in fission yeast, since this rod shaped cells constitute simple eukaryotic model system for cell polarity. The fission yeast member of the EB1 protein family, Mal3p, was identified in a screen for mutants that have defects in chromosome segregation (Beinhauer *et al.*, 1997). Deletion of Mal3p resulted in abnormally short cytoplasmic microtubules (Figure 2.15). The cells are hypersensitive to the microtubule depolymerizing drug TBZ and they are cold sensitive. Like EB1, Mal3p promotes microtubule growth and protects them from catastrophe. Since the microtubules in a Mal3p deleted cell become too short to reach the cell poles, important cell end marker proteins such as Tea1p would not be transported to the growing cell ends (Mata and Nurse, 1997; Behrens and Nurse, 2002), which results in miss-localization of other polar growth factors (La Carbona *et al.*, 2006). As a consequence, Mal3p deleted cells can have miss-positioned growth sites and thus exhibit abnormal morphologies (Beinhauer *et al.*, 1997; Fleig *et al.*, 2000). Over-expression of Mal3p leads to the formation of extraordinarily long cells and compromises spindle formation and function (Beinhauer *et al.*, 1997). Recent studies present Mal3p as a vital factor for the proper interaction of microtubule plus ends with the kinetochores during mitosis and for cooperation with the spindle checkpoint mechanism (Asakawa *et al.*, 2005; Asakawa and Toda, 2006). Additionally, Mal3p localizes to the SPB and other

fission yeast MTOCs, where it is speculated to be involved in γ -TuRC distribution or in other microtubule minus end-associated activities (Chen *et al.*, 2000). However, MTOC localization of Mal3p is expected to occur as an immediate consequence of new microtubule nucleation as this always coincides with the generation of a growing microtubule plus end.

Studies with GFP tagged Mal3p revealed that the GFP signal starts fading about 80 seconds prior to a catastrophe, and that Mal3p never accumulates at the plus end of a depolymerizing microtubule. This indicates that Mal3p may have to be removed from microtubule ends before a catastrophe can occur. Interestingly, Mal3p molecules only lose their ability to interact with the plus ends when the microtubules touch the cell poles and not when growing microtubules touch the cortex in central regions of the cell (Busch and Brunner, 2004). This is different for cells that do not express Tip1p: In *Tip1* deleted cells, Mal3p dissociates from the plus ends also when the microtubules touch the cortex at the cell center, resulting in premature catastrophes. This implies that Tip1p is important for the spatial regulation of Mal3p activity and that Tip1p mediates regional information, as it prevents the removal of Mal3p from microtubule tips specifically at the cell center but not at the poles.

2.9 Open questions and aim of this thesis

We like to understand how microtubule associated proteins (MAPs) interact and control microtubule dynamics. Fission yeast Mal3p belongs to the highly conserved end-binding protein 1 (EB1) family, and is considered to be classical plus end binding protein (+TIP) that localizes preferably to the growing microtubule plus ends. However, on many occasions EB1 proteins were also seen to be associated with the microtubule lattice. Lattice binding was observed *in vivo* under conditions where EB1 proteins were over expressed (Ligon *et al.*, 2003), but also *in vitro* when recombinant EB1 was co-polymerized with microtubules (Ligon *et al.*, 2006). In the case of Mal3p, a 10-fold over-expression of GFP-tagged Mal3p produced a faint but distinct signal along the entire lattice of all the microtubules of a yeast cell (Busch and Brunner, 2004). The situation is similar, but the fluorescent signal is weaker for Mal3p, fused to GFP via a 22 amino acid long linker, at endogenous levels in fixed cells (Figure 2.16), (Sandblad *et al.*, 2006). Although the dynamics and subcellular localization of EB1-family proteins have been investigated over the last few years in various eukaryotes (Mimori-Kiyosue *et al.*, 2000; Ligon *et al.*, 2003) including fission yeast (Busch and Brunner, 2004) still very little is known about the structural details regarding interaction of EB1-family proteins with

microtubules. However, essentially all previous microscopy studies have been carried out with light microscopy techniques that have a very limited resolution when it comes to solving structural detail of macromolecular assemblies. The aim of this work was to use cryo-EM techniques and *in vitro* systems to visualize the interaction of Mal3p with the microtubule lattice. A structural interaction study at molecular resolution would enhance our knowledge about how Mal3p promotes microtubule growth and prevents microtubules from catastrophic decay. Microtubule turbidity measurements and co-pelleting assays were to show how Mal3p influences microtubule polymerization kinetics, stabilizes and bind microtubules *in vitro*.

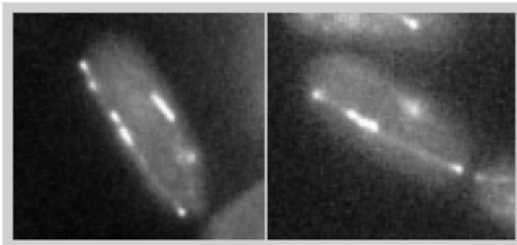


Figure 2.16: Mal3p-GFP in Fission yeast. Confocal microscopy images of *S. pombe* expressing endogenous levels of Mal3p tagged at its C-terminal with GFP via a 22 residue linker. Mal3p-L-GFP highlights the bundles of microtubules by associating with the entire set of microtubule lattices. In addition the protein accumulates at the microtubule plus ends. Images were kindly provided by Emanuel Busch.

Based on its homology to EB1, Mal3p is proposed to form a homodimeric complex between two chains composed of an N-terminal microtubule binding domain, called the CH-domain and a C-terminal coiled-coil and an acidic tail called the EB1-domain (Bu and Su, 2003; Hayashi and Ikura, 2003; Honnappa *et al.*, 2005). It has been suggested previously that Mal3p may be regulated by phosphorylation (Busch and Brunner, 2004). In addition, the combination between a basic CH-domain and an acidic tail implies that the molecule might have an intramolecular regulatory mechanism, similar to the self-inhibition proposed for CLIP-170 (Lansbergen *et al.*, 2004). To test this theory we investigated the microtubule interaction properties for a truncated Mal3p containing the microtubule binding domain and a residual linker peptide, but lacking the EB1-domain and therefore the ability to dimerize.

Our results revealed striking, novel properties and specific molecular details of how the MAP Mal3p interacts with microtubules and how such proteins may mediate microtubule stabilization and regulation of the dynamic behavior of microtubules. Obviously, these results triggered a series of new questions that will be the subject of future research.

3 Experimental methods and instrumentations

3.1 Molecular biology methods

3.1.1 Cloning

We designed expression constructs for different fusion proteins, including full-length Mal3p and several Mal3p truncation peptides (Figure 4.1A and 4.13C). All of them contained an N-terminal His6-tag with a TEV protease cleavage site. We cloned all these constructs using the same protocol; the *mal3* cDNA was amplified by PCR from an *S. pombe* cDNA library (constructed by B. Edgar and C. Norbury, ICRF, Oxford, UK) using Vent-polymerase (NEW ENGLAND BioLabs, Ipswich, MA, USA). Primers were synthesized by Thermo SCIENTIFIC (MA, USA: <http://www.thermo.com>), and listed in table 3.1. The PCR product was bound to QIAquick spin columns and purified according to the QIAquick PCR purification kit protocol (QIAGEN, Hilden, Germany). DNA fragments and vector pETM11 (G. Stier, EMBL-Heidelberg, DE) were digested with restriction enzymes NcoI and XhoI (NEW ENGLAND BioLabs). Linear DNA was separated by agarose gel electrophoresis and purified according to the QIAquick gel extraction kit protocol (QIAGEN). In cases where removal of larger fragments was not required the QIAquick nucleotide removal kit (QIAGEN) was applied.

Table 3.1: Primers

	Oligonucleotide sequence	Restriction site
aa 2 forward	ATAT <u>CCATGGG</u> GATCTGAATCTCGGCAAGAGC	NcoI
aa 308 reverse	ATTGCGGCCGCTTAAAACGTGATATTCTATCG	NotI
aa 308 reverse	CGGCGCTCGAGTTAAAACGTGATATTCTCATC	XhoI
aa 252 reverse	ATTCTCGAGTTAGGGTTGATCAGGTGGTAACTCA	XhoI
aa 203 reverse	AATTCTCGAGTTAATCAGTTCTCTCCAACCAAAC	XhoI
aa 166 reverse	ATTTCTCGAGTTATGCAGTCGAAGACACGTTATTG	XhoI
aa 123 reverse	AATTCTCGAGTTAAGCAGGTCTCTATTCCC	XhoI
aa 163 forward	ATAT <u>CCATGGG</u> GATCTTCGACTGCAAATACTGC	NcoI

The cDNA and the vector were ligated with T4-Ligase (NEW ENGLAND BioLabs) to circular DNA, transformed in to chemically competent DH5 α *E.coli* cells and plated on LB agarose plates supplemented with 30 μ g/ml Kanamycin. Positive clones were amplified in LB medium containing Kanamycin at 37°C over night. Plasmids were purified using QIAprep spin miniprep kit protocol or QIAfilter plasmid midi kit protocol

(QIAGEN). DNA concentration was measured with the NanoDrop ND-1000 (NanoDrop, Wilmington, DE, USA) at a wavelength of 260 nm and the plasmids were analyzed by sequencing, using the T7 and T7-terminator sequence as primer, as a last control.

3.1.2 Protein expression

Plasmids carrying a recombinant Mal3p coding sequence were transformed into *E. coli* expression cells BL21 (DE3: Novagen, San Diego, CA, USA). The cells were grown at 37°C in LB medium containing Kanamycin until the cell cultures reached a density measured by OD₆₀₀ of 0.4-0.6. Then, the expression of fusion proteins was induced with 0.1-0.4 mM IPTG at 32°C and cells were grown for an additional 4-5 hours. Cells were subsequently harvested by centrifugation at 6000 g and washed once before they were stored at -80°C.

3.1.3 Protein purification

E. coli cells were resuspended in equilibration buffer complemented with protease inhibitors (Complete EDTA-free tablets, Roche, Basel, Switzerland). 0.5% Triton X-100 and 0.01% β-Mercaptoethanol were added to increase solubility of the recombinant protein. During purification the samples were continuously kept at 4°. The *E. coli* cells were first lysed with a French press and the lysate centrifuged at 13,000 g to separate the membrane fraction from the Mal3p containing supernatant. In the initial protein purification step His6-TEV-Mal3p fusion protein was bound to TALON poly-His-tag binding affinity resin (BD Biosciences, Heidelberg, Germany). The protein bound to TALON was washed with equilibration buffer; 5 mM Imidazol in the washing buffer reduced unspecific binding of *E. coli* proteins. The fusion protein was eluted with 150 mM Imidazol (standard protocols from BD Biosciences). Before further processing, the Imidazol buffer was exchanged with equilibration buffer, either by Slide-A-Lyser dialyze cassettes or by Zeba desalting spin columns (both from PIERCE, Rockford, IL, USA). The His6-tag was cleaved from Mal3p by Tobacco etch virus (TEV) protease digestion by applying a ratio of 10 µl His-tagged TEV protease (Protein Expression and Purification Core Facility, EMBL-Heidelberg) to 1 mg fusion protein. The incubation took place overnight and the cleaved Poly-His-tags were removed with TALON. Alternatively, we also performed digestion with TEV protease overnight directly while the fusion proteins were still bound to the TALON. This procedure saved one elution and buffer exchange step and made the purification faster. However, it yielded less product, as only about 50% of the fusion proteins could be cleaved this way. The final purification step was gel-filtration on a HiLoad Superdex 200 column (Amersham Biosciences, Uppsala, Sweden),

2x Protein loading buffer:	100 mM Tris, HCl pH 6.8 4% SDS 0.2% bromophenol blue 20% glycerol 0.2 M DTT added before use.
Laemmli running buffer:	2.5 mM Tris Base 20 mM Glycine 0.1% SDS
MOPS running buffer:	2.5 mM MOPS 2.5 mM Tris 0.05 mM EDTA 0.1% SDS

3.1.5 Microtubule Polymerization

Tubulin was purchased from Cytoskeleton Inc. (Denver, CO, USA). Purified tubulin (2.2–45 μM) was polymerized to microtubules in BRB80 buffer, including 2 mM GTP (or alternatively 1 mM GMPCPP), 4 mM MgCl_2 , and 5-10% DMSO. Co-polymerization experiments were performed by mixing tubulin and Mal3p at various ratios in the polymerization buffer. Polymerization was initiated by raising the temperature to 37°C.

3.1.6 Turbidity Measurement

Protein polymers scatter light of 350 nm more strongly than protein monomers. Accordingly, the differences in adsorption are related to the amount of polymers in a solution. With this method microtubule polymerization can be monitored over time (Gaskin *et al.*, 1974). A 100 ml solution of 22 μM tubulin in polymerization buffer (BRB80 pH 6.8, 2 mM GTP, 4 mM MgCl_2), with or without Mal3p (2.5–10 mM) present, was pre-incubated for 10 min on ice. The cuvette was cooled to 18°C before the polymerization mix was added, (time point 0). Polymerization was induced by heating the polymerization mix to 37°C. Turbidity was measured and recorded every three seconds with a UV-1700 spectrophotometer with a temperature control unit from Shimadzu.

HEPES buffer: 25 mM HEPES
 50 mM Potassium Acetate
 1 mM MgCl₂
 1 mM EDTA
 0.1% Triton X-100, protease inhibitors were added before
 use.

3.1.10 Western blot

Specific proteins in the yeast extract were detected by standard Western blotting using monoclonal antibodies. Yeast extracts were diluted ten-fold and protein concentrations as low as 2 nM could be analyzed with this method. 5 µl of standard protein concentration gradients and yeast extract suspended in protein loading buffer were separated by SDS-PAGE and transferred to an Immobilon-P transfer membrane (MILLIPORE) that was pre-equilibrated in 100% methanol followed by ice-cold transfer buffer. We used a wet blotting setup operated at 4°C for >3 hours with a transfer current of 250 mA. The membrane was blocked with 5% milk powder in PBS-T (0.1% Tween-20) for 1 hour at room temperature. Primary antibodies were diluted 1:1000 and the Hybridoma cell supernatant was diluted 1:2 - 1:20 in 5% milk PBS-T, depending on quality and concentration of the antibody in the supernatant. Membranes were incubated for 2.5 hours and washed 3 x 10 min in PBS-T. We then used a secondary antibody, coupled to horseradish peroxidase (HRP: Amersham Bioscience, Uppsala, Sweden) that was diluted 1:2000 in 5% milk powder PBS-T and incubated and washed the same way. Chemoluminescence from HRP was induced by adding “Western lightning enhanced luminal” reagent (PerkinElmer life sciences, MA, USA) to the membranes and exposure to BioMax MR film (KODAK, Stuttgart, Germany).

The staining intensity on the film correlates directly with the concentration of the detected protein in the sample, which allowed us to estimate endogenous protein ratios. We used a concentration gradient of purified tubulin (45-180 nM) and recombinant purified Mal3p (2.4-38 nM monomeric protein) blotted on same membrane as a sample of yeast extract respectively. Membranes were stained with monoclonal antibodies against α -tubulin (SIGMA, Missouri, USA) or against Mal3p (Hybridoma cell lines was clones by Monoclonal Antibody Core Facility, EMBL-Monterotondo and Emanuel Busch, Hybridoma cell supernatant was expressed and characterized for this study; see supplementary material 6.2). Staining patterns on films were scanned and analyzed with

ImageJ (Wayne Rasband, National Institutes of Health, USA). Endogenous protein concentration ratios were estimated according to the protein standard curves.

Transfer buffer	2.5 mM Tris base
	25 mM glycine
	20% methanol

PBS	137 mM NaCl
	2.7 mM KCl
	10 mM Na ₂ HPO ₄
	2 mM KH ₂ PO ₄
	HCl pH 7.4

3.2 Electron microscopy

3.2.1 Negative staining for electron microscopy

For visualizing with an electron microscope (EM) samples have to resist high vacuum conditions. For a relatively quick approach that delivers high contrast, samples can be fixed by negative staining that soaks them with heavy metal salt prior to air-drying. The stain accumulates around the specimen by forming a high-density cast around the protein structures and enables visualization of molecular details to about 1 nm resolution.

Prior to cryo-EM, test samples were checked according to this standard protocol as a quality control of microtubules: Microtubules at a concentration of 4.5 μ M or less are suitable for negative staining. They were adsorbed for 1 minute onto formvar- and carbon-coated grids and washed twice in H₂O or BRB80, and subsequently stained in 1.5% uranyl acetate for 20 seconds. Images were recorded with a Mega-View III CCD camera on a FEI Morgagni transmission electron microscope (TEM).

For the “microtubule to sheet transition” assay a solution of 22 μ M tubulin was polymerized for 15 min at 37° in BRB80, supplemented with 1 mM GMPCPP, 4 mM MgCl₂ and 10% DMSO. To enhance sheet formation the samples were diluted to a tubulin concentration of 2.2 μ M in polymerization buffer. GMPCPP and DMSO stabilized microtubules adsorbed to carbon coated copper grids were washed with BRB80 only; experiments have shown that H₂O wash made GMPCPP microtubules sticky, so they aggregated and were washed away. These samples were imaged at 44,000x nominal

magnification on an FEI Morgagni TEM and recorded with a Mega-View III CCD camera with a resulting pixel size of 0.75 nm. Analyses and measurements of 50 images per preparation were performed with ImageJ. Each experimental condition was repeated 3-5 times individually, imaged and analyzed blindly. The total measured microtubule lengths for each preparation was between 117 and 277 μm .

For the GMPCPP nucleation studies, tubulin oligomers were polymerized in BRB80 without DMSO and the grids were washed with H_2O to improve the resolution and avoid salt crystals. These samples were imaged at 110,000x nominal magnification on an FEI Morgagni TEM and recorded with a Mega-View III CCD camera with a resulting pixel size of 0.53 nm

3.2.2 Freeze-drying and unidirectional shadowing of microtubules for electron microscopy

High-resolution unidirectional surface metal shadowing EM is a method that images exclusively the outer surface of macromolecular assemblies. The contrast of the heavy metal coat creates the impression of a pseudo three dimensional (3-D) appearance. Internal densities of the sample are neglected due to the strong contrast produced by the metal layer (Smith and Kistler, 1977). Conventional rotary and unidirectional shadowing techniques typically apply a thin layer of carbon on top of the metal layer to protect it from oxidation and from collapsing when the freeze-dried biological material is warmed to room temperature (Gross, 1987). However, if the samples remain protected from air and high temperatures at all times during preparation, transfer to the microscope and imaging, it is possible to use only a thin layer of Tantalum and Tungsten (Ta/W) without any carbon backing. Thereby the resolution of shadowed surface data can be improved to ~ 2 nm directly visible detail, and approximately 0.7 nm after averaging of two dimensional (2-D) crystalline samples (Walz *et al.*, 1996). To reach this goal the group of H. Gross at the ETH-Zürich, Switzerland, developed a unique cryo-vacuum transfer system (named MIDILAB) for shadowed specimens that greatly improves the capabilities of metal shadowing (Gross *et al.*, 1990). The MIDILAB shadowing unit performs freeze drying and unidirectional shadowing at an elevation angle of 45 degrees, and it is directly connected to a CM12 TEM. It delivered crucial data for the work presented here.

The preparation of specimens for the shadowing experiments were carried out as follows: 22 μM tubulin was co-polymerized with a 2.5x dimeric molar concentration of Mal3p in the presence of taxol for 30 minutes and diluted to a tubulin concentration of 2.0 μM

prior to absorption to glow-discharged carbon coated grids for 60 seconds. 5 μM *Neurospora* kinesin 355 (nK355) were used to decorate Mal3p-microtubules in the presence of 2.5 μM AMPPNP. The grids were then quick-frozen in liquid nitrogen and transferred into the MIDILAB (Figure 3.1). The samples were freeze-dried for 1.5 hours at -80°C , $< 10^{-5}$ Pa and unidirectional shadowed with Ta/W at an elevation angle of 45° . Then samples were then transferred under high vacuum conditions to the specimen stage of a modified GATAN cryo holder, allowing imaging at -170°C in a low dose mode. Micrographs were recorded at 35,000x nominal magnification with a GATAN 2K 794 Multi-Scan CCD camera, resulting in a pixel size of 0.53 nm.

3.2.3 Cryo-electron microscopy

Among the common EM specimen preparation methods, fixing samples in a frozen-hydrated state is the best method for preserving samples in their natural state. This is largely because drying and/or chemical fixation can be avoided. As a result, unstained frozen-hydrated samples of microtubules preserve the 3-D structure substantially better than negatively stained samples, revealing the internal structure and reducing flattening artifacts. Image contrast results only from the density difference between the protein and buffer. This difference is rather small and therefore frozen-hydrated samples require phase contrast enhancement that is produced in the microscope by large under-focus values (-2 to $-5\mu\text{m}$). Frozen hydrated samples are rapidly frozen in liquid ethane at a rate that prevents the formation of crystalline ice, but rather generates an amorphous state by a process called vitrification (Dubochet *et al.*, 1988). Further handling of the specimens is performed at liquid nitrogen temperatures with special cryo-specimen equipment. Vitrified specimens show a very high sensitivity to beam damage, and therefore they require strict low-dose conditions.

Polymerization studies were carried out with tubulin diluted to 22 μM in polymerization buffer. For co-polymerization studies this mix was supplemented with variable concentrations of Mal3p. The polymerization was induced by incubation at 37°C in the Vitrobot (FEI-Company, Eindhoven, NL). Initially a glow-discharged holey-carbon grid (Quantifoil, Jena, DE) was pre-warmed to 37°C at 80-90% humidity in the Vitrobot humidity chamber. 4 μl of the polymerization mix was adsorbed to the grid and incubated for varying times, followed by blotting and quick-freezing in liquid ethane.

Mal3p decoration studies on stabilized microtubules were performed by diluting microtubules to a final tubulin concentration of 2-4.5 μM . In order to achieve full decoration 4-

8 times more Mal3p than tubulin dimers were applied to taxol-stabilized microtubules, and incubated the final mix for 1-2 minutes. 3.5 μ of the mix was adsorbed onto glow-discharged holey-carbon grids for 1 min, followed by hand blotting and quick-freezing in liquid ethane using a manual plunger (Dubochet *et al.*, 1988).

Cryo-EM was performed on a FEI CM120-BioTwin TEM and on a FEI CM200-FEG TEM (FEI, Eindhoven, NL), using a GATAN-626 Cryo-holder (GATAN). Images were recorded at 37,000x (FEI CM120 BioTwin) or 38,000x (FEI CM200-FEG) nominal magnification on Kodak SO-163 EM film at an under-focus range from 1.5 to 2 and 2.5 to 3 μ m. Micrographs were scanned with a Zeiss-SCAI scanner at a step size of 21 μ m correlating to 0.5676 nm (BioTwin) or 0.5526 nm (FEG) respectively on the actual specimens.

3.2.4 Image processing and helical three dimensional reconstruction of cryo-electron microscopy images

The recovery of 3-D information from a specimen recorded as a series of 2-D projections under various angles (e.g. from an electron microscope) takes advantage of the “projection theorem”: The Fourier transformation of a 2-D projection obtained from a 3-D object is identical with one particular central section of the 3-D transformation of the object. Furthermore, if an object has symmetry, several of these sections can be assigned to one single projection (DeRosier and Moore, 1970). In a helical microtubule, e.g. a 15-protofilament microtubule, the smallest asymmetric unit consists of one $\alpha\beta$ -tubulin dimer and an associated tubulin binding particle (e.g. a Mal3p monomer, or kinesin motor domain). These units are arranged along a helical path that positions them with an even angular distribution. This helical path has a pitch of 16 nm and is convoluted with a protofilament supertwist with a pitch of about 800 nm. A complete isotropic 3-D reconstruction requires continuous projections of the asymmetric units between 0 and 180 degrees. Therefore, a single image of a helix is sufficient to generate two complete isotropic 3-D maps that are independent from each other (the near and the far side). Helical handedness, layerline numbering and assignment of Bessel orders in Fourier space are the parameters that define each individual helical path and that are required to execute a 3-D reconstruction (DeRosier and Moore, 1970). The Fourier transform of a 2-D projection from a helical object generates sets of continuous functions called layerlines that are arranged symmetrically around the center of the transform. The position of the layerlines depends on the repeating distance of an asymmetric unit. Each helical path creates its individual cylindrical wave function that is reflected in the shape of the Bessel

function (Stewart, 1988), of which the Bessel order corresponds to the number of identical helical starts for any given path. Bessel orders can be negative (-) for a left-handed helix and positive (+) for a right-handed helix. The amplitude and phase modulations along a layerline depend on the Bessel order and include structural characteristics (Figure 3.1).

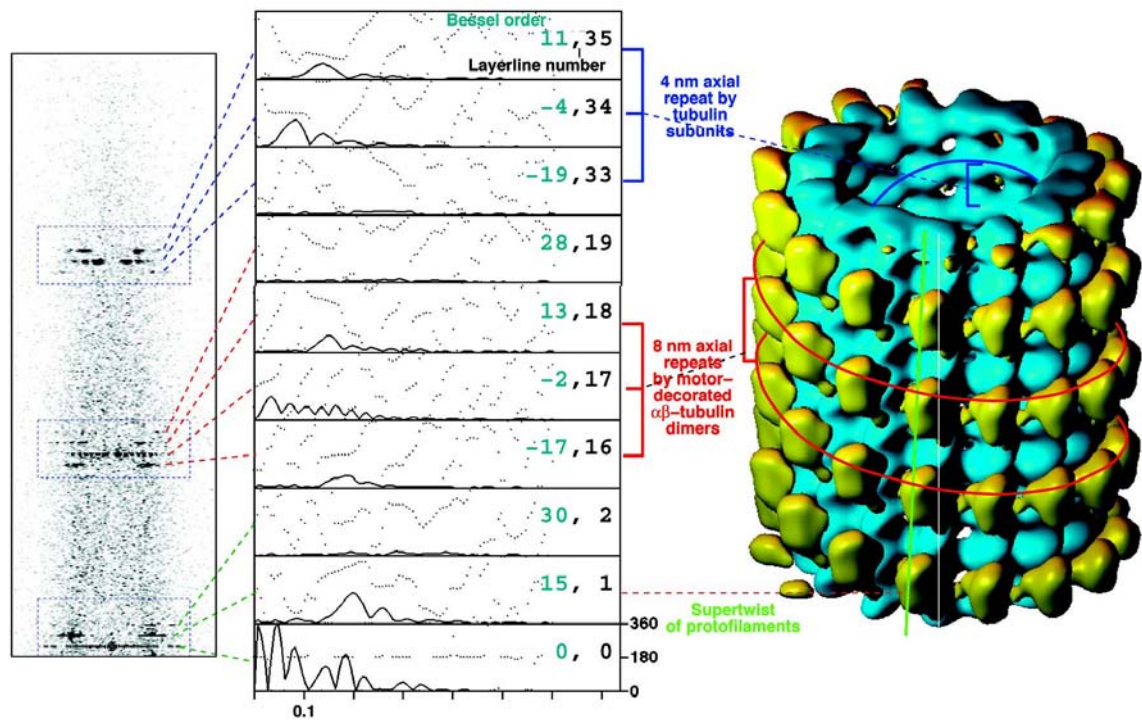


Figure 3.1: Correlation of diffraction pattern layerlines, Bessel order and real-space features of a helical microtubule. The upper half of the diffraction pattern of a 15 protofilament microtubule decorated with motor proteins is shown in the panel left. The obtained phases, drawn as dotted lines and the intensities (=amplitude²) drawn as continuous lines of selected microtubule characteristic layerlines are shown in the middle panel. In the right panel, the averaged reconstructed 3-D volume, visualized with VolVis. Adapted from Beuron and Hoenger, 2001.

Most native microtubules contain 13 protofilaments while the number of protofilaments in *in vitro* assembled microtubules may vary considerably more (Mandelkow *et al.*, 1986a; Wade *et al.*, 1990). In the case of microtubules composed of 13 protofilaments, the protofilaments are arranged parallel to the microtubule axis. However, in order to accommodate more or less than 13 protofilaments, the microtubule lattice forms a super-twist (Wade *et al.*, 1990). While microtubules composed of 13 protofilaments contain a so-called lattice seam (for visual proof see: Kikkawa *et al.*, 1994; Sandblad *et al.*, 2006) that interrupts helical symmetry, 15-protofilament microtubules with a right-handed

supertwist exhibit true helical symmetry according to a so-called B-type lattice (see section 2.6.4.4-2.6.4.6) (Amos and Klug, 1974). Hence, these microtubules can be used for helical 3-D image reconstruction. Helical 15 protofilament microtubules form a right-handed supertwist which constitutes the longest helical path in the lattice. Accordingly the supertwist generates a strong layerline (layerline 1) with a Bessel order of +15 (+ for right-handed, 15 for a 15-start helix as each protofilament forms its own helical start) (Figure 3.1). This layerline 1 is the dominating feature responsible for the sampling of layerlines with shorter repeats. A typical diffraction pattern of a kinesin-decorated 15-protofilament microtubule shows two more locations with clusters of strong layerlines, one at 1/8 nm and another one at 1/4 nm (Figure 3.1). Both clusters are convolutions of monomer repeats in the microtubule with the protofilament supertwist. The cluster at 1/8 nm corresponds to two parallel left-handed helices connecting motor domains laterally that are intertwined with an individual pitch of 16 nm and therefore form an axial 8 nm repeat. This corresponds to a Bessel order of -2. The cluster at 1/4 nm corresponds to the underlying α - β - α - β tubulin monomer repeat. In this case four left-handed parallel helices result in a 4 nm repeat due to the axial tubulin repeat (Figure 3.1) (Beuron and Hoenger, 2001). Images of helical microtubules are the 2-D projection of 3-D objects, meaning that the top and the bottom surfaces of the object are superimposed on each other, which can be separated in Fourier space (DeRosier and Moore, 1970). As mentioned above, two individual 3-D maps can be calculated theoretically from a single image of a helical object. In practice however, the low contrast of frozen-hydrated samples and the low-dose imaging result in noisy images. These conditions make it necessary to increase the signal-to-noise ratio by averaging many more asymmetric units than provided by one single image. For rapid 3-D reconstructions the resolution of the 3-D reconstructions of microtubules decorated with MAPs is typically 2-3 nm which can give us information about the binding geometry of MAPs to microtubules. Higher resolution requires substantially greater efforts such as collecting more data and correcting the contrast transfer function (CTF) modulations of the microscope (Hirose *et al.*, 2000; Krebs *et al.*, 2005; Sindelar and Downing, 2007).

15-protofilament/2-start helical microtubules were selected from micrographs according to their characteristic Moiré pattern (Beuron and Hoenger, 2001). Selected microtubules were processed with the help of the software suites PHOELIX (Whittaker *et al.*, 1995) and SUPRIM (Schroeter and Breaudiere, 1996). The microtubules generally exhibited a slight curvature along their length, which was corrected by a straightening procedure at the very beginning of the processing. Then the layerlines were extracted, according to the

helical selection rule the layerline numbers and Bessel orders were assigned, the amplitudes and phases are calculated, and the 3-D maps are prepared by Fourier-Bessel inversion of the layerline data (Whittaker *et al.*, 1995).

3.2.5 Statistical Difference Mapping

Statistical difference mapping was carried out with a Student's t-test routine adapted for 3D data of helical symmetry (Milligan and Flicker, 1987). Individual maps were calculated for each data set and phases were aligned with each other. Variance maps were calculated for each dataset by comparing persistent and variable densities among each individual data unit. The densities and their statistical fluctuations at equivalent positions in the two maps were compared by the Student's t-test routine that yielded a statistical difference map. For each voxel in this map the significance level was determined and displayed in an iso-value 3-D map. The value is determined according to the degrees of freedom by $n = (n-1) + (m-1)$ where n is the number of data sets of one experimental condition while m is for the number of data sets for the other experimental condition. In the presented work, differences >99% significance level, are taken into account. For 3-D visualization of the difference volume, we used the software VolVis (SUNY Stonybrook).

3.3 Internet based bioinformatic tools

Theoretical values for peptide specific extinction coefficients, molecular weights and isoelectric points/pH were obtained with Protein calculator (<http://www.scripps.edu/~cdputnam/protcalc.html>) by C. Putnam, Scripps, USA. Sequence alignments were carried out using MUSCLE from (<http://www.bioinformatics.nl/tools/muscle.html>) Laboratory of Bioinformatics, WUR, Netherlands. Coiled-coil propensities were analyzed with COILS (http://www.ch.embnet.org/software/COILS_form.html) by A. Lupas and Multicoil (<http://multicoil.lcs.mit.edu/cgi-bin/multicoil>) by E. Wolf (Lupas *et al.*, 1991; Wolf *et al.*, 1997).

4 Results

4.1 Expression and purification of Mal3p

Initially, we started an investigation of the structural and functional properties of full-length Mal3p. The first aim was to establish an optimal and reproducible expression and purification protocol. To achieve a stable product with high yield and few contaminations we choose a bacterial expression system (*E. coli*, *BL21 DE3*). We produced an expression construct containing full-length *mal3* fused with a TEV protease cleavage site and an N-terminal His6-tag (Figure 4.1A) that was then transformed into *E. coli*. The resulting His6-Tev-Mal3p fusion protein was expressed after induction with 0.4 mM IPTG and did not degrade in the cell lysate when it was supplemented with conventional protease inhibitors. In SDS-PAGE His6-Tev-Mal3p runs as a 40 kDa protein. The first affinity purification step for the fusion protein was performed on the poly-His binding resin TALON. 2 ml resin suspension of TALON binds up to 20 mg of recombinant Mal3 fusion protein. The binding phase was extended to 4 hours to saturate the TALON at 4°C (Figure 4.1B). Protease cleavage with TEV protease at 4°C is slow; accordingly, more than 4 hours of digestion at 4°C was required to cleave > 50% of the fusion protein (Figure 4.1B). To remove uncleaved fusion protein, free poly-His peptides and TEV proteases, we applied two additional rounds of TALON binding to separate uncleaved from cleaved product (Figure 4.1B). This procedure finally yielded highly pure Ma3p visible as a single 35 kDa band in SDS-PAGE and coomassie blue staining.

The final purification step was carried out with gel-filtration, which transferred the protein to BRB80 + 100 mM NaCl. Gel-filtration separated the main product from remaining *E. coli* proteins and Mal3p degradation products, and at the same time delivered a rough estimation of the size of the Mal3p molecule and possible oligomerization. Mal3p eluted from the HiLoad superdex 200 gel-filtration column within a relatively wide peak around 66.5 ml (Figure 4.1C). This gel-filtration column was calibrated using a set of standard proteins with known molecular weight (see section 6.1). Assuming that the protein would be completely globular the elution volume of Mal3p corresponded to a molecular weight of approximately 160 kDa. As the travel properties through the gel-filtration matrix are roughly related to an approximately globular volume of the protein complex, a molecular weight of 160 kD would suggest that the molecule has formed a tetramer or an even larger complex. However, Mal3p is a bi-globular protein with two domains linked to each other by a 50-residue random coil. Hence the predicted volume

from gel-filtration based on a globular shape highly overestimates the actual molecular weight. The human homolog EB1 dimerizes at the C-terminal domain (Honnappa *et al.*, 2006) and >50 amino acid long linker connects the globular CH-domains to the dimerization region, resulting in a rather flexible complex with unstructured elements (Figure 5.1). In addition, the width of the elution peak was also indicative of a rather flexible complex.

From 1 l of *E. coli* cell culture approximately 0.5 ml of 8 mg/ml purified full-length Mal3p was recovered.

For a better analysis of the Mal3p complex we performed analytical ultracentrifugation with the help of Valdimir Rybin from the Protein Expression and Purification Core Facility EMBL-Heidelberg. The analyses revealed a complex with a molecular weight of approximately 75 kDa, indicative of a dimeric Mal3p complex.

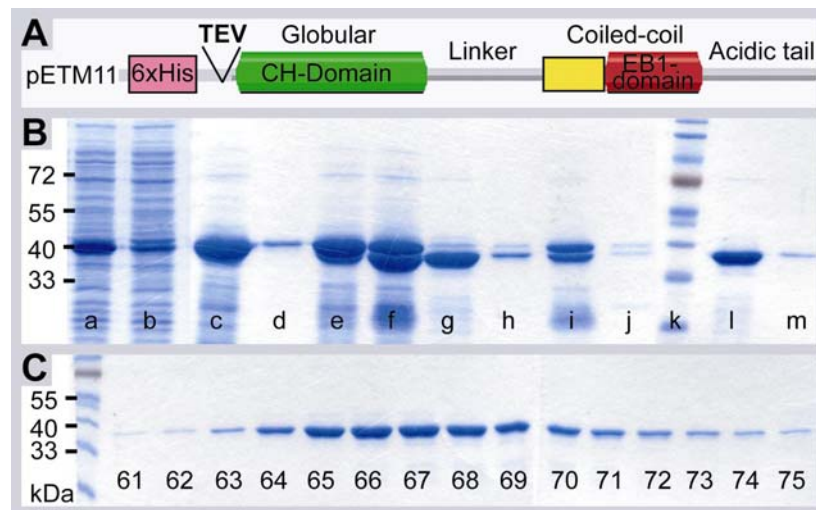


Figure 4.1: Expression and purification steps for Mal3p. (A) Graphical view of the pETM11-based expression construct. (B) Coomassie SDS-PAGE of affinity purification steps: (a) *E. coli* lysate; (b) Remaining lysate after first TALON binding; (c and d) First elution; (e) After buffer exchange; (f) After TEV cleavage; (g and h) Remaining sample after second TALON binding; (i and j) Waste elution of TALON bound fraction; (k) protein marker; (l and m) Remaining sample after third TALON binding. (C) SDS-PAGE of Gel-filtration fractions from full-length Mal3p.

4.2 Biochemical studies of full-length Mal3p binding to microtubules

4.2.1 Turbidity measurements

Analysis of microtubule dynamics in cells that were deleted for *mal3* suggested that the protein is a general promoter of microtubule growth. However, it was not known whether this is a direct effect of Mal3p binding to the microtubules or whether it involves additional factors. To gain further insight into the effects of Mal3p on the kinetics of microtubule polymerization *in vitro*, we performed standard turbidity experiments (Gaskin *et al.*, 1974) screening for the ratio of polymerized versus soluble tubulin. These experiments allow monitoring the generation of newly polymerizing microtubules in solution. Experiments were performed in the absence, and in the presence of various concentrations of Mal3p. Microtubule polymerization was initiated by a temperature shift from 18°C (time 0) to 37°C (+2 minutes; Figure 4.2). In the absence of Mal3p tubulin polymerization peaked after approximately 15 minutes and then decreased very slowly again (Figure 4.2). Already small amounts of Mal3p had a strong effect on the polymerization rate of tubulin, and the total amount of polymerized tubulin increased with increasing Mal3p concentrations. In the presence of Mal3p, nucleation occurred after 3-4 minutes and was followed by rapid polymerization. However, polymerization did not reach a true plateau but progressed gradually until the end of the experimental time frame (figure 4.2). These turbidity experiments clearly show that Mal3p promotes microtubule nucleation and polymerization *in vitro*, without any other MAPs present.

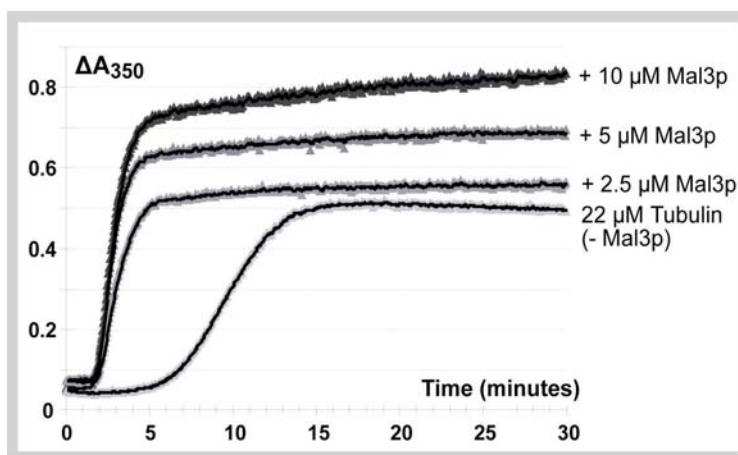


Figure 4.2: Turbidity caused by the polymerization of 22 μM tubulin under increasing Mal3p concentrations measured as a function of time. Compared to the control in the absence of Mal3p (light grey marks), increasing concentrations of Mal3p (darker grey scale marks) raised the ratio between free tubulin and polymerized tubulin in favor of polymer microtubules.

4.2.2 Co-pelleting Mal3p with microtubules

To test the microtubule binding capacity of recombinant Mal3p, we used a co-pelleting assay. We kept a constant Mal3p concentration of 2.3 μM and increased the amount of microtubules gradually from 0.6 μM to 18 μM , and repeated this centrifugation experiment 3 times. As expected, an increasing fraction of Mal3p co-pelleted with microtubules as the tubulin concentration in the preparation was raised (Figure 4.3A). Finally, at a concentration of 18 μM tubulin the Mal3p fraction was entirely adsorbed by microtubules (Figure 4.3B). Accordingly, we needed about eight times more tubulin to deplete Mal3p from the supernatant.

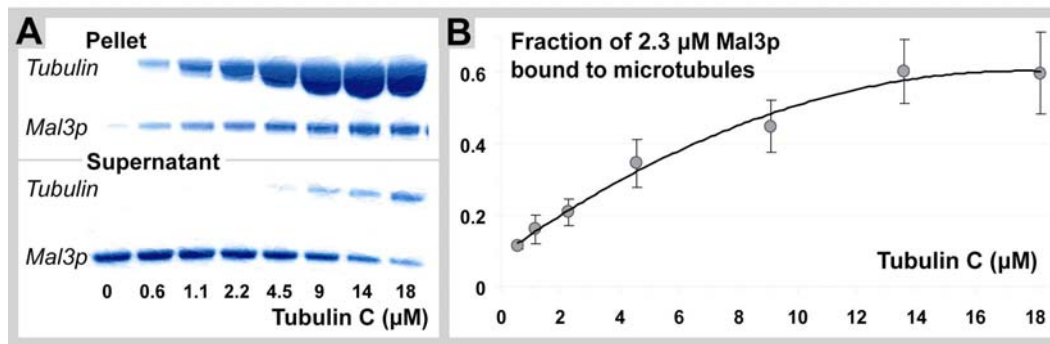


Figure 4.3: Co-pelleting Mal3p in complex with microtubules. Mal3p concentration was kept stable at 2.3 μM . (A) In the absence of microtubules (left column) Mal3p was found only in the supernatant. With increasing microtubule concentrations more Mal3p was found in the pellet. (B) The median of three individual experiments show that approximately 8 times more tubulin is necessary to saturate binding to microtubules of Mal3p. Accordingly, there are fewer Mal3p binding sites on a microtubule than there are tubulin dimers.

4.2.3 Subtilisin digestion does not affect Mal3p binding

Subtilisin specifically cleaves ~ 10 amino acids off the C-terminal end of α -tubulin and ~ 20 amino acids off the C-terminal end of β -tubulin (Serrano *et al.*, 1984). Several MAPs and motors interact with the very acidic C-terminal tail of β -tubulin, and subtilisin digestion interferes with their function (Serrano *et al.*, 1984; Santarella *et al.*, 2004; Skiniotis *et al.*, 2004). SDS-PAGE trimmed for a high separation power in the range of 50-60 kDa barely separated α - from β -tubulin. That separation became more pronounced after subtilisin treatment because β -tubulin loses a larger stretch of its C-terminal tail (β -runs below α -tubulin). However, unlike other MAPs (e.g. see Tau: Santarella *et al.*, 2004) the binding affinity of Mal3p to taxol stabilized microtubules before and after subtilisin digestion did not show any considerable difference (Figure 4.4). Hence, the acidic C-terminal amino acids on β -tubulin seemed to be irrelevant for Mal3p binding.

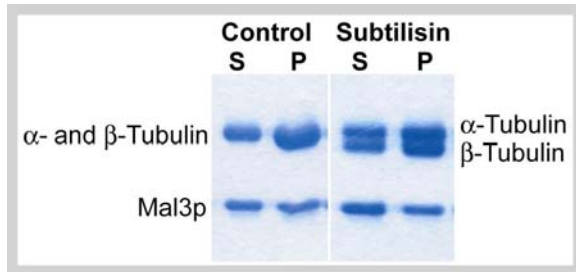


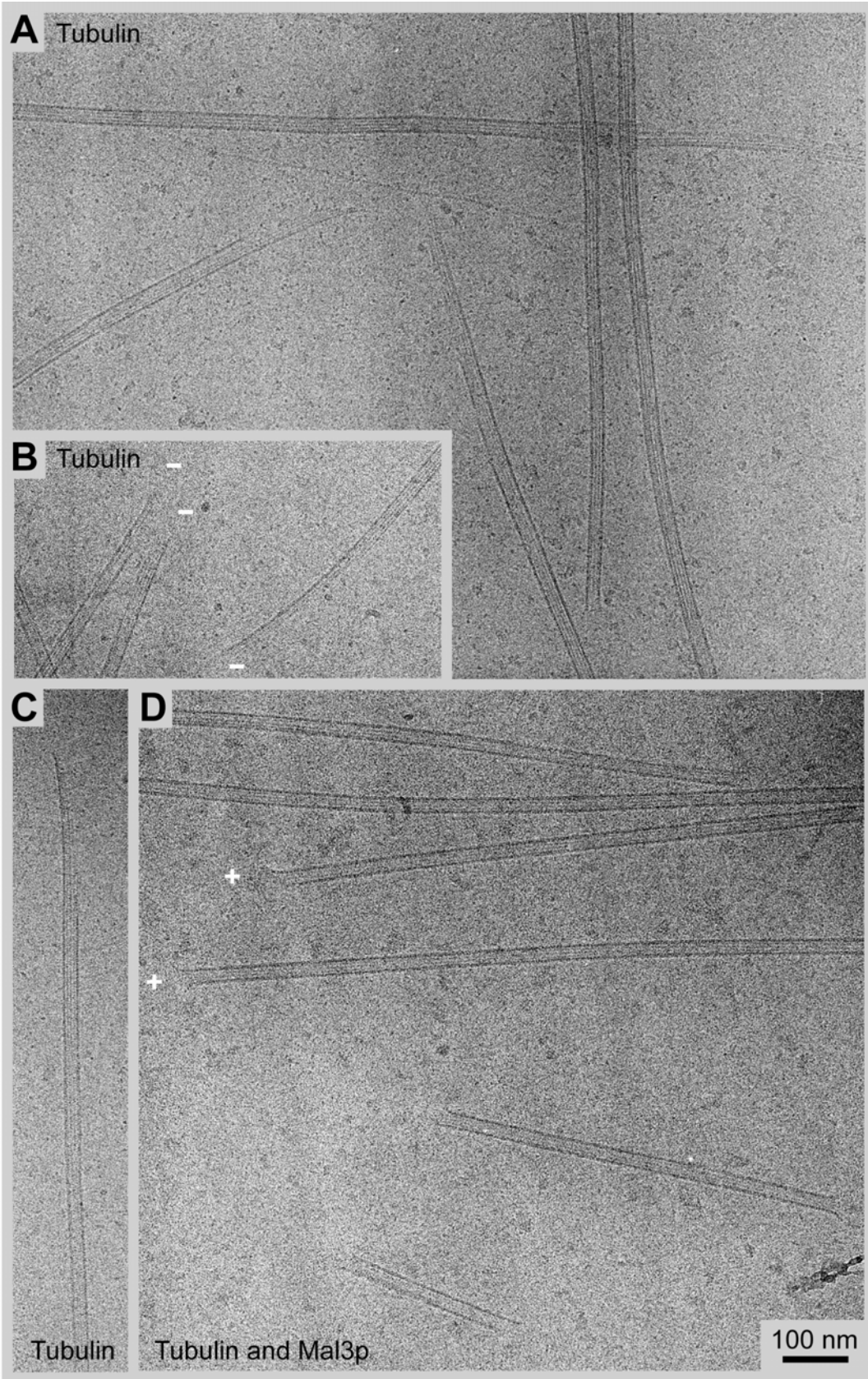
Figure 4.4: Ma3p bound to Subtilisin treated microtubules. Subtilisin cleaves the acidic C-terminal tail of β -tubulin, which is shown as a separation of α - and β -tubulin (right) by SDS-PAGE. Equal amounts of Ma3p were found in the pellet after centrifugation of untreated (left) or subtilisin treated (right) microtubules.

4.3 Visualization of Mal3 binding to microtubules by electron microscopy

4.3.1 Cryo electron microscopy of microtubules co-polymerized and decorated with Mal3p

In yeast cells Mal3p is predominantly found at the growing plus ends of microtubules (Busch and Brunner, 2004). Unfortunately visualizing the molecular structure of a growing microtubule end with fine structural detail *in vivo* is not yet possible. *In vitro*, microtubule plus ends were either seen as open tubulin sheets, sometimes also referred to as C-tubes (Chretien *et al.*, 1995), when they were in a growth phase or with protofilaments bending away from the tubes and disassembling into small oligomers during phases of decay (Mandelkow *et al.*, 1984; Mandelkow *et al.*, 1986a). As we know that Mal3p in particular accelerates the onset of polymerization (see section 4.2.1 and Figure 4.2), we used the quick-freeze capabilities of cryo-EM and plunge-froze plain microtubules and microtubules co-polymerized with Mal3p during the onset of their polymerization (Figure 4.5D). For microtubules that exhibit a protofilament supertwist it is possible to determine their polarity according to the Moiré pattern, which is characteristic for a particular protofilament number (Chretien *et al.*, 1996). Accordingly, we could specifically analyze the plus ends of supertwisted microtubules decorated with Mal3p (Figure 4.5D). Plain microtubules in a growth phase showed the characteristic open tubulin sheets at their plus ends (Figure 4.5A and C), but some sheets could also be found at the minus ends (Figure 4.5B). In contrast, microtubule-Mal3p complexes generally exhibited blunt ends instead (Figure 4.5D).

Figure 4.5: Cryo-EM of microtubules polymerizing in the absence (A-C) or presence (D) of Mal3p. (A-C) The ends of *in vitro* polymerizing unstabilized microtubules often exhibited open sheet structures (Chretien *et al.*, 1995), (B) Minus ends also show this conformation (marked with white -). (D) In the presence of Mal3p faster polymerizing microtubules generally exhibit blunt ends. According to the Moiré pattern, we were able to determine the polarity of some of the microtubules, here two growing plus ends are shown (marked with white +). See next page.

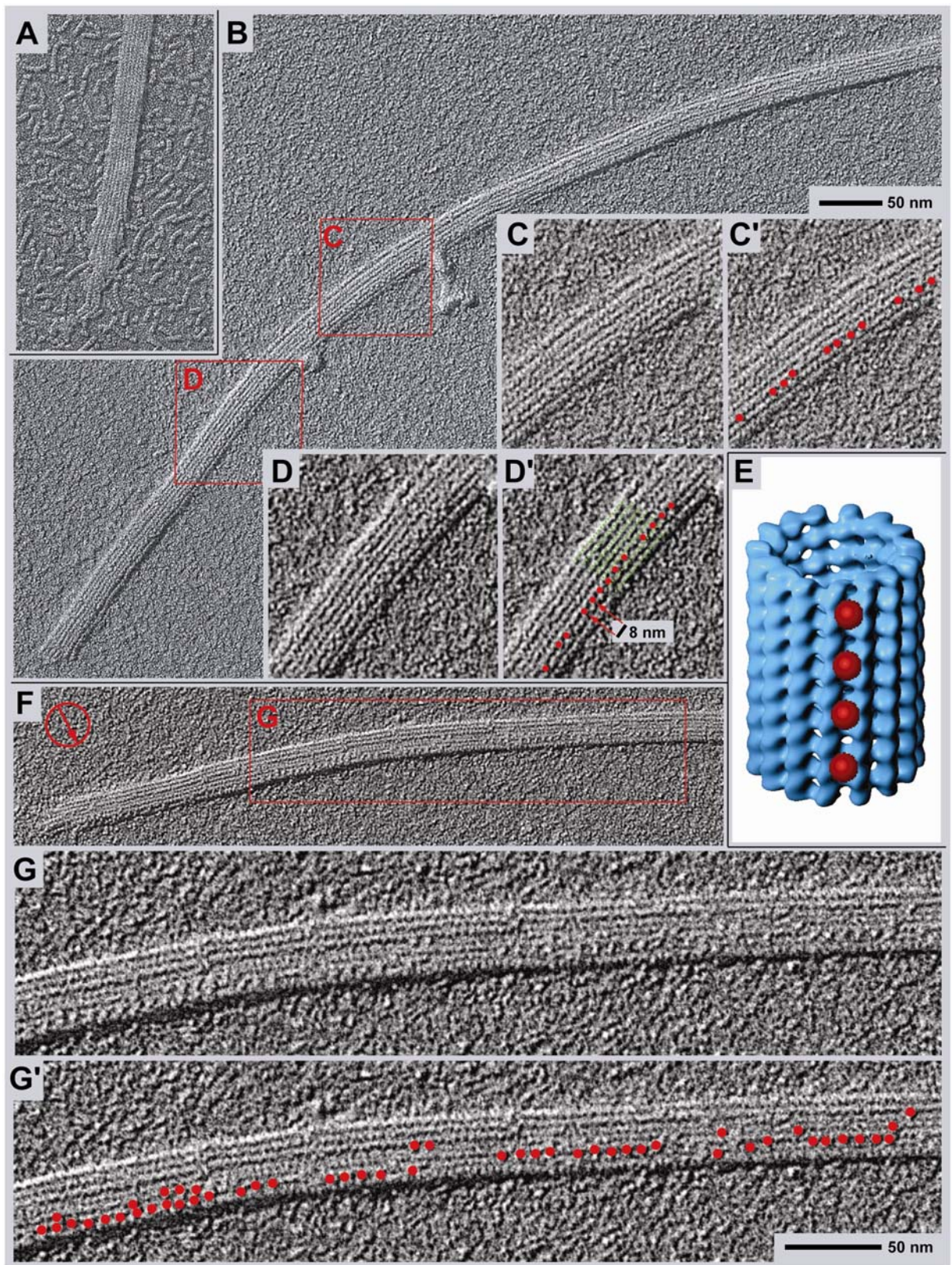


In the initial phase of this project we used cryo EM and helical 3-D image analysis (for an application to microtubules see: Beuron and Hoenger, 2001) in an attempt to elucidate the binding geometry of Mal3p dimers to the microtubule surface. To this end, samples with taxol-stabilized microtubules saturated with Mal3p were embedded in vitrified ice, and the images were analyzed accordingly. However, it quickly became clear that Mal3p did not pack the microtubule surface stoichiometrically, like it was observed with kinesin motor domains (Hoenger *et al.*, 2000b). Interestingly, even partial decoration should reveal a qualitative localization of a binding partner, however, with this strongly under-represented mass helical analysis of full-length Mal3p failed completely for mapping the Mal3p microtubule binding site. As disappointing this was at that time, it later became very obvious why this was the case through a very spectacular observation (see below section 4.3.2-3).

4.3.2 High-resolution shadowing electron microscopy reveal Mal3p binding at the groove between two protofilaments

After the negative results from cryo-EM and helical analysis we looked for other visualization methods to demonstrate that Mal3p interacts with microtubules in some way to confer its stabilizing effect. To do this we used high-resolution metal shadowing that allowed us to specifically investigate the surface binding properties of Mal3p. High-resolution (unidirectional or rotational) metal shadowing is an EM specimen preparation method that reveals a high contrast image of the surface of a sample (Gross, 1987). Here we employed unidirectional shadowing by applying an approximately 0.3 nm thick layer of tantalum tungsten (Ta/W) to the surface of our specimens, at an elevation angle of 45 degrees. Shadowing experiments were carried out in the lab of H. Gross at the Swiss Federal Technical High School (ETH-Hönggerberg, Zürich, Switzerland). This lab developed a unique device, named MIDILAB (Gross *et al.*, 1990), that holds the world record in resolution for metal shadowing (Walz *et al.*, 1996, Tittmann *et al.*, in prep.).

Figure 4.6: High-resolution unidirectional surface metal shadowing of microtubules complexed with Mal3p. This method allows imaging without any computational averaging or other signal enhancing methods. (A) A plain microtubule with a clean surface and the typical curved tubulin oligomers in the background. (B) and (F) show overviews of microtubules copolymerized with Mal3p. Red circled arrow delineates the shadowing direction. The boxed areas are shown magnified in (C), (D) and in (G), respectively. The green lines in (D') highlight the protofilaments and the red dots highlight clearly recognizable Mal3p particles (viewing the figure from a flat angle parallel to the long axis of the microtubule facilitates the identification of Mal3p). These normally locate directly into one of the grooves between two protofilaments, while the rest of the surface remains free of Mal3p. The row of aligned Mal3p particles occasionally has gaps but often finds its way back to the same groove. Imperfections within *in vitro* polymerized microtubules are not uncommon; therefore, the lattice seam may change position occasionally. (E) Shows a 3-D model integrating the results of Figure 4.6. See next page.



When applied to our Mal3p-microtubule complexes, high-resolution metal shadowing carried out in the MIDILAB allowed us to visualize individual molecular particles protruding from the surfaces of the microtubules. Thus we made a stunning discovery: Microtubules co-polymerized with Mal3p clearly revealed Mal3p particles on the surface of microtubules, however, only at very specific locations. Rather than fully decorating the entire microtubule surface, these particles reproducibly decorated only along a single line parallel to the long microtubule axis (Figures 4.6B-G). For a comparison with kinesin motor domains see Figure 4.6F and G and recent publications (Hoenger *et al.*, 2000a; Krzysiak *et al.*, 2006). Only few isolated Mal3p particles could be found elsewhere of the microtubule (Figures 4.6B-G). Clearly visible on shadowed specimens, the protein particles were always situated in the groove in between two adjacent protofilaments. Axially the shortest repeat of Mal3p molecules appeared to be 8 nm or multiples of that interval (Figures 4.6C, D and G), it should be stressed that this is the length of a tubulin dimer. The Mal3p alignments occasionally jumped over to a neighboring groove (Figures 4.6F and G) but typically filled only one single groove at any given position along the tube. This is in strong contrast to dynein and kinesin motor proteins or MAPs like Tau, which decorate the entire outer tubulin surface, typically interacting with the C-terminal and Helix 12 of β -tubulin (Sosa *et al.*, 1997; Hoenger *et al.*, 2000b; Mizuno *et al.*, 2004; Santarella *et al.*, 2004). Mal3p particles appear to interact with tubulin subunits from two adjacent protofilaments. This location does not seem to share much of its microtubule binding site with other MAPs (Al-Bassam *et al.*, 2002; Santarella *et al.*, 2004) or motor proteins (Hoenger *et al.*, 1995; Hoenger *et al.*, 2000b). Accordingly, we observe the same binding pattern for Mal3p on microtubules co-polymerized with Tau (Figure 4.7) as we do in the absence of Tau (Figure 4.6).

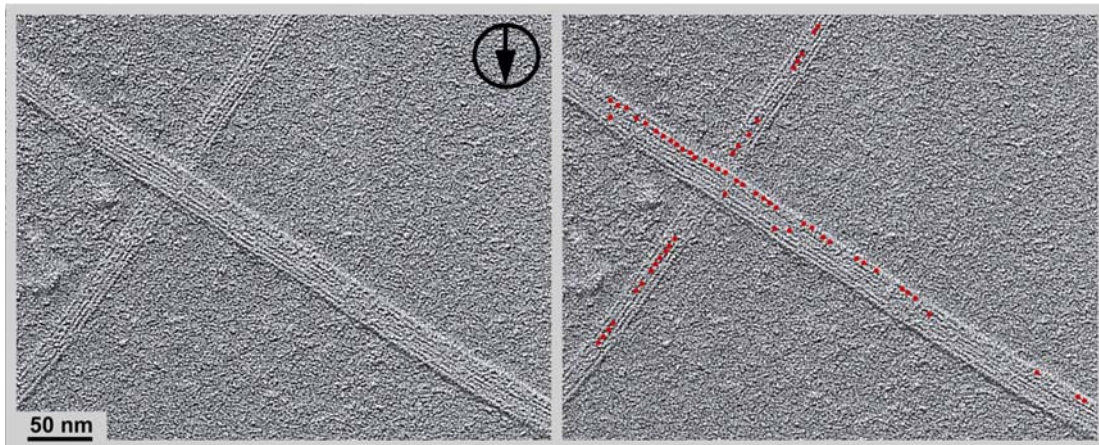


Figure 4.7: High-resolution unidirectional surface metal shadowing of microtubules co-polymerized with Tau and decorated with Mal3p. Two copies of the same image. In the right panel Mal3p particles are highlighted with red dots. Arrow indicates shadow direction.

4.3.3 Mal3p specifically interacts with the microtubule lattice seam

Obviously, the key question at this stage was why Mal3p bound predominantly to one single groove on a microtubule surface, and what was so special about this groove? The only feature on a microtubule surface running axially and that is structurally different from the rest of the microtubule surface is the microtubule lattice seam (Kikkawa *et al.*, 1994; Sosa and Milligan, 1996). This lattice seam (see Figure 4.8D,E and H) interrupts the predominant so-called B-lattice pattern (lateral α - α and β - β interactions) with an A-lattice interaction (lateral α - β interactions; Amos and Klug, 1974). Our findings suggested that Mal3p binds to this microtubule lattice seam in a configuration that recognizes a specific binding pocket that is only formed between two adjacent protofilaments interacting with A-lattice contacts. *In vivo* microtubules are most commonly composed of 13 protofilaments and these arrangements typically form one seam. However, at least *in vitro*, multiple seams may occur as well as so-called mixed lattice (Chretien and Wade, 1991; Kikkawa *et al.*, 1994; Dias and Milligan, 1999). Occasionally, we observed a microtubule with two adjacent rows of Mal3p densities, which could reflect the presence of two neighboring seams (Figures 4.8A-C,E and H). On plain, shadowed microtubules the structural similarity between α - and β -tubulin prevented a clear distinction between A- and B-lattices (Figures 4.6A). The B-lattice became visible under conditions where microtubules were fully decorated with molecular motors (Figure 4.8G, blue line and 4.9), which enhanced the relative positions of $\alpha\beta$ -tubulin dimers to each other. However, the presence of Mal3p in neighboring grooves now allowed us to indirectly measure the lateral stagger between three adjacent protofilaments that form Mal3p-binding sites. The lateral stagger of the Mal3p densities in the neighboring rows exactly corresponded to that of an A-lattice configuration (Figures 4.8C-D and H). For a normal B-lattice interaction the lateral stagger along the left-handed helical path forming the lattice would be approximately 0.92 nm corresponding to an inclination of 10.6° (Figure 4.8 G and H, blue line), whereas in the presence of a seam (A-lattice) it should be approximately 4.2 nm in the same direction or 3.2 nm with a right-handed twist, corresponding to an inclination of 38° (Figure 4.8H yellow line), (Amos and Klug, 1974). This confirmed the preferential binding of Mal3p to microtubule seams.

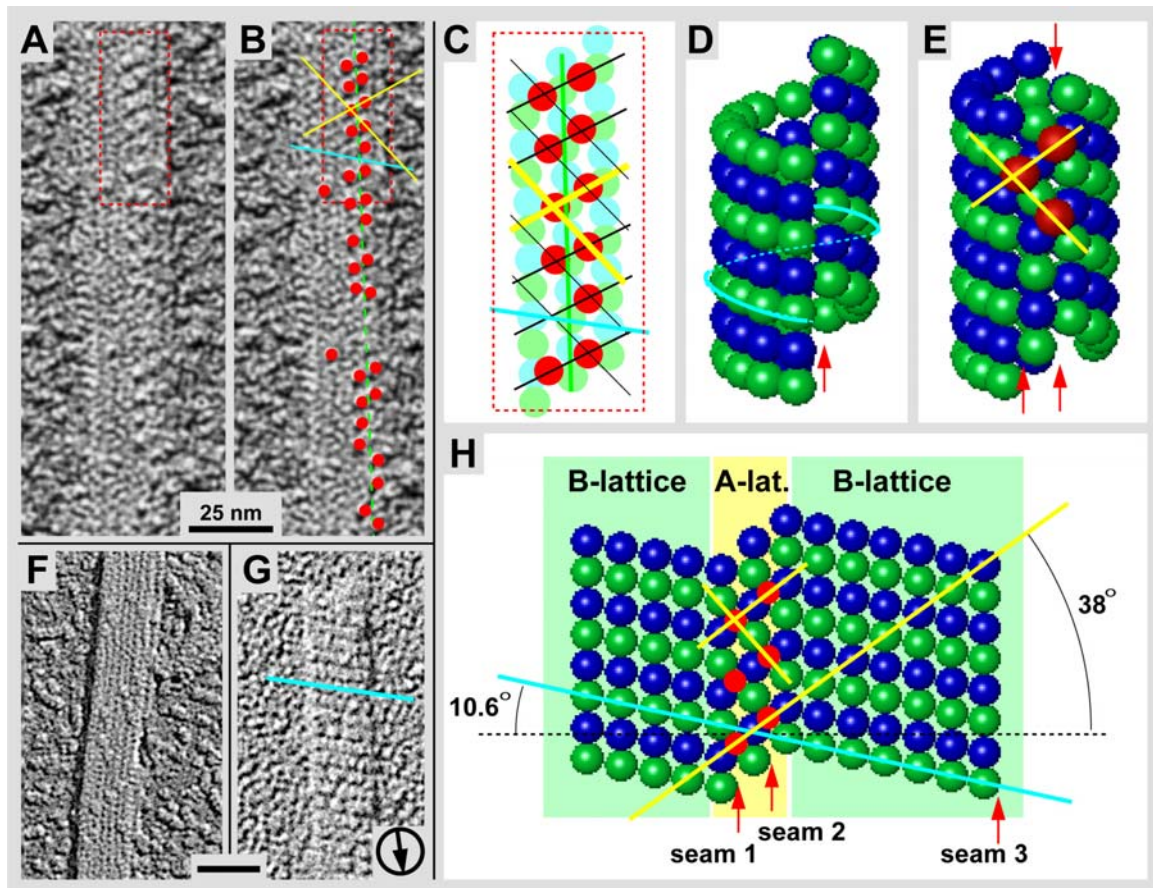


Figure 4.8: Mal3p Recognizes the Microtubule Lattice Seam. (A) Occasionally microtubules can be found where Mal3p aligns in two adjacent rows. (B) Same image as (A) but Mal3p particles are marked with red dots. These expose the microtubule lattice geometry (yellow lines), showing that Mal3p binds along an A-lattice interaction and clearly reveals the presence of a lattice seam. (C) A cartoon of Mal3p binding as in the case of figure (A). (D), (E) and (H) are models of the microtubule seam. (E) and (H) are models of the Mal3p and seam (red arrows) distribution that must occur on the microtubule shown in A. Most likely there are two adjacent seams as modeled as a closed tube (E), and flat sheet (H). A 13 protofilament microtubule would have to compensate for such a double seam with a third seam, which here is placed arbitrarily in the back of the tube. Multiple seams in microtubules are rare but do occur (Chretien and Wade, 1991; Dias and Milligan, 1999; Kikkawa *et al.*, 1994). (F) A microtubule surface decorated with a few kinesin motor head domains for comparison. These are randomly distributed over the entire surface. (G) Shows a microtubule decorated stoichiometrically with kinesin motor head domains that serve as “lattice geometry enhancers” and reveal the microtubule B-lattice geometry (blue line in all panels) as the predominant lateral protofilament interaction in microtubules (Song and Mandelkow, 1993). Without the use of such a lattice geometry enhancer, the lateral tubulin dimer arrangement is invisible at this resolution due to the strong structural similarities between α - and β -tubulin.

4.3.4 Mal3p stabilize the microtubule lattice seam

The microtubule binding of recombinant motor domains of kinesins such as *Neurospora crassa* kinesin 355 (nK355) has in the past been studied by high-resolution unidirectional surface shadowing (Hoenger *et al.*, 2000a; Song *et al.*, 2001). If microtubules were stoichiometrically decorated with these motor domains, their selective binding to the β -tubulin subunit would result in a binding pattern that perfectly revealed the protofilaments' B-lattice interaction. Interestingly, in such preparations A-lattice interactions that would correspond to seams, were never observed. It was thought that during adsorption and dehydration the microtubules collapsed and flattened, as this process would generate considerable tension on the lateral interactions between protofilaments.

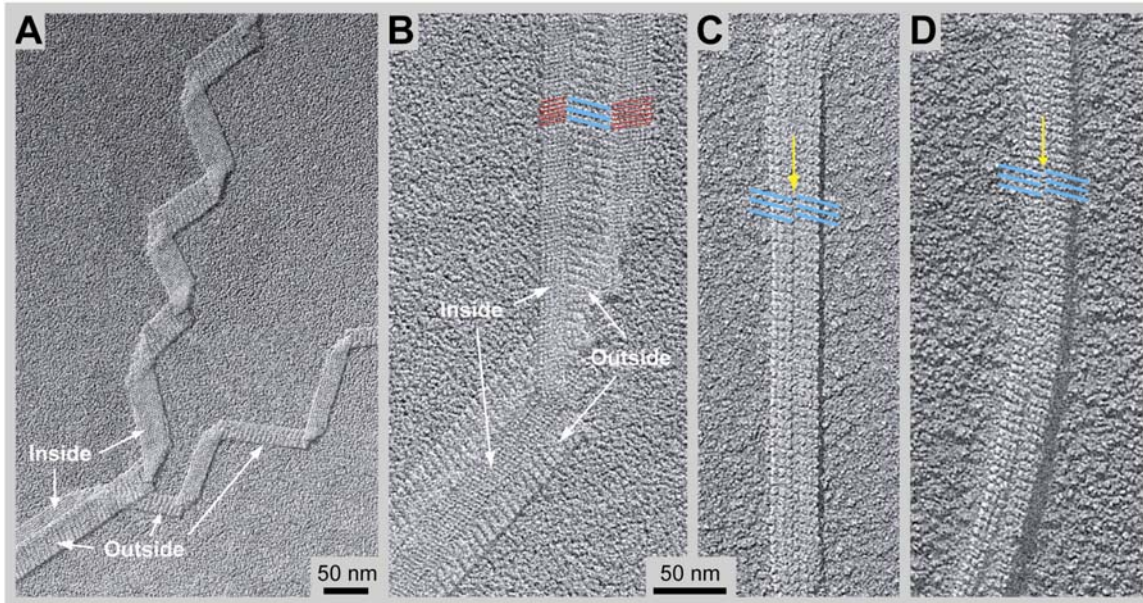


Figure 4.9: Kinesin motor domain decoration revealed the microtubule lattice seams stabilized by Mal3p. Decorations with monomeric kinesin motor domains strongly enhance the axial 8 nm $\alpha\beta$ -tubulin dimer repeat of the outer surface blue lines in (B)-(D). (A) Kinesin decorated microtubules often break into sheets during preparation for high-resolution unidirectional shadowing. (B) A case where three individual sheets remained laterally associated, in the upper part two flanking sheets exposing the microtubule's outer face, while the center sheet exposes the inner face that remains free of motor domains. In the lower right part the entire triplet has folded over and exposing the other corresponding surfaces (white arrows). Since motors do not decorate the inner microtubule surface, the predominant pattern on inner surfaces is the axial 4 nm $\alpha\beta\text{-}\alpha\beta$ monomer repeat (red lines in inset). Typically under the experimental conditions applied in (A) and (B), lattice seams cannot be seen, suggesting that these sheets break apart along the seams. (C) and (D) Kinesin decoration of Mal3p co-polymerized microtubules reveals a large fraction of flattened intact tubes that exhibit a lattice seam (yellow arrows), indicating that in the presence of Mal3p seams are no longer the weakest lateral connection and flattening tubes do not necessarily fold along seams any more.

The dominance of the B- over the A-lattice in microtubules indicates that the lateral interactions between protofilaments are significantly weaker in an A-lattice contact (Sept *et al.*, 2003). Therefore, it was argued that seams, in particular the ones exposed on the upper surface of the tubes, would break during microtubule flattening. This prediction was supported by numerous investigations of motor decorated sheets that never showed seams (Figure 4.9A and B). In contrast, our experiments showed a single row of Mal3p on the outer surface of intact tubes, suggesting that in the presence of Mal3p lattice seams should also be present on those surfaces. To test this we combined the two experiments using microtubules co-polymerized with Mal3p, and we fully decorated them with nK355. In many cases the predominant B-lattice arrangement of nK355 was now clearly interrupted by an A-lattice interaction, revealing a seam (Figures 4.9C and D). This observation not only provides further evidence for Mal3p seam binding but also strongly suggests that Mal3p is stabilizing microtubules by strengthening the lateral protofilament interactions of microtubule lattice seams.

4.4 Microtubule polymerization with GMPCPP and the influence of Mal3p

4.4.1 Microtubule polymerization with GMPCPP under different conditions

The stability and dynamic of microtubules is dramatically changed in the presence of the non-hydrolyzable GTP analog GMPCPP (Hyman *et al.*, 1992; Muller-Reichert *et al.*, 1998). As previously described, we could confirm that in the presence of GMPCPP tubulin polymerization occurs at extremely low concentrations. The critical concentration for nucleation at room temperature with 1 mM GMPCPP was 0.5 μM tubulin and the critical concentration for nucleation of GTP-tubulin was estimated to 20 μM at 37°C (Gaskin *et al.*, 1974; Arnal *et al.*, 2004). We induced rapid polymerization at 37°C and found that at low concentrations (2.2 μM) of tubulin and 1 mM GMPCPP very long microtubules were polymerized (Figure 4.10A and B) while at 22 μM of tubulin many short microtubule seeds were present (Figure 4.10C), but only few long tubes. When microtubules were nucleated in the presence of GMPCPP and 10% DMSO at a high tubulin concentration at 37°C and subsequently dilution to 2.2 μM at room temperature, the dilution enhanced a fast elongation from the seeds and polymers emerge as an open protofilament sheet conformation (Figure 4.10D and 4.11C). In this special polymerization condition about 70% of the microtubule lengths were in the form of open sheets (Figure 4.10D and 4.11C). Sheets were not only found at the ends of microtubules,

but could also be found within a tube as frequent zones where tubes partially opened. The structural characteristic of these polymers was considered as the control for further Mal3p co-polymerization studies (see next section 4.4.2).

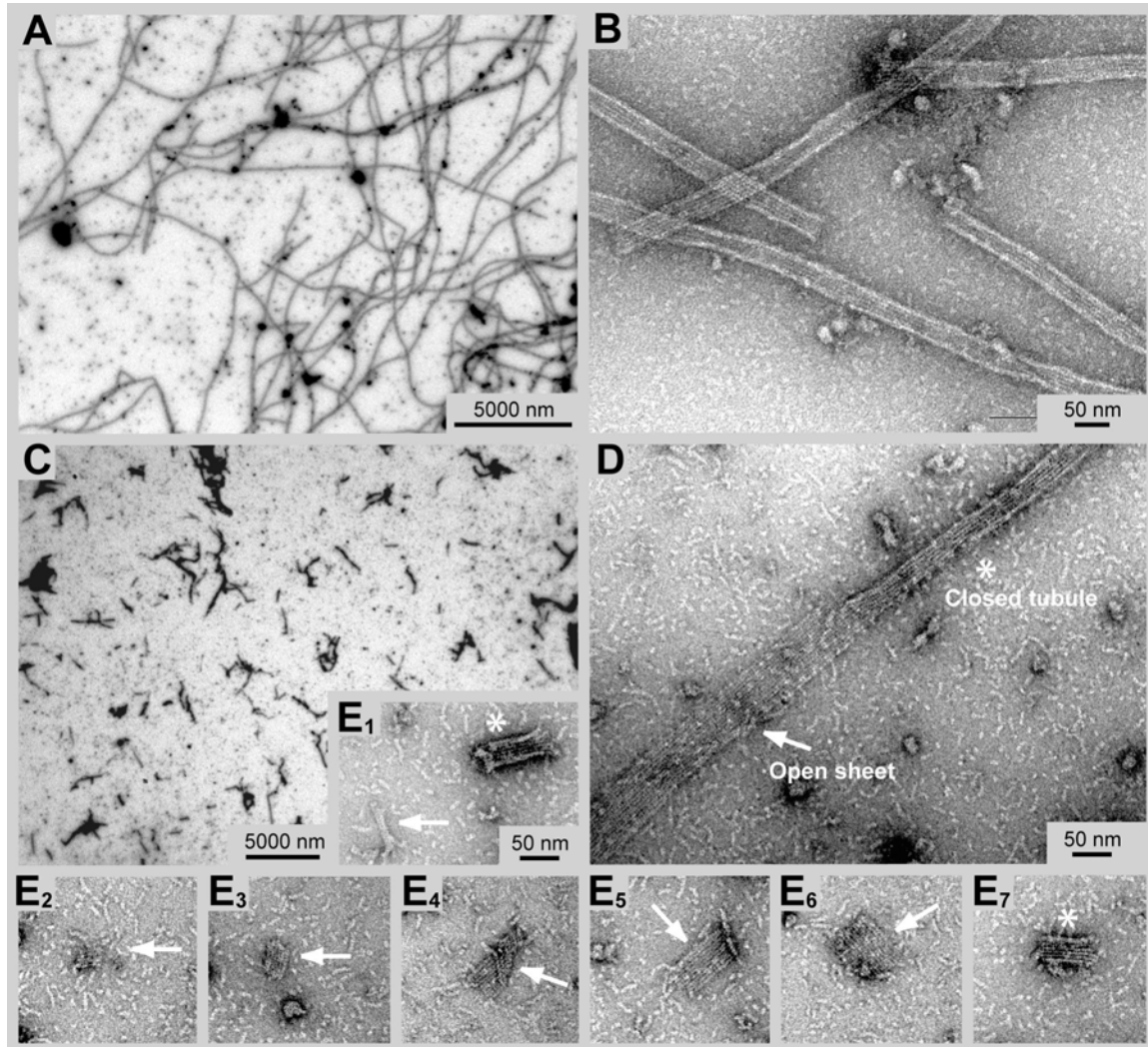


Figure 4.10: Negative staining EM of GMPCPP nucleated and stabilized microtubules. GMPCPP is an extremely effective nucleator. (A) At low tubulin concentrations long microtubules formed, mainly closed with blunt ends (B). (C) Nucleation at high tubulin concentrations resulted in numerous short seeds. (D) Dilutions of the seeds in the presence of DMSO resulted in a general open sheet conformation (which is used as control in the “sheet to tube” transmission assay, see section 4.4.2). (E) Snapshots of tubulin oligomers. A new microtubule nucleates through lateral association of short oligomers into a tubulin sheet, marked with white arrows, to which further oligomers are laterally attached until the sheet is large enough to close into a short tube, marked with white stars (E₁ and E₇).

GMPCPP and DMSO enhanced nucleation gave further insight into the process of microtubule nucleation in the absence of γ -tubulin. With negative staining EM several nucleation and polymerization intermediates were observed (Figure 4.10E₁-E₆). In the background tubulin oligomers, in form of short protofilaments of variable length, ~1-8 dimers, were visible. Tubulin oligomer protofilaments form before microtubules nucleate (Mozziconacci et al., in prep.) and are the product of microtubule depolymerization (Mandelkow and Mandelkow, 1985; Mandelkow *et al.*, 1991). Here we were able to visualize how two short tubulin oligomers associate to form a sheet (Figure 4E₁ marked with an arrow). Further observations supported a nucleation model with lateral addition of short protofilaments into a laterally expanding sheet (sheets of different width highlighted with arrows, Figure 4.10E₂-E₆), which subsequently closes into short cylinders (Figure 4.10E₁ and E₇, marked with stars). Very short seeds of closed microtubules could be found, the smallest with approximately 8 tubulin dimers length.

4.4.2 Mal3p stabilizes a closed conformation of GMPCPP microtubules

The current model of microtubule growth is that sheet-like structures with a B-lattice pattern are first formed at the plus end that eventually close into a tube, thereby forming an A-lattice type seam if lattice constraints make it necessary (i.e. if the lateral interactions and the number of protofilaments are not consistent with B-lattice formation). We used the GMPCPP polymerization system (see section 4.4.1) to further test the effect of Mal3p on tubulin sheet maintenance and/or closure. Here we investigated the structure of GMPCPP microtubule complexed with Mal3p by using EM and analyzed characteristic patterns such as tube versus sheet formation. Copolymerization with 2.5 μ M Mal3p revealed mostly closed tubes (Figure 4.11D-G) while the control, using only tubulin (2.2 μ M), in the absence of Mal3p showed a greater number of open sheets (Figure 4.11A and C). The samples were imaged by cryo- (Figure 4.11A and B) and negative staining EM. Using negative stain EM one can easily discriminate closed-tube and open-sheet configurations and visualize the transition points (Figure 4.11C-G). In the control experiments we observed on average about 32% tube structures versus 68% sheet structures, which was substantially more than in the presence of Mal3p. Even sub-stoichiometric amounts of Mal3p (0.25 μ M Mal3p/2.2 μ M tubulin) raised the percentage of tubes to approximately 68% (Figure 4.11H). Higher amounts of Mal3p further increased the amount of closed tubes to almost 90%. That value was reached at an equimolar ratio of Mal3p to tubulin (2.5 μ M). Therefore, we conclude that Mal3p promotes closed tube formation.

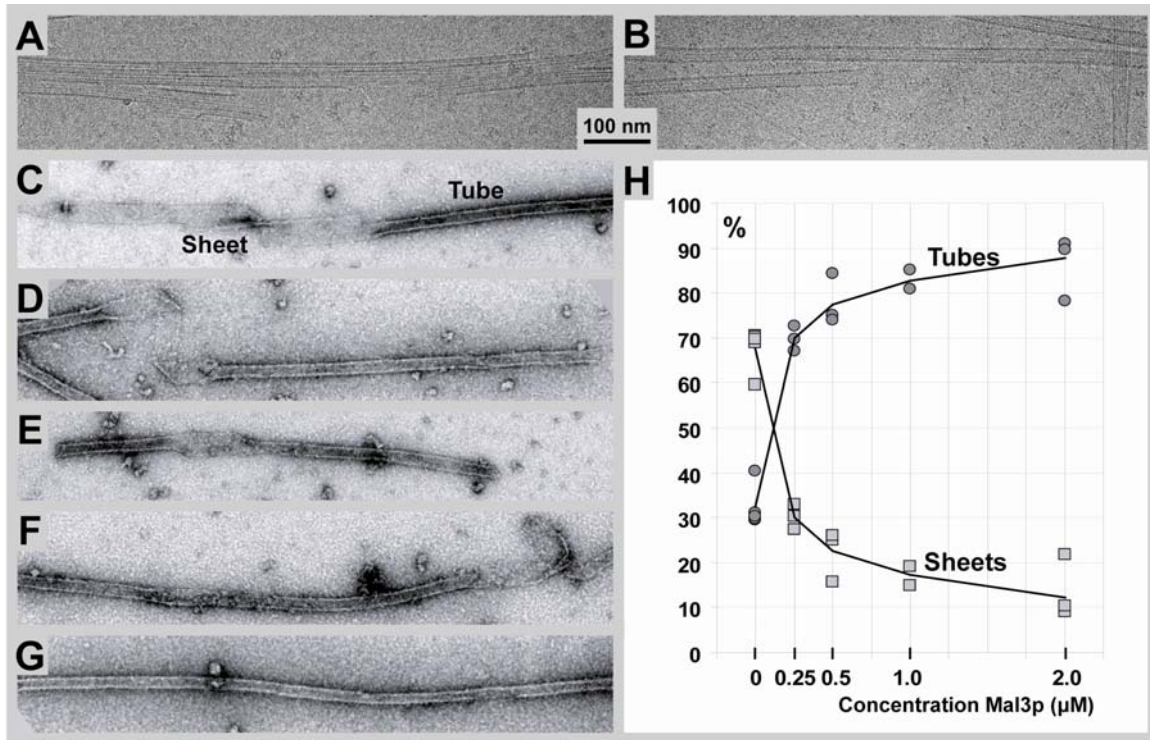


Figure 4.11: Mal3p forces microtubule sheets into a closed-tube conformation. (A) These GMPCPP polymerization conditions favor the formation of open tubulin sheets. By Cryo-EM of GMPCPP microtubules the determination of closed-tubes and open-sheets was impossible, since sheets are randomly arranged and cross over each other in the 3-D ice volume. (B) In the presence of Mal3p microtubules are predominantly closed. (C)-(G) By negative staining EM the sheets and microtubule are flattened onto the carbon on the grids, which make them easy to distinguish. In all preparations the final microtubule concentration was 2.2 mM. Microtubules were polymerized in the presence of GMPCPP with increasing concentration of Mal3p; (C) only tubulin with approximately 70 open-sheet conformations; (D) 0.25 μM Mal3p; (E) 0.5 μM Mal3p; (F) 1 μM Mal3p; (G) 2 μM Mal3p. (H) Graph summarizing measurements of negative staining images. The percentage of tubes and sheets per the total microtubule length were plotted against increasing Mal3p concentration. Every mark represents an individual experiment. With increasing Mal3p concentration, sheets progressively closed into tubes. At 2.0 mM Mal3p, only 12% sheets remain.

4.5 Comparing *S. pombe* endogenous concentrations of tubulin and Mal3p

Until this point all experiments were carried out *in vitro* providing conditions where the microtubule-Mal3p complex could be studied in isolation. However, these conditions did not reflect the concentrations and molecular ratios of a cellular environment. To clarify cellular concentration ratios between tubulin and Mal3p we performed a series of Western blot experiments. By comparing the signal intensity of monoclonal antibody reactivity, we could estimate the amount of each of the two proteins in yeast extract. We compared the wild type *S. pombe* extract concentrations of tubulin and Mal3p to a

dilution series with defined amounts of purified bovine tubulin and recombinant full length Mal3p (see supplementary material 6.3). The yeast extract contained 1.5 μM tubulin and 0.0044 μM monomeric Mal3p. This revealed an approximately ratio of 300:1 tubulin heterodimers to Mal3p monomers, but the experimental procedure applied here has a very large error factor. In fact, the situation *in vivo* is more complicated since this overall ratio does not reflect the actual ratios in specific local compartments of the cell, for example, at the cell tips or the region around the spindle pole bodies (SPB). The concentrations during interphase and mitosis are also likely to be different, since both tubulin and Mal3p are transported into and out of the nucleus during the cell cycle.

4.6 Truncated peptides of Mal3p

4.6.1 Homology, conservation and tertiary structure predictions define the boundaries between protein domains

Members of the EB1 protein family are highly conserved. Fission yeast, *S. pombe* and budding yeast, *S. cerevisiae*, both possess a single EB1 homolog, whereas higher eukaryotes and vertebrates have multiple paralogs. Humans have 3 paralogs, EB1, EB2 (RP1) and EB3 (Su and Qi, 2001), and also possess multiple splice variants that show tissue specific expression patterns. In evolutionary terms, fission yeast and budding yeast are as divergent from each other as they both are from vertebrates (Wood *et al.*, 2002). The situation is similar for the phylogenetic tree of the EB1 protein homologs. The *S. pombe* Mal3p amino acid sequence is 30% identical to *S. cerevisiae* Bim1, 29% to *Drosophila* EB1, 24% to *C. elegans* EB1, 29% to *Xenopus* EB1 and 31% to human EB1. Human and *Xenopus* EB1 are 83% identical, whereas the three human paralogs are more divergent and share only 60% of their amino acid sequence (Figure 4.12).

EB1 proteins are composed of a N-terminal globular CH-domain and a C-terminal coiled-coil domain including an EB1-domain linked together by a very flexible random coil region (Figure 4.13A). These structural properties make crystallization of the full-length protein very difficult. Hence, the globular and coiled-coil domain have been crystallized and solved to atomic detail as individual domains (CH-domain: Hayashi and Ikura, 2003; coiled-coil domain: Honnappa *et al.*, 2005). The N-terminal CH-domain, although also known as an actin binding motif (Gimona *et al.*, 2002), in Mal3p actually serves as a microtubule binding domain (Bu and Su, 2003; Hayashi and Ikura, 2003). The C-terminal acidic coiled-coil region includes the EB1-domain (Hayashi *et al.*, 2005; Honnappa *et al.*, 2005).

To determine conserved regions of the Mal3p amino acid sequence and the protein domains we used the internet-based sequence alignment program MUSCLE to align Mal3p, human EB1 and further members of the EB1-family (Figure 4.12). As expected, we could confirm high sequence similarity between the N-terminal, globular CH-domains of all species. The role of the CH-domain in microtubule binding indicates a highly conserved mechanism for that interaction. In addition, two further extremely conserved sequences were found in the EB1-domains. This domain mediates most of the known interactions with other proteins and its coiled-coil region enables dimerization (Bu and Su, 2003; Honnappa *et al.*, 2005). Accordingly, the nature of EB1-MAP interactions may also be highly conserved. All EB1-family proteins have an extremely acidic C-terminal region that can vary considerably in its distance to the EB1-domain. The least conserved region in EB1 proteins is the flexible region that links the CH-domain with the EB1-domain.

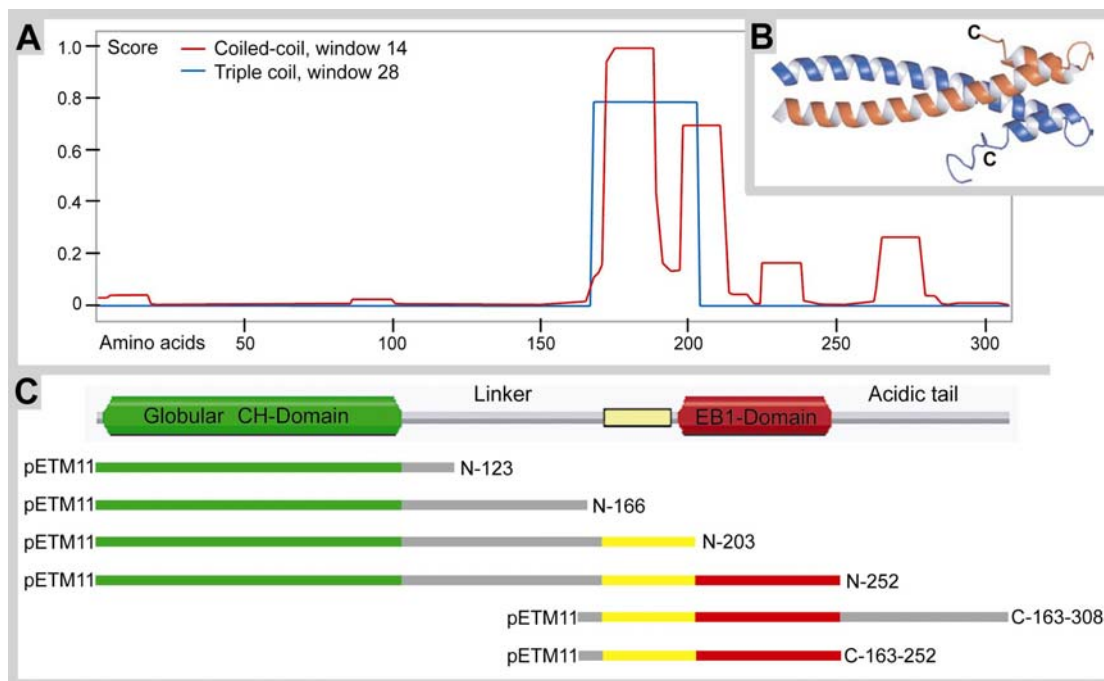


Figure 4.13: Coiled-coil prediction and design of truncated Mal3p expression constructs.

(A) A coiled-coil prediction calculated the probability of the sequence to form an α -helical coiled-coil structure. The red line indicates that Mal3p is very likely to have a coiled-coil conformation after amino acid ~170 and in the first part of the EB-domain. The blue line shows the probability for a triple coil and indicates that Mal3p is likely to interact with other proteins e.g. MAPs in this region. (B) The crystal structure of the EB1-domain of human EB1 (Honnappa *et al.*, 2005). Because of the high sequence homology it is likely that Mal3p also arranges the coiled-coil in to a dimer like human EB1. However, the total C-terminal tail could not be detected in the crystal structure, and Mal3p's longer C-terminal tail is likely to be even more flexible. (C) A graphical view of Mal3p's protein domains compared to all cloned truncated Mal3p expression constructs.

MUSCLE (3.51) multiple sequence alignment

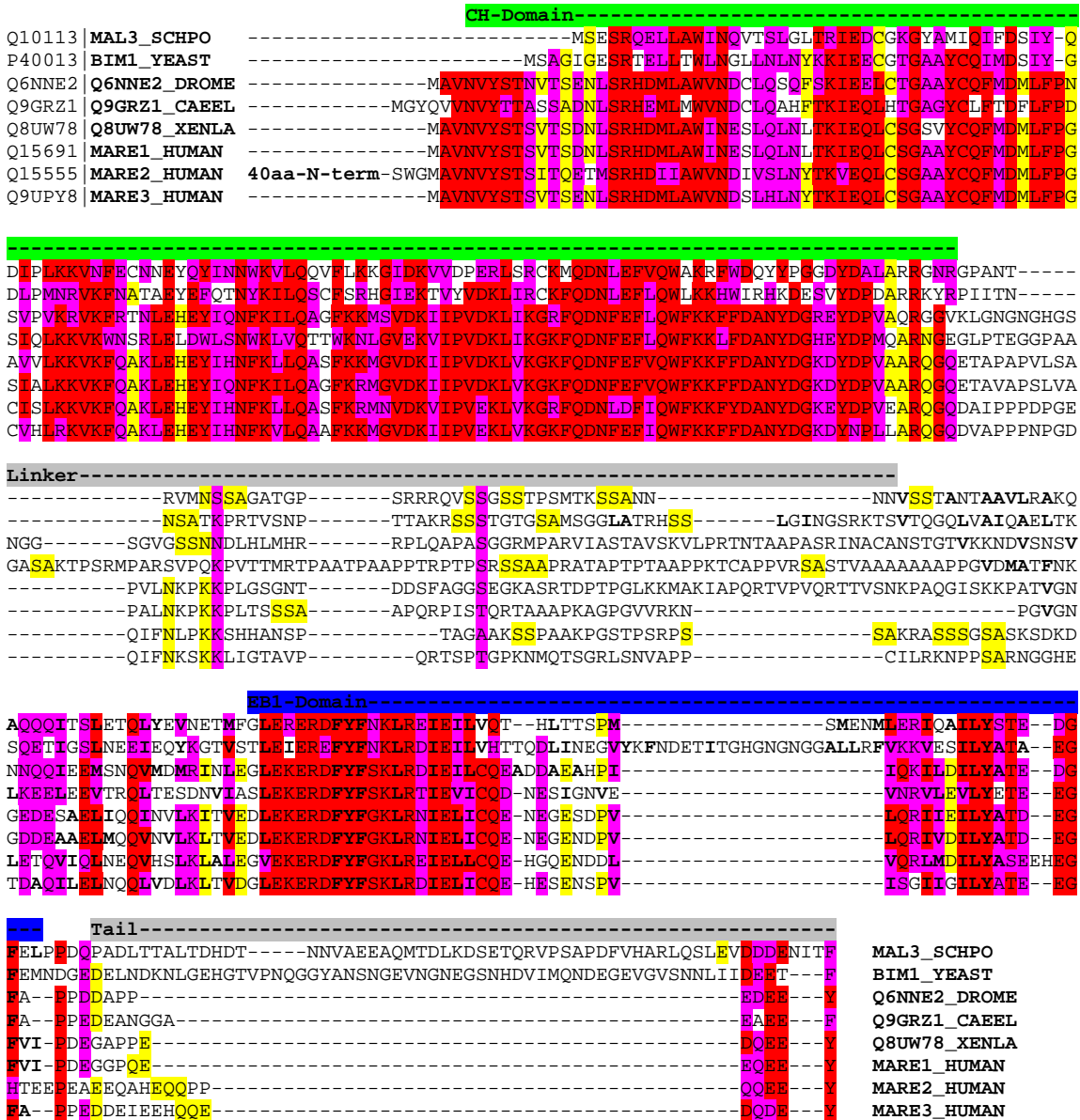


Figure 4.12: Sequence alignment for members of the EB1 protein family. Muscle alignment show high similarities in the CH-domain (green) and in the EB1-domain (blue), but also the last amino acids of the C-terminal tail are extremely conserved among all eukaryotes. Highly conserved residues with identical amino acids are colored red, highly conserved residues of equivalent amino acids are colored pink, less conserved residues, as well as conserved motives in the linker and the tail (both grey) are colored yellow. Hydrophobic amino acids contributing to the heptad in the coiled-coil structure are written in bold. The yeast homologs Mal3p and Bim1 have a slightly smaller EB1-domain, probably a more extended coiled-coil region, and a longer C-terminal acidic tail, then the higher eukaryotic homologs.

Coiled-coil structures are characteristic for their heptad-repeat pattern that places hydrophobic residues at particular positions in the amino acid sequence along the α -helices. Seven amino acids constitute two turns of the α -helix. The repeat in the amino acid sequence at the so-called a and d positions (out of a-g) form a hydrophobic face that forms the contact point between the monomers (bold letters in Figure 4.12), while the other side of the α -helix is predominantly hydrophilic. Mal3p contains longer heptad-repeat sequences than higher eukaryote EB1-family proteins. Bioinformatic predictions for Mal3p revealed a high probability of a coiled-coil region shortly before and within the EB1-domain, with short intercepts that are likely to be stutters, causing short interruptions in the coiled-coil region (red curve in Figure 4.13A). Furthermore, these regions could be a target for additional EB1-MAP interactions as the α -helices show triple interaction tendency (blue curve in figure 4.A). However, due to the high degree of conservation between Mal3p and human EB1, its EB1-domain is likely to be arranged like the human EB1 (Honnappa *et al.*, 2005), (Figure 4.13B). All this information was used for the design of truncation constructs of Mal3p (Figure 4.13C). Eventually, we used similar domain boundaries as previously used in biochemical studies for mapping of the interaction between Mal3p and Tip1p (Busch and Brunner, 2004).

4.6.2 Purification of Mal3p truncated peptides

Expression constructs for all Mal3p truncation proteins (Figure 4.13C and 4.14) were cloned following the same procedures as used for the full-length construct (see section 3.1.1 and 4.1), inserted after a N-terminal His6-tag and a TEV protease cleavage site. These fusion proteins expressed very efficiently and were purified similarly to the full-length Mal3p (see section 3.1.2-3 and 4.1). All N-terminal constructs were further purified for structural analysis by gel-filtration. This method gave us an estimation of the size and oligomerization property of the different Mal3p constructs (Table 4.1). Like the full-length Mal3p, the construct Mal3p-N-252 also eluted in a wide peak mimicking a much larger protein complex than it actually was. We believe this is due to the very flexible conformation of a dimer. All the shorter N-terminal constructs eluted within a relatively distinct peak at a large elution volume (V_e) respectively. The gel-filtrations show that Mal3p-N-203, N-166 and N-123 are monomers. Figure 4.14 shows SDS-PAGE analysis of all Mal3p constructs. However, to date of all constructs Mal3p-N-203 has given us the most interesting results with EM. In the following last part of the results section primarily this protein construct is discussed. The other constructs will be investigated in the future.

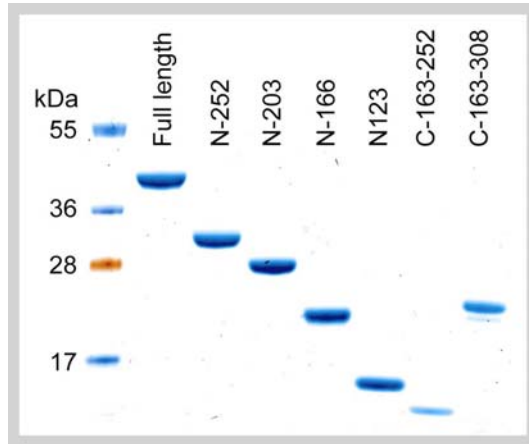


Figure 4.14: SDS-PAGE of all purified Mal3p constructs. All constructs could be purified without contaminations and degradations, visualized by coomassie staining.

Table 4.1: Theoretical and experimental data concerning all Mal3p constructs							
Mal3p construct	Full-length	N-252	N-203	N-166	N-123	C-163-252	C-163-308
Theoretical size (kDa)	35.0	28.8	23.1	18.8	14.5	10.4	16.6
Theoretical Isoelectric point	5.0	6.0	9.0	9.2	7.6	4.5	4.3
Theoretical extinction coefficient (for A_{280} , (mg/ml) \cdot 1 cm $^{-1}$)	1.0	1.2	1.4	1.7	2.2	0.37	0.23
Gel-filtration elution volume, V_e (ml)	66.5	70	86	89	96	-	-
Estimated molecular size (kDa)	160	120	29	22	12	-	-

4.7 Mal3p-N-203 microtubule binding

Full-length Mal3p has been demonstrated to be an extremely potent microtubule nucleator and stabilizer. Mal3p-N203 has the same microtubule binding domain, the CH-domain, as the full-length protein. It includes the flexible linker as well as the first coiled-coil segment, but this segment was not enough to dimerize Mal3p-N-203. Additionally Mal3p-N-203 lacks the EB1 domain and the acidic tail. Mal3p-N-203 could not associate with other MAPs (Busch and Brunner, 2004). But how important is dimerization for Mal3p function? Surprisingly, we found Mal3p-N-203, unlike the full-length version decorates microtubules *in vitro* over the entire lattice and not only along the seams. Hence, a more detailed analysis of this truncated protein may give further insight into the mechanisms involved in seam-specific binding of full-length Mal3p.

4.7.1 Turbidity

To examine the microtubule nucleation and stabilization capacity of Mal3p-N-203 we performed the same turbidity experiment as for full-length Mal3p (see section 4.2.1). We recorded the absorption at 350 nm of polymerizing microtubules in solution over time with 10 μM dimeric Mal3p or 20 μM monomeric Mal3p-N-203. (Since the Mal3p effect is concentration dependent, small variations in absorption can be caused by errors in concentration measurements. The concentration measured at OD_{280} is based on theoretical extinction coefficient values, and might vary from the extinction coefficient of the folded protein.) 22 μM unstabilized microtubules nucleated slowly and reached a maximal value after approximately 15 min, which then decreased slightly (black curve in Figure 4.15). Mal3p-N-203 facilitated microtubule nucleation and stabilized at approximately the same level as the full-length protein. This demonstrated that the fast nucleation caused by Mal3p was not a cross-linking effect caused by Mal3p dimers linking adjacent microtubules.

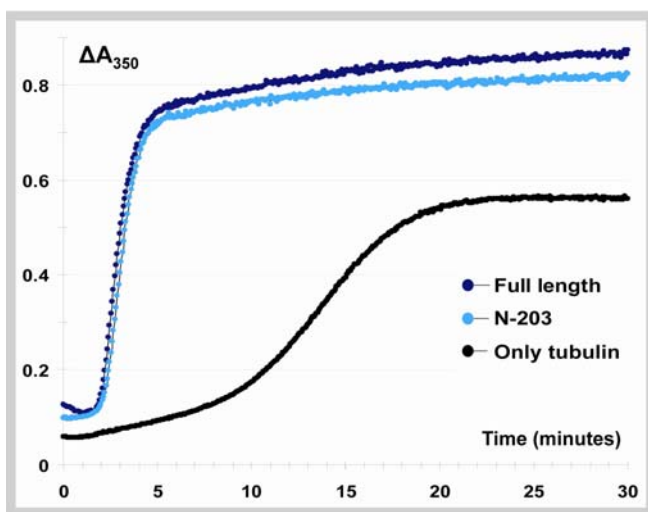


Figure 4.15: Monomeric Mal3p-N203 and full-length Mal3p had a similar influence on microtubule polymerization. 22 μM tubulin polymerized at 37°C. The black curve shows the turbidity as a function of time of a tubulin reaction in the absence of any binding factors. Full-length Mal3p (dark blue) and Mal3p-N-203 (light blue) are equally effective promoters of nucleation and stabilizers of the dynamic reaction. In the presence of any form of Mal3p the amounts of microtubules continue to increase and do not reach a stable plateau.

4.7.2 Cryo-electron microscopy of microtubules co-polymerized and decorated with Mal3p-N-203

To visualize the microtubule structure under influence of Mal3p-N-203 we used the same method as for analyzing the full-length protein. Samples of polymerized tubulin and Mal3p adsorbed to holey carbon film coated grids were vitrified by plunging them into liquid ethane. Cryo-EM of vitrified samples reveals the true protein density without staining and supporting film. 22 μM tubulin (without taxol) was co-polymerized with 60 μM Mal3p-N-203, and diluted 1:2 in pre-warmed BRB80 quickly before freezing. These

conditions were equivalent to the turbidity measurements (see section above 4.7.1), and microtubules polymerized very well and were stabilized by Mal3p-N-203 (Figure 4.16A). Further more, taxol-stabilized microtubules decorated with Mal3p-N-203 were imaged with cryo-EM, comparison of the undecorated microtubules (Figure 4.5A-C and 4.16B) with Mal3p-N-203 decorated tubes revealed that decoration became visible through somewhat darker edges in the projection (Figure 4.16D-C), indicating the presence of additional protein all over the tubular surface. 20-30 μM monomeric Mal3p-N-203, incubated 3-5 minutes with 3.4 μM microtubules before plunging saturated the entire microtubule surface (Fig. 16D-C).

Co-polymerization, of Mal3-N-203 and tubulin or decoration of taxol-stabilized microtubules revealed no difference within the structure of the Mal3-N-203-microtubule complex. Closed microtubules co-existed with long and straight protofilament sheets. Occasionally, a tube separated into independent sheets, some of which were only two parallel protofilaments wide (Figure 4.16A and C, marked with arrow). As taxol-stabilized microtubules were generally closed before addition of Mal3p-N-203, the truncated form of Mal3p seemed to break lateral protofilament interactions and open up microtubules into sheets. Interestingly, the Mal3p-N203 stabilized sheets remained straight after splaying apart from a closed tube. They did not curve like depolymerizing GDP protofilaments or GMPCPP sheets (Mandelkow *et al.*, 1991; Muller-Reichert *et al.*, 1998). Certainly, the acidic C-terminal tail and the EB1-domain (which were deleted in this construct) influence Mal3p's binding properties, even if the actual binding site is at the CH-domain (Gimona *et al.*, 2002; Hayashi and Ikura, 2003).

4.7.3 Helical reconstruction of undecorated, Mal3p-N-203 and *Neurospora* Kinesin-355 decorated microtubules

The globular motor domain of many kinesins and MAPs like Tau bind repeatedly to the microtubule lattice. This property enables structural determination by cryo-EM (Beuron and Hoenger, 2001). While helical 3-D analysis of microtubules incubated with full-length Mal3p was unsuccessful due to its specific affinity for the microtubule lattice seam, the truncated construct Mal3p-N-203 behaved very differently. This construct lacked the C-terminal tail and lost its specificity for the seam but rather decorated the entire surface. Achieving complete decoration now allowed us to use a 3-D helical reconstruction approach.

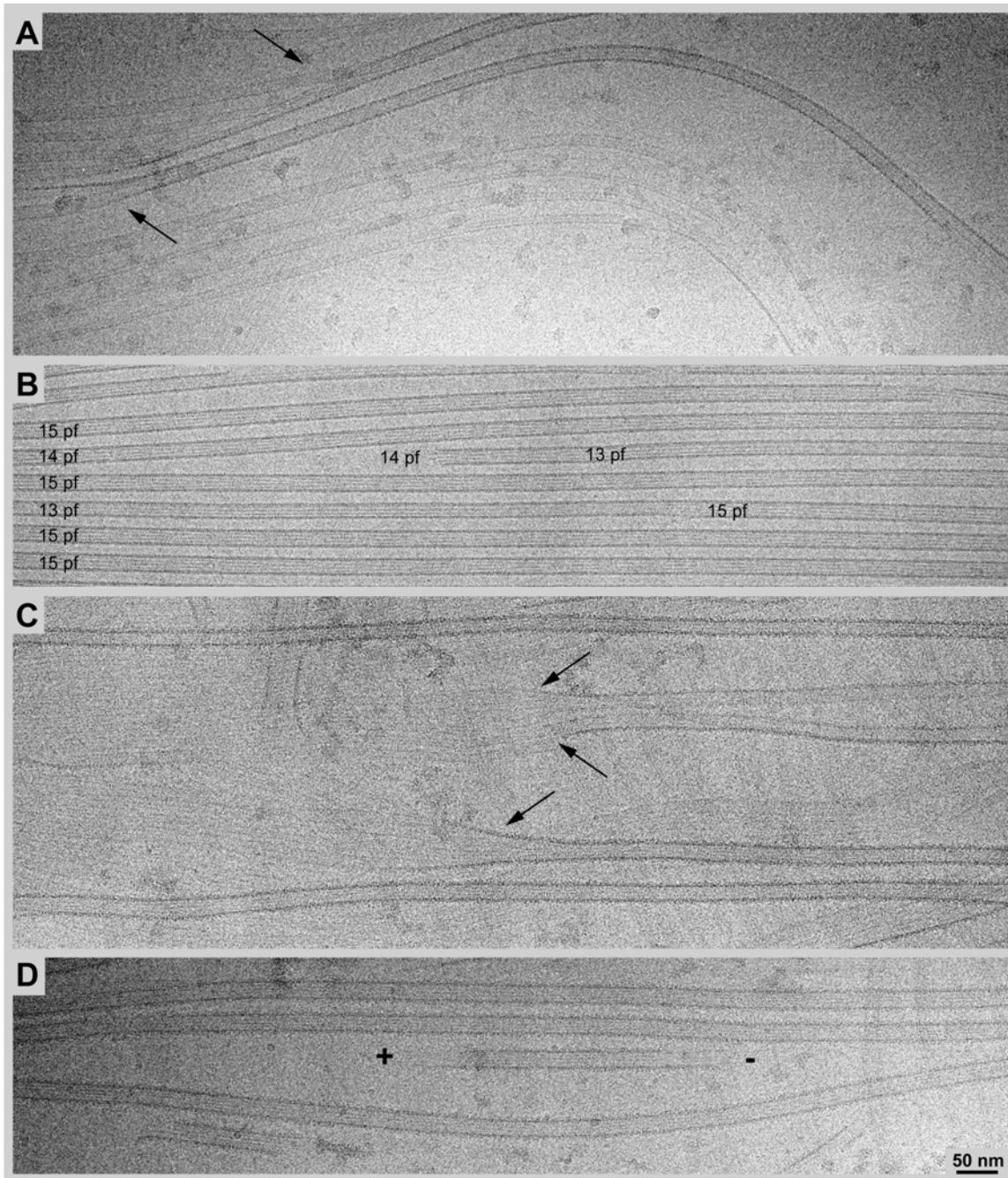
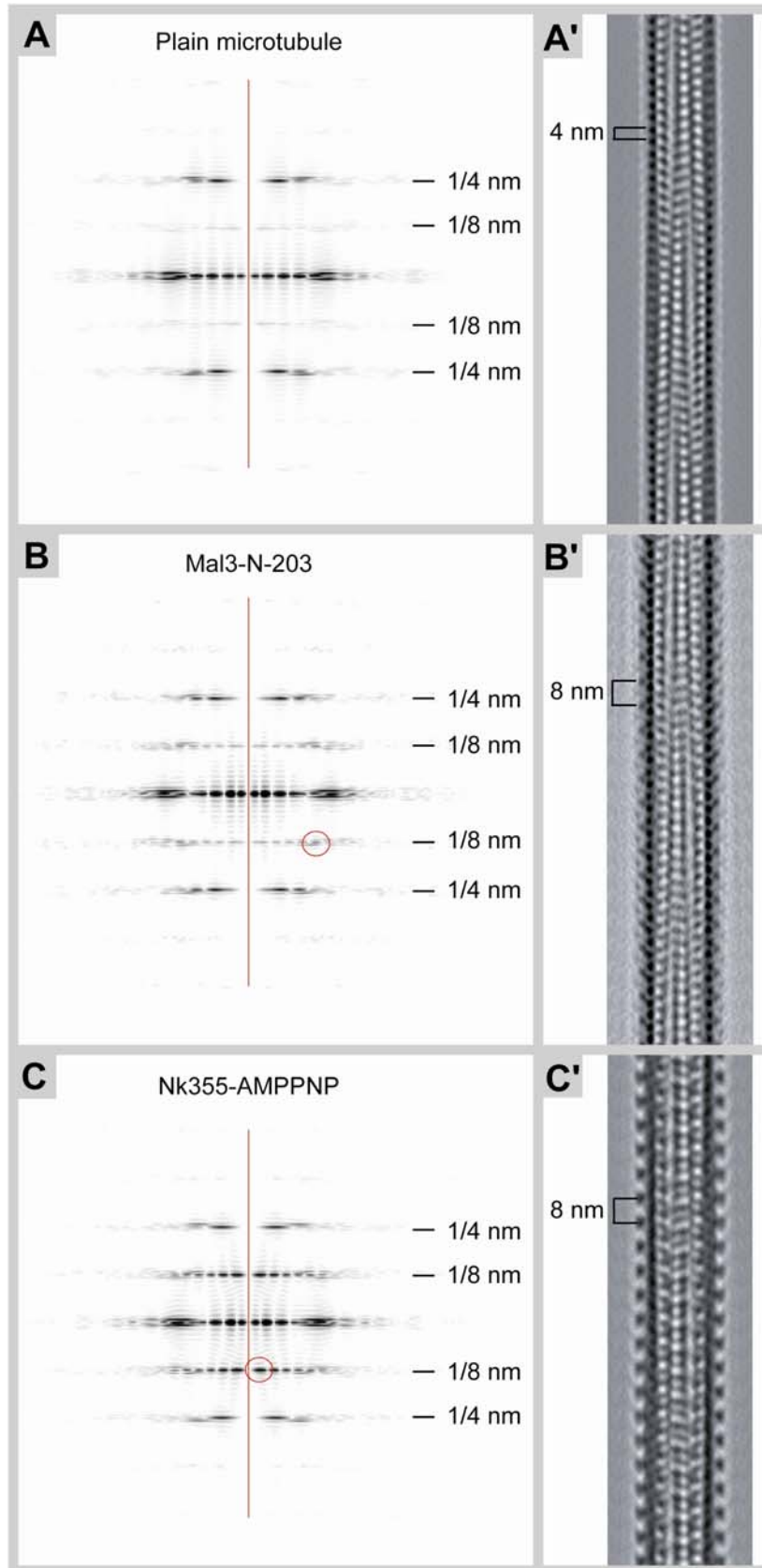


Figure 4.16: Cryo-EM of microtubules in complex Mal3p-N-203. (A) Tubulin co-polymerized with Mal3p-N-203. (B) Taxol-stabilized undecorated microtubules, the number of protofilaments (pf) were determined according to the observed Moiré Pattern (Chretien *et al.*, 1996). In two of these microtubules shifts in protofilament number were observed. (C and D) Pre-polymerized stabilized microtubules decorated with Mal3p-N203 at 1:8 stoichiometry. Decorated microtubules were used for 3-D helical reconstruction. In samples, both with Mal3p-N203 co-polymerized and with decorated microtubules, some closed microtubules and a large number of long and straight protofilaments were observed. Transitions from closed tubes to open sheets were common (black arrows in (A and C). In (D) black + and - indicate the polarity of a short seed, both ends are in the form of short straight sheets.

Diffraction patterns of individual microtubule decorated with Mal3-N-203 showed a weaker intensity peak at the 1/8 nm layerline cluster than microtubule-motor complexes, but still significantly higher than that of native microtubules. The concentration for optimal stoichiometric binding was approximately 8 Mal3p monomers per tubulin heterodimer. This mix was incubated 3-5 minutes in BRB80. Images of nK355 decorated microtubules in the presence of AMPPNP, kindly provided by Dilem Hizlan (EMBL-Heidelberg, now MPI for Biophysics, Frankfurt, Germany) were used to compare the binding pattern of a conventional kinesin motor domain with that of the truncated Mal3p. Control images of undecorated microtubules were processed the same way. Averaging of all three data series and 3-D reconstruction resulted in three very different structures. Both Mal3p-N-203 and nK355 decoration data were aligned to the undecorated average. Finally, ~37.000 asymmetric units went into the undecorated microtubule reconstructed structure, ~11.000 into the mal3p-N-203 structure and ~16.000 into the nK355 structure

Real space 2-D projections from the 3-D averaged volume (Figure 4.17A'-C') and Fourier space diffraction data (Figure 4.17A-C) clearly showed the repeating characteristic of plain and decorated microtubule averages. NK355 decorated microtubules showed a very strong 1/8 nm layerline cluster that corresponded to the regular motor domain binding to each $\alpha\beta$ -tubulin dimer with an 8 nm axial repeat along protofilaments (Figure 4.17C and 4.18C). NK355 motor domains place themselves further from the tubulin center than Mal3p-N-203, which locates more into the groove between protofilaments (Figure 4.17B and 4.18B). The 1/8 nm layerline of the Mal3p-N203 decoration was weaker, but still much more pronounced than in plain microtubules (Figure 4.17). Figure 4.19 show the amplitudes and phases of selected characteristic layerlines from the diffraction pattern of the three averaged maps.

Figure 4.17: Averaged 3-D reconstructions of microtubules visualized as diffraction patterns of the Fourier transforms and 2-D projections. (A) Undecorated microtubules have a strong 4 nm repeat representing every tubulin monomer. The minor difference between α - and β -tubulin is almost invisible in the 1/8 nm cluster of the diffraction pattern. (B) Mal3p-N-203 decorated microtubules exhibit a weak but significant 8 nm repeating density representing the CH-domain. (C) Kinesin motor domain nK355 decorated microtubules exhibit a strong 8 nm repeat according to the large globular motor domain interacting with every β -tubulin. Noteworthy is that the strongest intensity (marked with red circle) in the 1/8 cluster in the nK355 diffraction pattern is close to the meridian (red line), but in the Mal3p-N203 diffraction pattern the strongest intensity is far away from the meridian (see also the layerlines in Figure 4.19). In the 2-D projection of the reconstructed volumes (right column A'-C') the supertwisted protofilaments from both sides give rise to the Moiré pattern. The clearly visible arrow like pattern is characteristic of a 15 protofilament microtubule. In this right handed supertwist helix the arrows point towards the plus end. See next page.



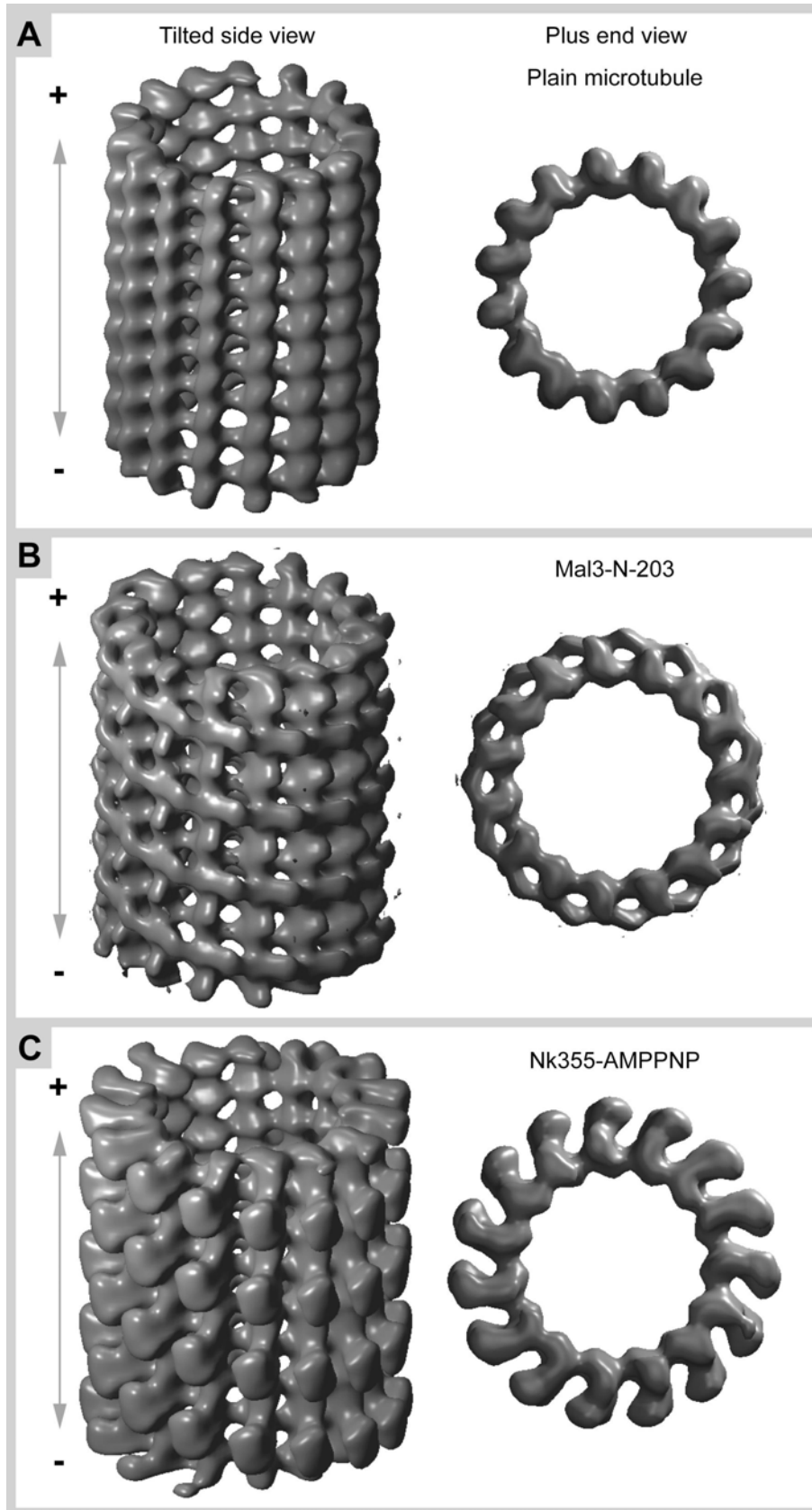
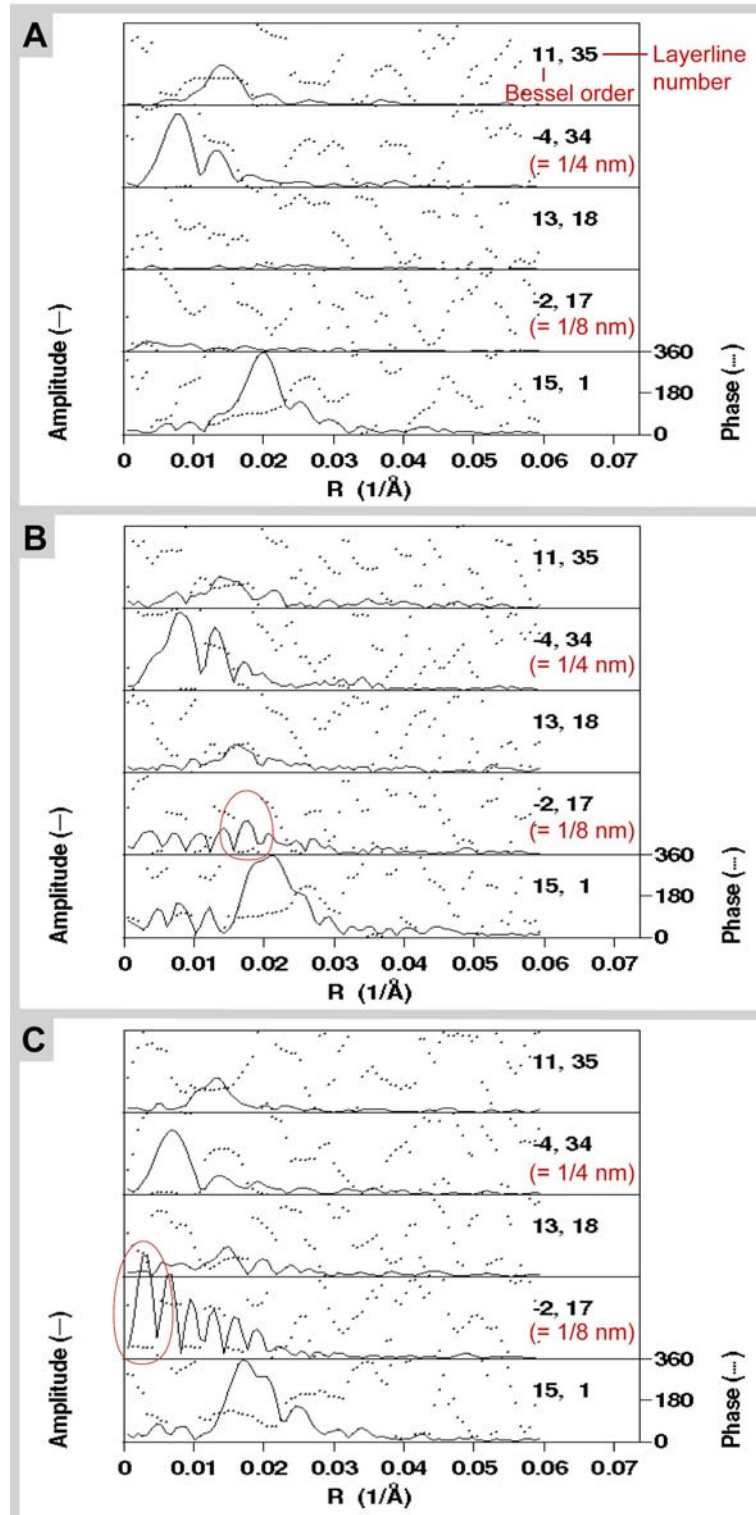


Figure 4.18: Helical 3-D reconstruction of microtubules, visualized as isosurface rendering of the averaged electron density. The polarity of the microtubules is indicated as + and -, with the plus end pointing upwards in the side view, and towards the observer in the end view (In this plus end view the protofilaments of the microtubule point counter clock wise). (A) Undecorated microtubule, with 15 protofilaments, each globular tubulin subdomain is visible in the tight longitudinal interaction of the protofilaments, the minor difference between α - and β - tubulin is visible as different sized windows between the lateral interaction, large and slightly smaller windows repeat every 8 nm. (B) Mal3p-N-203 decorated microtubules exhibit a globular protein density between the protofilaments. This particle, which we consider likely to be the CH-domain, interacts with one subunit on each neighboring protofilament, bridging the protofilaments repetitively every 8 nm. The first level of noise appears 4 nm away from the strongest density in the supertwist direction, indicating an occasional miss-averaging of CH-domains, likely to be caused by seam interruptions in the B-lattice. (C) The kinesin motor domain nK355 decorated 3-D reconstruction show that this conventional kinesin binds microtubules at a different interaction site than Mal3p (Original data for the nk355 reconstruction was kindly provided by Dilem Hizlan). These monomeric globular domains bind to one interaction region on the outer surface of the protofilaments. See previous page.

In Figure 4.18 the reconstructed 3-D electron density maps were visualized as a 3-D isosurface volume, observed from a tilted side view (Figure 4.18 left column) and a plus end view (Figure 4.18 right column). In this visualization the supertwisted microtubule protofilaments and the individual monomers present the microtubule architecture at approximately 2 nm resolution. Mal3p-N-203 binds in between the protofilaments (Figure 4.18B), similarly to the full-length protein, although the full-length protein binds specifically only to the seam protofilament groove (see section 4.3.2-2). Currently we believe that the mass attributable to the truncated version of Mal3p is in fact one globular CH-domain at each 8 nm position while the linker sequence itself, including the short stretch of α -helix from the EB1-domain is too flexible to be visualized by averaging techniques. In its position within the groove between protofilaments the CH-domain bridges tubulin dimers laterally. These findings imply that a Mal3p monomer has two different microtubule binding sites on each side of a protofilament. This is very different from the kinesin binding site that is on top of the outer protofilament surface in close proximity to helices H11 and H12 of β -tubulin (Figure 4.18 C), (Hoenger *et al.*, 2000b; Song *et al.*, 2001). This could mean that Mal3p and kinesin both may bind at the same time in close proximity, without competing for space on the microtubule surface and Mal3p would not interfere with kinesin-mediated transport.

Figure 4.19: Selected layerlines from the averaged helical 3-D reconstructions. The amplitudes (continuous line) and phases (dotted line) are plotted as functions of the radius in the diffraction patterns. (A) Average of undecorated microtubules; (B) Mal3p-N203 decorated microtubules; (C) Conventional kinesin motor domain nk355 decorated microtubules. The phase is stable when the amplitude is high but may flip 180 degrees where amplitudes go to zero. Both the Mal3p-N203 average and the nk355 average were aligned to same phase as the plain microtubule average. Bessel order 15 represents the supertwist of the 15 protofilaments. Bessel order - 2 represents the tubulin dimer left-handed helix in a B-lattice. Bessel order 13 is the convolution

of 15 and -2. Bessel order -4 represents the monomeric subunit left-handed helix. Bessel order 11 is the convolution of 15 and -4. The undecorated microtubule has low amplitude and an almost random phase in layerline 17, Bessel order -2. The Mal3p-N203 and nk355 exhibit stronger 8 nm repeating features, which correspond to higher amplitude in this layerline. Interestingly, the highest amplitude of the Mal3p-N-203 map found at a longer radius (R) than the highest amplitude of the nk355 map, marked with red circles.



5 Discussion

This thesis provides an important step towards further understanding of the structure and function of microtubule plus end tracking proteins (+TIPs). Microtubule +TIPs play a crucial role in regulating microtubule dynamics within the cell (Akhmanova and Hoogenraad, 2005). Here we investigated in detail the structure and function of Mal3p, the fission yeast, *Schizosaccharomyces pombe*, homolog of mammalian EB1 (Su *et al.*, 1995; Beinbauer *et al.*, 1997; Tirnauer *et al.*, 2002b) and as such, a member of the highly conserved EB1 protein family. This work revealed an entirely new and unexpected molecular mechanism of how Mal3p interacts with the microtubule lattice and how microtubule dynamics and stability are regulated in a very economic fashion: Mal3p is capable of specifically recognizing the microtubule lattice seam and thereby stabilizes the potentially weakest lateral interactions between protofilaments in a microtubule extremely effectively and with minimal perturbation of the remaining microtubule surface. This discovery was only made possible by preparing specimens for EM by a high-resolution metal shadowing procedure that took advantage of a unique cryo-vacuum transfer setup operated at the ETH-Zürich (Switzerland) by the group of Dr. H. Gross. By applying this method, we found that Mal3p binds to the microtubule along a single line and in between two protofilaments most often at 8 nm intervals but also at 16 nm or 24 nm intervals (Figure 4.6). The occasional occurrence of a double seam in *in vitro*-polymerized microtubules allowed us to demonstrate that these lines of Mal3p do indeed correspond to a lattice seam. While microtubules typically exhibit so-called B-lattices, adjacent lines of Mal3p densities matched that of an A-lattice, a geometry that defines the lateral interaction between protofilaments at seams (Figure 4.8).

The conclusion that Mal3p binds preferentially to lattice seams is further supported by the finding that in the presence of Mal3p the lattice seams become stabilized. This can be visualized indirectly by fully decorating microtubules with kinesin motor domains that enhance the 8-nm repeating structure of the underlying tubulin lattice. In absence of Mal3p seams have never been observed, neither on flattened tubes nor unfolded sheets, presumably because they are too weak to withstand the shearing forces created during preparation that flatten the microtubules. In the presence of Mal3p, however, the seam is maintained and becomes visible as a typical 4 nm shift between two adjacent protofilaments in the otherwise regular arrangement of motor heads (see Figure 4.9). Reinforcement of the microtubule lattice by Mal3p is further supported by findings showing that Mal3p is capable to induce microtubule protofilament sheets to close into

cylindrical tubes (Figure 4.11). The last lateral protofilament interaction when sheets close to tubes was suggested to be the lattice seam (Chretien *et al.*, 1995; Chretien *et al.*, 1999).

The EB1-domain and the dimerization process of Mal3p are not directly involved in stabilization of microtubules; we detect similar nucleation and stabilization capacity for the full-length protein and a truncated version of Mal3p containing only the first 203 amino acids of the protein, Mal3p-N-203. The Mal3p-N-203 construct, which lacks most of the C-terminal EB1-domain is capable of interacting with the entire microtubule lattice independent of lattice conformation. We discovered a stochastic binding of Mal3p-N-230 to the microtubules, and were able to reconstruct the 3-D structure of a CH-domain-decorated microtubule (Figure 4.17-19). The structure proposes microtubule stabilization through cross-binding over two adjacent protofilaments, which implies that each Mal3p-N-203 molecule features two separate microtubule binding sites.

5.1 Mal3p binds and stabilizes microtubules *in vitro*

5.1.1 Turbidity studies reveal polymerization kinetics

Several biochemical approaches were used to study the kinetics of Mal3p microtubule interactions *in vitro*. First, we recorded turbidity as a measure of tube formation during microtubule nucleation and the first 30 minutes of polymerization. This method is based on the principle that polymers, in this case microtubules, scatter light of 350 nm wavelength more strongly than monomers. This is a traditional method, which was used to explore the fundamental properties of microtubule polymerization, for example the tubulin concentration-dependent nucleation and growth rate (Gaskin *et al.*, 1974). We used a stable tubulin concentration, and variable Mal3p concentrations, ranging from a 10:1 to 1:1 ratio of tubulin to Mal3p (Figure 4.2). Increasing Mal3p raises the total amount of polymerized tubulin, however, the nucleation rate remains the same. Even minute amounts of Mal3p trigger a much higher nucleation rate than tubulin alone, but this rate does not change much at higher Mal3p amounts. Interesting, is the slow increase of microtubules over the entire time in the presence of Mal3p, compared to the slow decrease of polymers after reaching the maximum in absence of Mal3p (Figure 4.2). The control polymerization experiment with only tubulin is dynamic, and microtubules polymerize at high free tubulin concentrations until the free tubulin dimers are used up. Depolymerization makes recycling of tubulin dimers possible, as long as GTP is present. In the turbidity curve the consumption of GTP is visualized as a slow depolymerization.

Possibly, Mal3p stabilizes microtubules and makes them less dynamic. In stabilized microtubules the “turn-over” is lower and if Mal3p recruits new dimers to the ends, even at low free tubulin concentrations, the total amount of polymers will continue to increase, albeit slowly.

Turbidity analysis is a measurement of the total amount of polymers above a certain size. We do not know what the critical size or shape to induce scattering is. Furthermore, we cannot measure any kind of length distribution, nor can we distinguish sheets from closed tubes. With this experiment we showed that recombinant Mal3p in BRB80 buffer exhibits similar functional properties to the native protein in a cellular environment (Busch and Brunner, 2004). It is indeed remarkable that Mal3p promotes microtubule growth without any additional MAPs present.

It is possible that Mal3p and other EB1 family members are regulated differently. Fission yeast does not have the same MAP repertoire as found in higher eukaryotes. In contrast to our findings for Mal3p, EB1 has previously been shown not to nucleate microtubules, but rather to increase polymerization from microtubule (GMPCPP-stabilized) seeds (Ligon *et al.*, 2003; Hayashi *et al.*, 2005). In the same experiments EB1 nucleation rate and stabilizing activity was enhanced by the presence of p150^{Glued}, a +TIP known to activate EB1 through interaction with the EB1-domain. In another study the interaction with APC, also an EB1 interacting +TIP, activates EB1 or Mal3p to enhance microtubule polymerization (Nakamura *et al.*, 2001). Nakamura and colleagues used N-terminal GST-fusion proteins and claim that Mal3p alone cannot induce microtubule polymerization. According to our experience, N-terminal labeling of Mal3p without a linker sequence between Mal3p and the tag inhibits its ability to bind microtubules, but not MAP interactions *in vivo* as well as *in vitro* (unpublished data). The use of protein tags in the previous experiments in addition to the different protein ratios could explain the variable results and prohibits a direct comparison of these studies in detail.

5.1.2 Mal3p binding to taxol-stabilized microtubules

EB1 from cell extract (Berrueta *et al.*, 1998), as well as recombinant EB1, has been shown to co-pellet with taxol-stabilized microtubules (Tirnauer *et al.*, 2002b). However, it has been demonstrated *in vitro* and *in vivo* that EB1 family members do not appear to associate with soluble tubulin (Tirnauer *et al.*, 2002b; Gache *et al.*, 2005). A direct biochemical interaction between free tubulin dimers and MAPs is difficult to observe, for example it not possible to measure by calorimetry (ITC), since tubulin dimers tend to

oligomerize and this interaction interferes with the result. We found that Mal3p binds to taxol-stabilized microtubules *in vitro*. From a constant pool of Mal3p, the fraction of microtubule-bound Mal3p increased with a rising tubulin concentration. To bind the pool of Mal3p in a sample more than 8 times more tubulin than Mal3p was necessary, which is shown as the plateau of the binding curve (Figure 4.3). From this result we concluded that full-length Mal3p does not bind stoichiometrically to tubulin dimers in the microtubules lattice. According to the globular structure of Mal3p, it is also unlikely that a Mal3p molecule would cover more than 2 tubulin dimers, e.g. unlike the elongated and flexible Tau molecule that contains up to four separate microtubule binding sites (Littauer *et al.*, 1986; Mukrasch *et al.*, 2007). It seems more likely that the binding sites for Mal3p are limited on the microtubule surface. Further EM experiments confirm this prediction, and show Mal3p preferentially interacts with the rare A-lattice conformation that exists only at the lattice seam. *In vivo* this would imply one or more Mal3p per 13 tubulin dimers. However an exact estimation of the binding ratio of tubulin to Mal3p is not possible as microtubule protofilament and seam numbers may vary *in vitro*.

5.2 Mal3p microtubule interaction is not detectable using cryo-electron microscopy

Several cryo-EM approaches to visualize recombinant full-length Mal3p binding to microtubules were initially implemented. Neither pre-polymerized microtubules decorated with an abundance of Mal3p in the solution nor co-polymerization of Mal3p and tubulin revealed Mal3p molecules interacting with microtubules. We used a 3-D helical reconstruction approach, based on averaging of asymmetrical subunits from several complete helical 15 protofilament microtubules (Beuron and Hoenger, 2001). At first it was quite puzzling that we could not find any interaction between Mal3p and microtubules, since we could observe binding to taxol-stabilized microtubules and growth promoting activity on dynamic microtubules. However, further high-resolution unidirectional shadowing experiments showed a specific seam binding pattern (Figure 4.6-4.8), which explained our negative results on the seamless helical 15-protofilament microtubules. Accordingly, these microtubules were not able to bind full-length Mal3p along the closed microtubule wall.

The advantage of using cryo-EM is that the native structure of macromolecular assemblies is preserved within milliseconds of freezing, in a frozen-hydrated state. Micrographs of vitrified samples show a 2-D projection directly obtained from protein density. We fixed microtubules during the onset of polymerization by plunge-freezing

directly from a 37°C humidity chamber. In the absence of any stabilizing factors microtubules exhibit long extending plus end sheets during polymerization (Chretien *et al.*, 1995; Chretien *et al.*, 1999). In contrast, Mal3p co-polymerized microtubules grow faster, and they also have almost exclusively blunt plus ends (Figure 4.5). In these preparations we rarely found 15 protofilament microtubules, but encountered mainly 13 and 14 protofilament microtubules. This could imply that Mal3p forces the microtubule to close with smaller angles between the protofilaments, as is reported for the neural microtubule stabilizer DCX (Moore *et al.*, 2004). Alternatively, Mal3p may preferentially co-polymerize with microtubules that exhibit a mixed A- and B- lattice (Wade *et al.*, 1990; Sosa and Milligan, 1996; Dias and Milligan, 1999), which would strongly reduce the occurrence of helical 15 protofilament microtubules. Further studies support the second alternative: the presence of Mal3p induces mixed lattices (see section 5.6).

5.3 Geometry of interaction of dimeric Mal3p with the microtubule lattice seams

High-resolution unidirectional shadowing EM reveals exclusively the surface of a sample with high contrast. Images of microtubules show the surface with 2-3 nm resolution. The protofilaments and the tubulin monomers are clearly recognizable by this method. Also, the short curved protofilaments, representing polymerization and depolymerization intermediates are visible in the background on the carbon surface (Figure 4.6). The continuous axial rim of protofilaments on the outer surface of a microtubule is clearly distinguishable from the more corrugated inner surface. From the inside, the geometry of the left-handed tubulin monomer helix with a 10° inclination is unambiguously identifiable, but appears right-handed on inside views (Figure 4.9A and B). The structural differences between α - and β -tubulin are too small to be visible on the surface of an undecorated microtubule, which makes it impossible to distinguish between A- and B- lattices. However, the use of kinesin motor domains that bind regularly to every β -tubulin on the outside of a microtubule strongly enhances the contrast of the tubulin dimer 2-start left-handed helical path (Hoenger *et al.*, 2000a).

5.3.1 Mal3p observed by unidirectional shadowing

We used two experimental approaches to visualize recombinant Mal3p in complex with microtubules: Microtubules were co-polymerized with an abundance of Mal3p and taxol, and Mal3p were decorated on pre-polymerized taxol-stabilized microtubules. Samples were unidirectionally shadowed with Ta/W that revealed a “pseudo 3-D” image of the surface of microtubules in the presence of Mal3p. Both preparation methods produced

very comparable results, confirming that Mal3p does not bind to microtubules through co-polymerization with tubulin. These images revealed arrays of particles within the groove of two adjacent protofilaments. These particles were clearly attributable to Mal3p, the only MAP present in the experimental setup.

Detailed analysis of the microtubule surface provided the first evidence for a seam binding preference of Mal3p. Globular particles were bound to one single groove per tube and in between two protofilaments on the microtubule lattice (Figure 4.6). There is essentially only one structural feature within the microtubule lattice that is different between two adjacent protofilaments as compared to the rest of protofilament interactions, and this is the lattice seam (see section 2.6.4.6). The seam constitutes an axial line on the microtubule which potentially provides very distinct binding properties for MAPs on the microtubule surface that are different from the remaining lattice (Kikkawa *et al.*, 1994; Song and Mandelkow, 1995). In our observations Mal3p is typically found along one single protofilament groove per tube, and the smallest axial repeat between particles is 8 nm, corresponding to the axial tubulin repeat. Mal3p binding may leave smaller or larger gaps in multiples of the 8 nm repetition but still continues in the same groove (figure 4.6). We rarely observe switches from one protofilament groove to the next, and even more rarely do we see variations in the number of lines of Mal3p binding. In an *in vitro* microtubule polymerization experiment occasionally microtubules change protofilament number within an intact tube and include minor lattice defects, (Chretien *et al.*, 1992). Accordingly, this could produce lateral dislocation of the seam or introduce one or two more seams on the same microtubule, as we observed in Figure 4.6 and 4.8. Unidirectional shadowing only visualizes one side of a cylindrical structure, the side away from the carbon support film. Microtubules polymerized *in vitro* exhibit a high degree of uncontrolled variation of protofilament number (Figure 4.16B). In addition, the number of seams per microtubule has been shown to vary in kinesin-decorated microtubules, from zero to three (Sosa and Milligan, 1996; Dias and Milligan, 1999). More seams are theoretically possible, but energetically not favorable (Sept *et al.*, 2003). Therefore, it is likely that in many cases we may not detect Mal3p binding because the seam is on the “back side” of the microtubule.

5.3.2 Mal3p matches the geometry of the seam

To our advantage, we found a case where two parallel protofilament grooves were decorated at the same time. The exposed geometry of the two parallel binding sites for Mal3p represents the geometry of a microtubule A-lattice conformation (Figure 4.8). An

A-lattice was originally proposed to be the conformation of the A-subtube, and the B-lattice the conformation of the B-subtube in microtubule doublets that can be found in cilia and flagella (Amos and Klug, 1974). However, decorating microtubules with kinesin motor heads revealed that the A-lattice is only present at seams and possibly at the interaction between A- and B-subtubes (Song and Mandelkow, 1995). Geometrically, a microtubule of 13 protofilaments, if it wants to adapt the least possible protofilament supertwist, has to form at least one lateral interaction of the A-lattice type to close into a cylinder (Wade *et al.*, 1990). Seams with an A-lattice conformation have been visualized by freeze-fracturing of both *in vitro* microtubules and mouse nerve cell microtubules decorated with kinesin motor domains (Kikkawa *et al.*, 1994) and by cryo-EM of kinesin-decorated microtubules analyzed by a backprojection 3-D reconstruction (Sosa and Milligan, 1996). In the case of Mal3p co-polymerization we cannot determine the conformation of the entire underlying microtubule, unlike with regular kinesin decoration. The inclination between two lateral Mal3p particles is 38° when following a right-handed helical twist. The smallest lateral stagger is approximately 3 nm and the highest is approximately 4 nm. As Mal3p along one protofilament always maintains 8 nm repeats or multiples of 8 nm, we assume that the interaction site is defined by two adjacent dimers interacting with A-lattice geometry, and therefore Mal3p must exhibit significant affinity for both, α - and β -tubulin, although on two separate interaction faces. Although the flattening of the hollow cylinder during the preparation for shadowing the geometry of a microtubule helical turn is slightly disordered, the geometry of the Mal3p particles still matches the predicted A-lattice configuration perfectly. The higher inclination and the right-handedness is clearly an A-lattice conformation (Figure 4.8). All these observations strongly support the conclusion that Mal3p preferentially binds to the microtubule lattice seam. In the previous decoration studies with kinesin motor heads, double seams were also observed (Kikkawa *et al.*, 1994; Sosa and Milligan, 1996). For this interpretation we assume that the rest of the microtubule exhibits a B-lattice conformation, to which Mal3p must have much less affinity to than to the seam.

5.3.3 Orientation of a dimeric Mal3p along the seam

The Mal3p binding sites along a seam repeat at intervals of minimally 8 nm, which corresponds to the length of an $\alpha\beta$ -tubulin dimer. High-resolution surface shadowing does not reveal very accurate values for the volume of a particle protruding from a surface. However, judging by their size and shape, the particles observed on microtubule surfaces (Figures 4.6-8) appear to represent a single CH-domain rather than an entire dimer. We combined the crystal structures from the human Mal3p homolog EB1 CH-

domain (Hayashi and Ikura, 2003) and the C-terminal α -helical dimerization domain (Honnappa *et al.*, 2005), and we modeled possible binding configurations, taking into account the long and flexible linker between the CH-domains and the dimerization motive (Figure 5.1A). Hence, a dimeric construct could theoretically occupy two binding sites. According to our model, these two binding sites may not necessarily be next to each other because the flexible linker between the CH-domains and the C-terminal coiled-coil region is composed of a rather unstructured 50 residue polypeptide that may reach between two binding sites that are separated by more than 8 nm (Figure 5.1B).

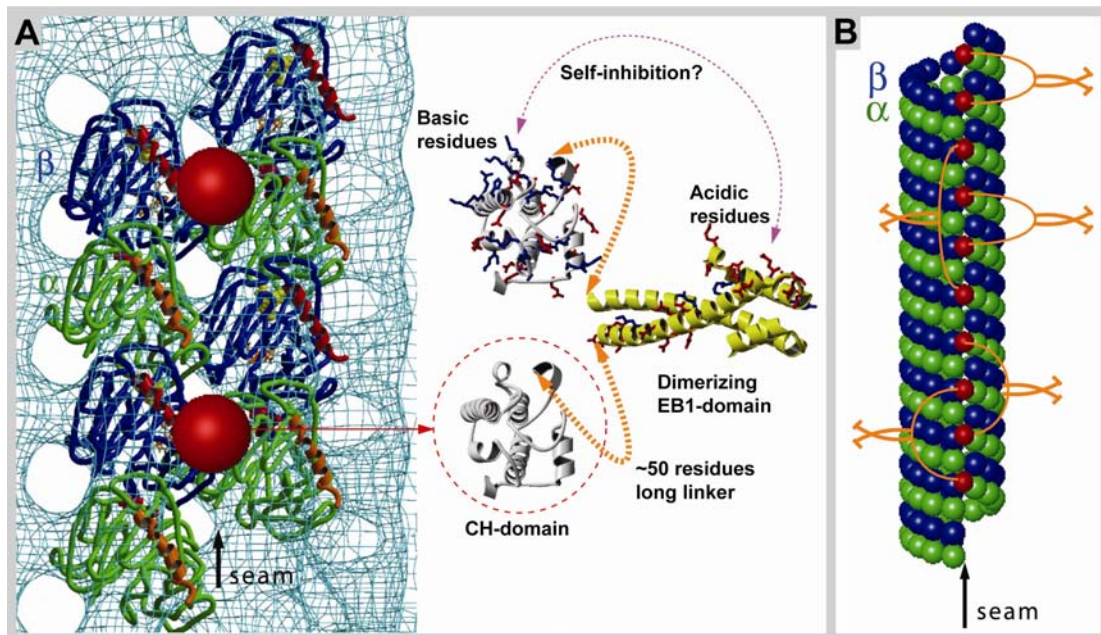


Figure 5.1: Model of the Mal3p dimer and its binding along the microtubule lattice seam. (A) EB1 protein family members form a homodimer. Crystal structures were obtained from the human Mal3p homolog, EB1. The globular structure of a single CH-domain (Hayashi and Ikura, 2003) was modeled as a dimer together with the coiled-coil C-terminal domain (Honnappa *et al.*, 2005). According to this model, the CH-domain and the C-terminal domain of Mal3p are connected by about 50 amino acids that presumably form a rather flexible linker. The size of the individual dots found on our shadowed images must represent single CH-domains. Accordingly, one dimer can occupy two different binding sites on the microtubule surface. Its preference for the microtubule lattice seam suggests that the CH domain, through its highly basic region, contacts two adjacent protofilaments in a way that creates a better binding environment in a seam than in a B-lattice interaction. As indicated, Mal3p binding repeats every 8 nm along a groove between protofilaments, but we cannot say if the position shown is correct or shifted by 4 nm on the tubulin heterodimer. (B) Model of Mal3p binding to the microtubule lattice seam. Mal3p could occupy two adjacent binding sites, but because of the flexible linker it may also span larger distances.

5.3.4 Selective binding rather than cooperative binding

Kinesin motor proteins sometimes bind to the microtubule lattice in a cooperative fashion (Wendt *et al.*, 2002). EM observations have shown microtubules in the same sample, where kinesin preferred to fully decorate one particular microtubule while others remained undecorated (Vilfan *et al.*, 2001; Hizlan *et al.*, 2006). This was described as a cooperative effect, where the binding of one kinesin molecule changes the microtubule surface in a way that increases the affinity for further motors to bind. Mal3p binds like a string along one protofilament groove with a constant repeat in short sequences. This could be the result of a cooperative effect during binding, where one associated Mal3p molecule opens up this protofilament groove, thereby enhancing the probability of another Mal3p binding to the next pair of tubulin dimers along the same groove. However, after a gap in the string of 8 nm repeating Mal3p binding, the next string of Mal3p particles generally stays on the same protofilament groove. As all protofilament grooves do not have the same affinity for Mal3p, this cannot be explained only as a cooperative binding effect, but rather that Mal3p selectively bind the seam.

5.4 A Novel mechanism for microtubule stabilization

A B-lattice, where lateral interactions between adjacent protofilaments occur from α - to α -tubulin and β - to β -tubulin, is energetically more favorable than an A-lattice, where subunits alternate (Sept *et al.*, 2003). However, to form a microtubule with 13 protofilaments, which is most common in nature (Tilney *et al.*, 1973), it is geometrically necessary that at least two protofilaments interact with an A-lattice conformation; this is the lattice seam (Wade *et al.*, 1990). The seam only occurs if lattice constraints make it necessary, and therefore it has been proposed that during polymerization the seam is formed at the final closing of the tube (Chretien *et al.*, 1995; Chretien *et al.*, 1999). Unfortunately, the lattice cannot be visualized directly since the microtubule lattice is only visible in combination with molecular motor domains or MAPs; accordingly this sheet closure model has to be seen as speculative.

Most described MAPs stabilize microtubules through protecting the protofilaments from curling outwards as they usually do during depolymerization (Mandelkow *et al.*, 1985). For example, XMAP215 and Tau bind to several interaction sites on the microtubule surface, keeping protofilaments in a straight conformation (Cassimeris *et al.*, 2001; Al-Bassam *et al.*, 2002; Santarella *et al.*, 2004). This is a somewhat opposite mechanism to that of microtubule destabilizing molecules like stathmin, colchicine and vinblastine that force protofilaments into curls and trigger disassembly (Ravelli *et al.*, 2004; Gigant *et al.*,

2005). The MAP doublecortin (DCX) is an exception compared to this classical model of stabilization created by filamentous proteins. DCX, a globular protein, crosslinks the protofilaments in a protofilament number dependent way (Moore *et al.*, 2004), without specificity for microtubule A- or B-lattice.

5.4.1 Mal3p stabilizes the microtubule lattice seam

Mal3p appears to use a similar mechanism when it comes to bridging protofilaments laterally, but it uses a novel strategy that enhances microtubule stability selectively at its weakest site. Because Mal3p, like its homologs in other organisms, accumulates at the plus ends of growing microtubules, it was assumed that it controls microtubule dynamics at this location. Our results raise an intriguing alternative and suggest that Mal3p may stabilize microtubules by reinforcing the lateral interaction of the two seam protofilaments, thereby “clamping” the seam together. Obviously this function does not rule out an additional stabilizing role for Mal3p at the growing plus ends.

The Hoenger group has performed numerous microtubule decoration experiments with different kinesin motor domains (Hoenger *et al.*, 2000a; Hizlan *et al.*, 2006; Krzysiak *et al.*, 2006), but seams have never been observed (Figure 4.9, and section 4.3.4). Apparently, the lateral interactions of the seam were too weak to stand the mechanical stress the microtubules encounter during adsorption onto a carbon film. The globular motor domains strongly facilitate the visualization of the B-lattice of the underlying microtubule, and therefore, seams, if they were present should be recognized easily. The situation changed significantly when Mal3p was present: Microtubules co-polymerized with Mal3p followed by decoration with the motor domain of the conventional *Neurospora* kinesin nK355 still flattened onto the carbon coated grid surface, but they did not break preferably at the seam anymore. Now, Mal3p stabilized the weakest lateral interactions and seams appeared as interruptions in the B-lattice on the surface (see Figure 4.9).

5.4.2 Mal3p causes a closed microtubule conformation

In standard *in vitro* polymerization reactions microtubules are generally closed tubes, even if the fast growing plus ends have been observed as an open sheet. The conformation and the closed and open states cannot be totally manipulated but can be significantly influenced by the buffer composition. We used GMPCPP-induced nucleation and stabilization and found a “tube closure” sensitive polymerization condition, where only 30% of the polymers had a closed conformation. Mal3p induced

closure during polymerization and increased the amount of closed cylindrical tubes to 90% of all polymers.

We used negative staining and cryo-EM to image GMPCPP-stabilized microtubules with and without Mal3p. It turned out to be impossible to analyze the control condition statistically in the cryo-EM images, because these images are projections of microtubules randomly organized in the ice volume; overlaying or tilted sheets were not possible to analyze as individual microtubules (Figure 4.11). In contrast, negative staining was not only easier and faster to perform, but this method resulted in images that simplified this analysis. With negative staining, microtubules are dried flat onto the carbon coated grids (Figure 4.11). The defined angle of lateral protofilament interactions defines the cylindrical curvature of a polymerizing sheet. For example a “c”-shaped structure, was likely to dry as a sheet and closed parts of the same microtubules remained closed even if the segments were very short. These two structures would be impossible to separate on cryo-EM images. The quick preparation and the simple image analysis made it possible to analyze a large total microtubule length. Also, the fact that all EM imaging and image analyzes were carried out blind made this an unbiased, reliable method.

5.5 Molecular interactions on the microtubule

Full-length Mal3p interacts specifically with the microtubule lattice seam and with high-resolution unidirectional shadowing EM we find the globular molecules in the protofilament groove on the microtubule surface (Figure 4.6). However, atomic interaction studies are not suitable with this method. A frequently used method to gain 3-D information of microtubules and motor proteins or MAPs at high resolution is cryo-EM and helical 3-D reconstruction (Beuron and Hoenger, 2001). However, helical methods failed in the case of microtubule-Mal3p complexes since full-length Mal3p does not decorate microtubules stoichiometrically.

To further investigate Mal3p microtubule binding properties we performed a series of experiments with Mal3p truncation constructs. Deletion of the C-terminal of Mal3p causes the protein to lose its specificity for the microtubule lattice seam, and it now decorates the entire microtubule wall. This makes a structural analyze of the CH-domain through helical based averaging possible.

5.5.1 Mal3p-N-203 binds the entire microtubule wall and no longer shows A-lattice specificity

Helical 3-D reconstruction of 15 protofilament microtubules decorated with Mal3p-N-203, reveals a globular protein density in between the protofilaments (Figure 4.17B and 4.18B). This protein bridges the protofilaments every 8 nm, so every tubulin dimer has one interaction with adjacent subunits. The volume of the protein density in this map is comparable to the CH-domain of Mal3p. The protofilament groove localization seems identical to the localization in the groove of the seam observed for the full-length protein with shadowing EM.

However, something in the EB1-domain and the last acidic amino acids of the tail makes this truncated construct less likely to associate with the predominantly occurring B-lattice, so that seam interactions are preferred. Theoretically, the difference must be that full-length Mal3p preferentially bridges A-lattice interaction protofilaments connecting one α -subunit and one β -subunit with every CH-domain and that the Mal3p-N-203 also is able to connect the same subunit type in a B-lattice, e.g. α - α or β - β . According to the high structural homology between α - and β -tubulin these interactions could be similar, but obviously not identical.

A speculative explanation is for example that the charge distribution on a A- or B-lattice could be different, since β -tubulin exhibits a longer and more charged tail than α -tubulin (Tuszynski *et al.*, 2006). These charges in a B-lattice could prevent an interaction with the C-terminal of Mal3p by electrostatic repulsion, as Mal3p also has a charged tail as tubulin.

5.5.2 Does Mal3p associate with α - or β -tubulin

Kinesin motor domains interact with β -tubulin (Song and Mandelkow, 1993), Tau binds along the protofilament but displays its highest density in its interaction with α -tubulin (Santarella *et al.*, 2004). It is not known which subunit EB1-family proteins preferentially associate with. At the seam Mal3p interacts with both α - and β -tubulin. When the reconstructed map of Mal3p-N-203 and nK355 decorated microtubules were aligned to the same undecorated microtubule map, it was seen that Mal3p-N203 interacts with the same subunit as nK355. This indicates a Mal3p interaction with the β -tubulin subunit. However, the alignment is not a totally reliable method when the data sets are as diverse as Mal3p and nK355, because the structural differences between α - and β -tubulin give rise to very weak signals, which may be obscured by the strong signal of symmetrical

decoration. In contrast to our rather weak indications, an α -tubulin mutation in the fission yeast *atb2* gene (amino acid replacement V260I) was described to result in an altered Mal3p interaction with the microtubules (Asakawa *et al.*, 2006). If α -tubulin is essential for proper Mal3p localization this mutation may be part of the Mal3p interaction surface, however no direct subunit associations have been demonstrated. Chemical cross-linking and co-decoration experiments with Mal3p-N-203 and Kinesin are certainly necessary to solve this open issue.

5.5.3 Stabilization of lateral protofilament interactions

The free binding energy is lower in a B-lattice, the general microtubule conformation, than in an A-lattice, the conformation of the seam. The differences are mainly caused by the “stickyness” of the M-loops, dependent on composition of charges and conformation, and this is influenced the neighboring N- and L-loops of tubulin (Sept *et al.*, 2003; Drabik *et al.*, 2007). For example, taxol effects the conformation of the M- and N-loops of β -tubulin and has a stabilizing effect on the lateral interactions. The CH-domain has no direct interaction with the M-loop and the helix H3 region on the neighboring subunit, but binding in close vicinity to this region may also influence the conformation and “stickyness” of the M-loop. Interestingly, Mal3p interacts with tubulin in close proximity to this region. Possibly, Mal3p especially enhances the stability of the weakest α - β -tubulin interactions, thereby causing a more stable seam.

5.5.4 Intramolecular regulation of EB1 family proteins

Full-length Mal3p forms a dimer in solution. The structure of this dimer is extremely flexible, as shown by gel-filtration. The C-terminally-deleted expression construct Mal3p-N-203, remains monomeric but the microtubule binding potential remains. The C-terminal EB1-domain is essential for interactions in the +TIP network (Bu and Su, 2003; Busch *et al.*, 2004; Honnappa *et al.*, 2006).

It has been speculated that EB1-family proteins may have a self-inhibitory mechanism. With the flexibility of the long linker region, the acidic C-terminus could reach over and interact with the basic CH-domain and prevent the CH-domain from interacting with microtubules. EB1s microtubule growth promoting effect was proposed to be enhanced by the presence of other MAPs, e.g. APC and p150^{Glued} (Nakamura *et al.*, 2001; Hayashi *et al.*, 2005). According to this model, other MAPs would release Mal3p from its self-inhibition. This mechanism was proposed to be similar to another structurally related (but not homologous) MAP CLIP-170, as demonstrated with scanning force microscopy. Full

length CLIP-170 forms a ring shaped structure with the C-terminal binding to the N-terminal globular microtubule binding domains (Lansbergen *et al.*, 2004). We detect an effective microtubule growth promoting capacity for full-length Mal3p, and this effect is not altered when C-terminal truncated versions of Mal3p are used (Figure 4.15). However, the cellular regulation of Mal3p is also likely to be achieved by different post-translational modifications (Busch and Brunner, 2004; Peth *et al.*, 2007) which were not taken in to consideration in these experiments .

5.5.5 The EB1-domain and dimerization are not necessary for microtubule stabilization

Surprisingly, we found that the C-terminal EB1-domain was dispensible for Mal3p's microtubule growth-promoting capacity. Indeed, the C-terminal truncated construct Mal3p-N-203 exhibited equivalent nucleating and stabilizing properties as the full-length Mal3p (Figure 4.15).

It was previously shown that a point mutation (I224A) in the EB1-domain rendered the protein unable to dimerize (Slep *et al.*, 2005). With this mutation it was demonstrated that post-translational modifications like phosphorylation and protection against proteolytic degradation are dependent on dimerization (Peth *et al.*, 2007). Though dimerization seems to be important for cytoplasmic stability or cell cycle regulated activity. We could demonstrate by turbidity analysis that dimerization is unnecessary for microtubule nucleation and stabilization *in vitro* (Figure 4.15). This function is managed by the CH-domain and the linker only.

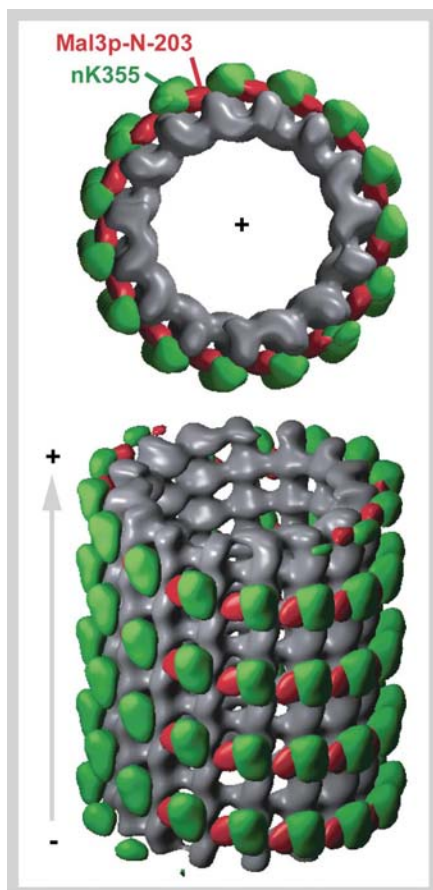
5.5.6 Microtubule nucleation *in vitro*

In vivo microtubules nucleate from γ -TuRC complexes (Raynaud-Messina and Merdes, 2007), which recruit the subunits and serve as a template for 13 protofilament microtubules. *In vitro* nucleation also occurs without the γ -TuRC complex. When nucleation and polymerization of microtubules were induced by GMPCPP we were able to observe several intermediate oligomeric tubulin states from tubulin dimers to closed tubular seeds. Finding short oligomers associating laterally into sheets, these would close after reaching a certain width (Figure 4.10E). As full-length Mal3p and Mal3p-203 promote the nucleation and initial growth phase, (Figure 4.15), one could speculate that Mal3p plays a role in the assembly of the nucleation intermediates *in vitro*. Since Mal3p associates with both sides of a protofilament it might recruit oligomers to each other, and facilitate the closure of a sheet. This hypothesis has to be investigated further. However,

tubulin assembly and microtubule conformation with GTP are not always comparable to the assembly situation with GMPCPP as the nucleotide.

5.5.7 Mal3p avoids traffic jams

Mal3p interacts with microtubules in a very different way to molecular motors or MAPs. Truncated Mal3p could decorate the entire surface of a microtubule, but the full length protein leaves the B-lattice free. Both kinesins (Hoenger *et al.*, 1995; Hirose *et al.*, 1995; Kikkawa *et al.*, 1995) and dyneins (Mizuno *et al.*, 2004), bind to the outer surface of β -tubulin forming an 8 nm repeating pattern on top of every protofilament, with the highest density at a larger radius from the tube center than displayed by Mal3p-N203 (figure 5.2). Tau-like proteins associate longitudinally along protofilaments (Al-Bassam *et al.*, 2002) but may also cross over protofilaments and hold them together laterally (Santarella *et al.*, 2004). In any case, we could detect full-length Mal3p seam binding also in the presence of Tau (Figure 4.7). In contrast to kinesin and Tau (Santarella *et al.*, 2004; Skiniotis *et al.*, 2004), Mal3p binding to microtubules is not affected by removal of the C-terminal acidic tail on β -tubulin, which further supports the conclusion that multiple binding sites on the microtubule surface are responsible for the different MAP interactions.



MAPs and motors typically decorate the entire microtubule surface (Hoenger *et al.*, 2000a; Santarella *et al.*, 2004). When overproduced, they may cause traffic jams and stall microtubule-based transport (Ebneith *et al.*, 1998; Seitz *et al.*, 2002). Mal3p, in contrast, leaves most of the microtubule surface free, which leaves ample room for other microtubule binding factors.

Figure 5.2: Mal3p-N203 and nK355 interact with different regions of the microtubule surface. A student's T-test (99% confidence) shows the difference map between a plain microtubule and Mal3p-N-203 decorated microtubule (red volumes show the Mal3p portion), or a nK355 decorated microtubule (green volumes indicate the motor domain). Mal3p-N-203 binds in between the protofilaments and conventional kinesin interacts only with the distal surface of the protofilaments. However, the full-length dimeric Mal3p is only found at the seam and not in all grooves as its truncated version.

5.6 Mal3p influences the microtubule structure

Helical reconstruction of the C-terminally truncated Mal3p-N-203 revealed a full stoichiometric decoration of the microtubule lattice (Figure 4.16 and 4.17). Careful analyses of the Fourier space diffraction pattern of the 3-D reconstructed Mal3p-N-203-microtubule complex revealed a mixture of A and B-lattice, which might be induced through Mal3p-N-203 interference (Figure 4.19). According to the relatively low number of asymmetric units that went into the reconstruction of the Mal3p-N-203 microtubule complexes the noise level is higher in this reconstruction than in the other ones (plain tubulin and nK355-microtubule complexes). However, apart from pure image noise the Mal3p-N-203 microtubule complex may have internal inconsistencies as well. Presumably, the truncated Mal3p-N-203 construct enhances the possibility of producing multiple seams due to its seam-stabilizing activity. The reconstruction procedure for a helical microtubule assumes a clean B-lattice conformation. If this lattice is interrupted by A-lattice contacts, even if they compensate for each other, the reconstruction procedure averages over different positions without actually recognizing them. Indicative of that possibility for Mal3p-N-203 microtubule complexes, the amplitude peak of the 1/8 nm layerline (Bessel order -2) is much further out from the equator than in the nK355-microtubule complex, although the amplitude oscillations still correspond to a Bessel order of -2 (Figure 4.19B-D). While a helical B-lattice microtubule has a Bessel order of -2 in the 1/8nm layerline cluster (corresponding to the axial tubulin dimer repeat), a clean A-lattice 15 protofilament microtubule would have a Bessel order of -7 and 8 at the same 1/8 nm location and this would correspond to the lateral position of the amplitude peak that we find in Mal3p-N203 microtubule complexes (Figure 4.17B and 4.19B). Therefore it seems likely that the microtubules used for the Mal3p-N203 microtubule complex reconstruction may contain multiple seams. But other alternatives, like irregular or equal α - or β -tubulin binding affinity cannot be ruled out, as we still lack detailed structural and biochemical information about how the EB1-family proteins interact with tubulin.

5.7 Comparing *in vitro* results with cellular observations

In cells microtubules generally nucleate from centrosome, SPB or other γ -TuRC locations and extend through the cell. Growing microtubules in all eukaryotic cell types are accompanied by plus end tracking of EB1 protein family members that affect microtubule dynamics (Beinhauer *et al.*, 1997; Morrison *et al.*, 1998; Tirnauer *et al.*, 1999; Rogers *et al.*, 2002). EB1 as well as the fission yeast Mal3p is known to accumulate like a comet at the growing plus ends, but dissociates as soon as a microtubule undergoes catastrophe and starts to depolymerize (Tirnauer *et al.*, 2002b; Busch and Brunner, 2004), (Figure

5.3). At the same time, fluorescent fusion proteins of EB1 and Mal3p were observed at lower concentrations along the entire microtubule, independent of their dynamic state (Mimori-Kiyosue *et al.*, 2000; Tirnauer *et al.*, 2002b; Busch and Brunner, 2004). The lattice binding was assumed to be concentration dependent, enhanced upon over-expression but still detectable at endogenous concentrations (Ligon *et al.*, 2003; Sandblad *et al.*, 2006). Lattice binding but no plus end tracking on taxol-stabilized microtubules was detected *in vitro* for EB1 (Ligon *et al.*, 2006). However, our recombinant Mal3p is able to plus end track as well as weakly associate to the entire wall on dynamic microtubule *in vitro* (Bieling *et al.*, manuscript in preparation).

5.7.1 Endogenous concentration ratios

Most experiments in this thesis are *in vitro* biochemical experiments; we aimed to reconstitute a simplified version of the cellular function and organization. With an *in vitro* system single protein key players of a process can be investigated without the disturbance of cellular complexity. We used approximately cellular ionic strength in the microtubule polymerization buffer. To accomplish a total saturation of Mal3p on the microtubule lattice we often co-polymerized or decorated microtubule in an abundance of Mal3p. To get an idea of protein ratios and concentrations within a cell we have performed western blots with a dilution series of extract from a defined cell number and a dilution series with defined amounts of purified Mal3p and tubulin, respectively, to get a measure of the amount of protein in cells. We find that there is in the order of 300 times more α -tubulin than Mal3p molecules in the cell (see section 6.3). However, this is a bulk experiment with a very large error margin and may not reflect the actual stoichiometry at the plus ends of microtubules. EB1 family proteins could also be detected in close proximity to the MTOCs (Louie *et al.*, 2004). This indicates that there exist regions of higher Mal3p concentrations and activation of cellular Mal3p, therefore a proper ratio for *in vitro* studies is hard to define and not very relevant, since EB1 family proteins are extremely dependent on other MAPs in the cellular environment.

5.7.2 Influence of taxol

Taxol has a strong influence on the microtubules structural conformation; it is a powerful microtubule stabilizer. Taxol binds only to β -tubulin, and from its binding site on the inside of the protofilament it affects the conformation of the M-loop (Xiao *et al.*, 2006). However, it could also interfere with the nucleotide dependent conformation of Helix H3; both functions would stabilize lateral interactions (Nogales *et al.*, 1999). At the same time, taxol may enforce a straight longitudinal interaction, which would be bent upon

GTP hydrolysis. This way taxol would strengthen the longitudinal interactions (Amos and Lowe, 1999). When interphase cells in cell culture are treated with taxol, microtubule dynamics are suppressed although the microtubules remain long and stable. Plus end tracking by EB1 is eliminated upon taxol treatment but EB1 association with the microtubule lattice remains unaffected (Morrison *et al.*, 1998; Mennella *et al.*, 2005). This supports our findings that Mal3p binds the entire microtubule length along the seam. Since we used taxol at low concentrations to stabilize microtubules in all our shadowing experiments, it is also reasonable that we do not observe a strong microtubule plus end accumulation.

In contrast, we assume that with the turbidity experiments in the absence of taxol, we measure the effect of plus end interaction and microtubule stabilization at the plus ends and the lattice simultaneously. We propose that the molecular interactions between tubulin and the Mal3p CH-domain are the same at the microtubule tips as along the lattice, but that the cellular microtubule plus ends exhibit a conformation more suitable for Mal3p association (see section 5.8 below).

With high-resolution unidirectional metal shadowing EM we were able to visualize the seam through Mal3p and kinesin motor domain decoration. We cannot directly observe a seam on a cellular microtubule, and also not on an *in vitro* polymerized microtubule using any kind of light microscope. To detect the seam or seam binding proteins a resolution below 4 nm, transmission EM is the only technique available to date.

5.8 What is going on at the microtubule plus end?

Our experiments were designed to address the question of how Mal3p binds to tubulin with the intention of gaining a better understanding of what happens at growing microtubule plus ends where most of the Mal3p protein accumulates, and influences microtubule dynamics. Our findings are not easily reconcilable with the current models of plus end growth; however, very little is known about the actual structure of the microtubule plus end *in vivo* because our contemporary EM imaging methods do not yet produce a sufficiently high signal to noise ratio. Studies of the +TIP CLIP-170 proposed that it treadmills on growing microtubule plus ends through association with free tubulin, co-polymerization and subsequent dissociation from the lattice (Arnal *et al.*, 2004).

It is possible that more Mal3p binds to microtubule plus ends because the properties of Mal3p plus end binding are different from those of microtubule lattice binding. For

example, tubulin conformation-dependent binding; GTP-tubulin has a different conformation than GDP-tubulin, but Mal3p binding could not be enhanced in the presence of the GTP analog GMPCPP, which indicates that the nucleotide state of tubulin does not influence Mal3p affinity.

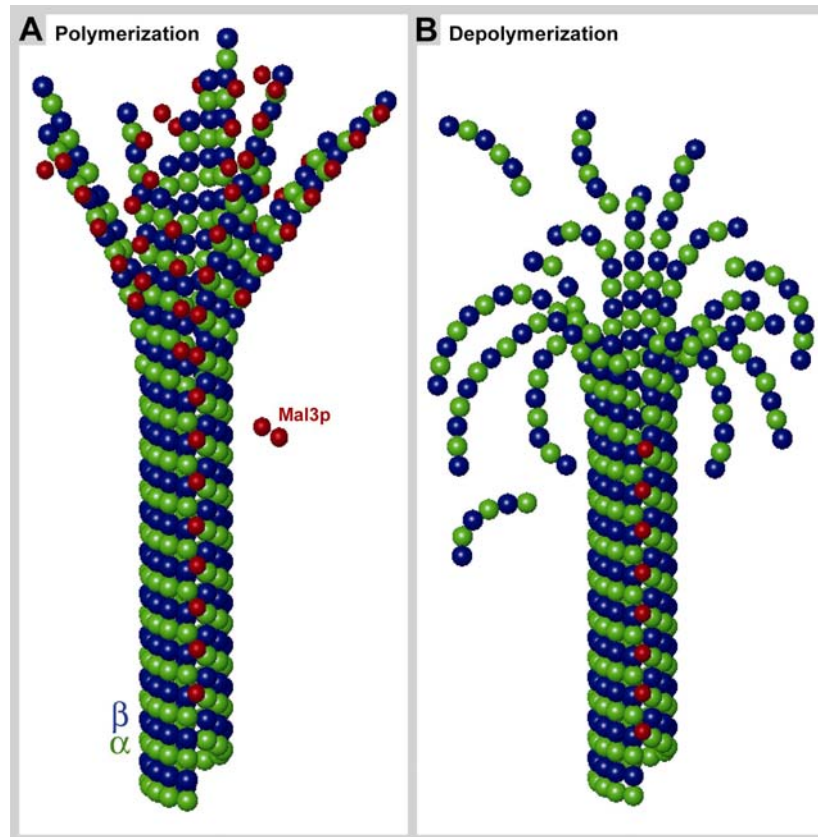


Figure 5.3: Model of Mal3p-Microtubule complex during polymerization, pause in growth and depolymerisation. (A) Polymerizing microtubule with Mal3p “surfing” on the plus end. The sheets of straight but flared protofilaments at the plus end accommodates numerous binding sites for Mal3p, but when the protofilaments subsequently close into a tight laterally interacting B-lattice Mal3p dissociates, and Mal3p only remains at the seam of the altering microtubule wall. In this funnel-like polymerizing state, the microtubule could interact with the kinetochores or membranes to exert force in form of motion. (B) A depolymerizing microtubule exhibits curled and flared protofilaments which gradually fall off as oligomers and can only accommodate Mal3p along the seam. We presume Mal3p has no affinity for the curling tubulin conformation.

We have shown that on tubulin subunits Mal3p preferentially binds specific sites that only form at the lattice seam. It is conceivable that more of these sites are exposed at growing plus ends if the protofilaments are not yet laterally attached. This could give an additional twist to the idea that growing plus ends form sheet structures, as was previously proposed based on cryo-EM studies (Chretien *et al.*, 1995; Arnal *et al.*, 2000). *In vivo*, these sheet structures may contain loose flared protofilaments that are laterally

connected by Mal3p. This model implies that Mal3p treadmills through binding to the straight but loosely interacting protofilaments at the plus ends. When the protofilaments subsequently close, which may be induced by the presence of Mal3p, Mal3p dissociates, because it cannot bind the closed B-lattice conformation (Figure 5.3). The protein could then diffuse to a new interaction site at the growing plus end. Intriguingly, microtubule plus ends appeared mostly flared in more recent electron tomography studies (Austin *et al.*, 2005; Hoog *et al.*, 2007), which support the idea of unattached protofilaments. This mechanism would raise the intriguing possibility that Mal3p not only clamps the seam but also promotes growth by controlling the “zippering” of protofilaments at growing microtubule plus ends.

5.8.1 MAP network at the growing plus end

EB1 family proteins are in charge of regulation at the growing microtubule plus end. In fission yeast, Mal3p plus end accumulation is independent of other MAPs, like Tip1p and Tea2p, however the plus end accumulation of Tip1p and Tea2p seem to be regulated by Mal3p (Busch and Brunner, 2004; Busch *et al.*, 2004). The situation in mammalian cells is even more complex. The EB1-domain possesses overlapping interaction sites for most other +TIPs; interactions with CAP-Gly domain family proteins like CLIP-170 and p150Glued were proposed to activate EB1. Furthermore, EB1 microtubule plus end localization is maintained in the absence of APC, CLASPs, CLIP-170 and p150Glued (Morrison *et al.*, 1998; Akhmanova *et al.*, 2001; Komarova *et al.*, 2002a). This extensive network is one of the reasons why definition of the plus end tracking mechanisms for individual +TIPs has been so difficult. Structurally this transient and dynamic macromolecular complex is still totally uncharacterized; for this purpose *in vitro* studies like ours have to be extended for entire complexes.

5.8.2 Depolymerisation

Catastrophe and depolymerisation can only take place if EB1 family proteins have been removed from the microtubule plus end (Mennella *et al.*, 2005). Whether depolymerization forces EB1 to fall off, or if EB1 is actively removed to allow depolymerization is still an unsolved problem, which may involve regulation by other MAPs. However, EB1 seems to be involved at the onset of depolymerisation. In *Drosophila*, Klp10A a depolymerizing kinesin, is recruited to microtubules by EB1 during polymerization (Mennella *et al.*, 2005). When the plus end accumulation of EB1 disappears Klp10A is activated, which lead to catastrophe. Two models have been proposed for the mechanism that depolymerizing kinesins use to destabilize microtubules from the plus

end. Kinesin-13 motor domains have a slightly convex binding surface with high affinity for the tubulin dimer, which may force the protofilaments to curve, and curl away from the microtubule (Moores *et al.*, 2002; Moores *et al.*, 2003; Ogawa *et al.*, 2004; Tan *et al.*, 2006). Depolymerization is counteracted by MAPs that straighten the protofilaments, e.g. XMAP215 (Kinoshita *et al.*, 2001). Another destabilizing kinesin XKCM1 may also curl the protofilaments, although a second mechanism was suggested (Desai *et al.*, 1999; Niederstrasser *et al.*, 2002). The dimeric kinesin could bind two adjacent protofilaments and use its motor activity to separate the protofilaments from each other; this would disrupt the microtubule lattice. When the protofilaments lose their lateral interactions they would theoretically depolymerize. Hence, in the presence of EB1 family proteins, microtubules might be protected from depolymerization through protofilament cross-bridging at the plus ends.

5.9 The sense of the seam

The way in which Mal3p interacts with microtubules adds a new perspective to the discussion concerning the microtubule lattice seam. The structure of the seam is poorly investigated and the biological function of the seam seems to be neglected in most previous studies. From an evolutionary viewpoint it almost looks like Mal3p made use of a structural peculiarity that at a first glance appears to be an imperfection in the microtubule lattice. The appearance of a seam is enforced by the fact that the microtubule building block is a heterodimer. Since prokaryotes only possess a monomeric tubulin analog, namely FtsZ, that assembles into filaments rather than tubes (Oliva *et al.*, 2004), it looks as if dimeric tubulin occurred later in evolution and with it the closed tube and a seam together with further functional variations for the protein. In any case, the dimeric building block was obviously not lost due to evolutionary fitness pressure, nor did nature rely on seamless microtubules (i.e., 15 protofilament microtubules). Instead, nature chose to use mostly 13 protofilament microtubules, possibly because they show no supertwist. Seamless and therefore helical microtubules do exist in certain cell types e.g. in sperm cells (Afzelius *et al.*, 1990) and as a subpopulation of the microtubules in *C. elegans* neurons (Savage *et al.*, 1989), but these are rare exceptions. Therefore, the seam may indeed play a more important role than just matching up the lattice of a tube in an imperfect way. The entire microtubule can be stabilized by fewer Mal3p molecules as compared to tubulin, since only one Mal3p molecule binds per helical turn of the microtubule. Microtubule stabilization along the seams appears to be very economical and leaves ample room on the microtubule surface for other factors such as motor proteins to operate. It is therefore conceivable that the seam is used as a platform for the

direct regulation of microtubule stability through site-specific interactions with molecules such as Mal3p.

5.10 Perspective for Mal3p and the +TIPs

5.10.1 The EB1 protein family

As human EB1 can substitute for Mal3p function *in vivo* (Beinhauer *et al.*, 1997; Browning *et al.*, 2003), it is likely that the function we propose for Mal3p is conserved, which now needs to be shown. So far, no other EB1 protein family members have been structurally investigated by EM. The only existing structural data are crystallography structures of the separate domains (Hayashi and Ikura, 2003; Honnappa *et al.*, 2005). It is likely that the flexibility of the full-length protein in solution is too high to crystallize. EM certainly brings more insight into the organization and function of EB1 family proteins. In contrast to fission yeast, higher eukaryotes possess multiple EB1 homologs. Where investigated it appears that functions identified for EB1 can be replaced by EB3 but not EB2/RP1 (Bu and Su, 2003). This suggests that there exist EB1 protein variants that have specialized for some of the Mal3p functions and that each of the three mammalian homologs have not necessarily inherited all properties of Mal3p from their common EB1 ancestor respectively. At the same time the distribution of Mal3p function emphasizes the central importance of this class of proteins as regulators of microtubule dynamics. To understand which properties are essential and conserved, the functional differences and microtubule binding properties of all the three mammalian paralogs need to be investigated in a comparative way.

5.10.2 Microtubule plus end structure

When comparing our high-resolution EM images of *in vitro* polymerized microtubules with cellular dynamic microtubules imaged with light microscopy (Busch and Brunner, 2004; Akhmanova and Hoogenraad, 2005), several questions arise: Is the microtubule lattice conformation and plus end structure equivalent *in vivo* as *in vitro*? How can the microtubule plus end accommodate the large amount of different +TIPs, which cause the bright tip staining observed by fluorescence techniques? Microtubules polymerized *in vitro* normally exhibit open sheets of protofilaments at the growing plus end (Chretien *et al.*, 1995; Arnal *et al.*, 2004). Polymerization in the presence of the total MAP repertoire in *Xenopus* oocyte extract shows an equivalent structure (Arnal *et al.*, 2000).

The most detailed 3-D view of cellular microtubule ends present to day are tomograms of cryo-immobilized freeze-substituted semi-thick sections, stained with uranyl acetate and osmium tetroxide. In a *C. elegans* cell, microtubule minus ends were described as capped or blunt and plus ends as open flared or blunt (O'Toole *et al.*, 2003). The non-astral microtubules in a plant cell display an even more variable conformation of the plus ends, from blunt ends, some straight sheets, to backwards curling protofilaments and also more straight separately flared protofilaments in a funnel form (Austin *et al.*, 2005). In fission yeast, where the microtubule plus ends interact with the cell poles, a funnel shaped end was also observed to interact with the cortex, with a diameter double that of a microtubule at the protofilament membrane connection (Hoog *et al.*, 2007). This implies that protofilaments splay apart but remain straight and stable as long the microtubule interacts with the cell pole cortex. In these funnel shaped or straight sheet structures is it easy to imagine that Mal3p may find a lot of possible interactions sites, which are otherwise not accessible in a closed lattice. However the signal to noise ratio in this preparation does not allow recognition of any +TIPs. The quick high pressure freezing is proposed to preserve the cellular organization and should not initiate microtubule depolymerisation, although the water exchange against plastic and heavy metal contrast enhancement may cause aggregation and other artifacts within the cellular structures. Further, the individual protofilaments in these tomograms are generally not distinguishable. A better structural preservation, and high enough resolution to separate all individual protofilaments and to define the polarity was achieved through cryo-EM and tomography of vitreous sections (Garvalov *et al.*, 2006; Bouchet-Marquis *et al.*, 2007). Next, the microtubule ends have to be analyzed with this method, to create a refined view of the microtubule plus end, if possible including the +TIP complex. However, new methods regarding cellular labeling for tomography of vitreous section EM would be necessary to prove the localization of individual MAPs. This is of particular importance for small MAPs like EB1 and more unstructured filamentous MAPs like XMAP215 that, in cryo-tomograms cannot be identified directly.

Cryo-electron tomography is a powerful method to visualize large asymmetric macromolecules and complex cellular organelles. To further understand the plus end microtubule promoting mechanisms, the next step after this work is to add other MAPs (e.g. Tip1p, Tea2p) to the same *in vitro* system. These assemblies can then be studied in 3-D by cryo-electron tomography (Sui and Downing, 2006).

5.10.3 Structure and function of truncated Mal3p and microtubules

For most studies of motor protein interactions with microtubules only the globular head domains, or other and defined microtubule binding domain were used (NCD-tail; Wendt et al., 2003). Here we took a reversed approach as we showed that full-length Mal3p preferentially binds the microtubule lattice seam of stabilized, *in vitro* polymerized microtubules. Furthermore, we found that seam-specific binding is abolished when the C-terminal acidic tail of the protein is removed. Even if the CH-domain is the actual microtubule binding domain of the protein, the rest of the molecule regulates the binding specificity. The full function of a protein cannot be proposed if only one of the protein domains is studied, but in comparison with the full-length protein, domain studies may dissect the functional properties and allocate them to the responsible region of the protein.

We have already cloned a series of Mal3p truncations (Figure 4.13-4.14). One of our constructs Mal3p-N203 remains a monomer and binds stochastically on the microtubules but exhibits the same nucleation and depolymerisation activity as full-length Mal3p. Optimization of Mal3p-N203 (or other constructs with similar activity) and tubulin co-polymerization conditions and further microtubule binding analyses may shed more light onto the Mal3p property responsible for specific recognition of the seam. If truncated Mal3p that therefore is not only directed to the lattice seam, is able to induce more A-lattice interactions in a microtubule, this also questions whether the B-lattice always is the favored conformation or if this conformation is caused by the presence of kinesin motor domains or taxol. Hopefully the future will bring even more interesting results regarding microtubule and MAP interactions and counteractions.

6 Supplementary information

6.1 Standard curve for HiLoad Superdex 200 prep grade 16/60

We used a low molecular weight calibration kit (Amersham Biosciences) of globular proteins to run a standard gel-filtration and draw a standard curve for the molecular weight according to the elution volume. For each standard protein the elution volume V_e was determined. K_{av} was calculated according to $K_{av} = (V_e - V_0) / (V_t - V_0)$ to create a standard curve as a function of the logarithmic molecular weight (Figure 6.1). From the elution volume (V_e) for each protein, the corresponding K_{av} was calculated and used to approximately determine the MW from the trendline equation:

$$MW = 1700 e^{-7.1 \times K_{av}}$$

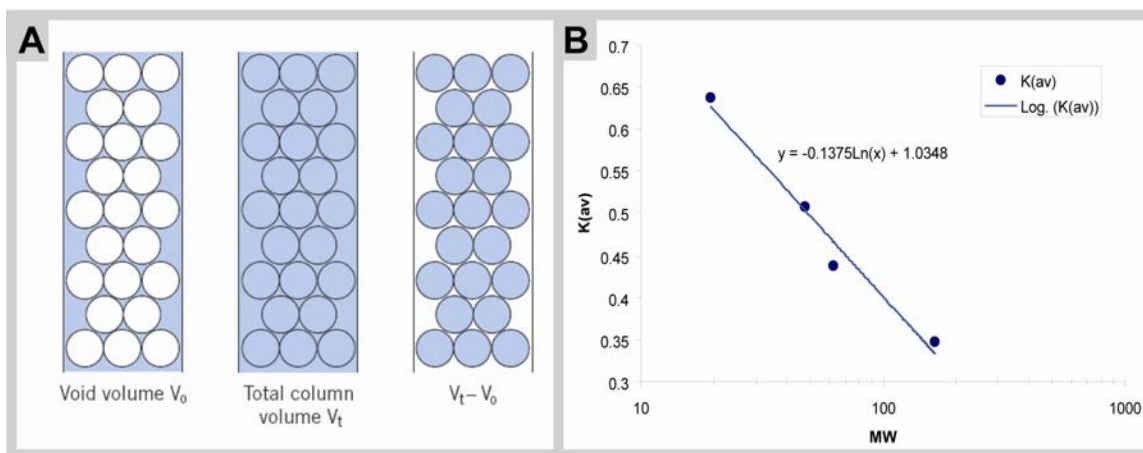


Figure 6.1: Gel-filtration calibration. (A) Model of a Gel-filtration column. Void volume V_0 is the volume outside the gel matrix; particles too large for the matrix meshwork would be eluted in this volume, which is 40 ml for HiLoad Superdex 200 prep grade 16/60. Total volume V_t is the total soluble phase of the matrix; the buffer is eluted in this volume, which constitutes 120 ml for this column. (B) Standard curve for HiLoad Superdex 200 prep grade 16/60 and equation of the logarithmic trend line.

6.2 Monoclonal anti-Mal3p-antibody expression and characterization

Hybridoma cells are mutated mouse blood cells expressing and secreting IgG antibodies (Abs). Cell lines used here were created from GST-Mal3p-immunized mice at EMBL-Monterotondo, Italy, by Alan Sawyer. Cells cloned into monoclonal strains can be cultured and the expressed monoclonal Abs can be collected and used directly from the cell supernatant.

14 original monoclonal hybridoma strains were originally created, supernatant collected and stored in 2003. We thawed 4 α -Mal3p clones, from which 3 expressed Mal3p specific IgG Abs. The original clones were called α -Mal3p-18F8, -20D5, and -1D1.

6.2.1 Hybridoma cell culture

During the work with hybridoma cells, constant care was taken to work under sterile conditions. All media were filtered through 22 μ m sterile filters prior to use.

6.2.1.1 Defrosting

Aliquots of 1 ml frozen hybridoma cell cultures were thawed directly by adding 10 ml 37°C HM20 supplemented with 10% hybridoma cloning factor (HCF, EMBL-Monterotondo, Italy), through mixing in the pipette and transfer to a Falcon tube. The cells were centrifuged 100 g for 5 minutes and resuspended two times in 10 ml 37°C HM20 + 10% HCF. After the last centrifugation they were resuspended in 1 ml of the same medium and transferred to a 24 well plate. In a dilution series the cells were split 1:2 four times in new wells on the plate in order to find a dilution for the cells to recover. The cells were cultured at 37°C in a humidified incubator with 5% CO₂.

Hybridoma Medium 20 (HM20)	DMEM (Gibco, Invitrogen, Karlsruhe, Germany)
	20% FCS (Hyclone, UT, USA)
	1% L-Glutamine 200 mM (Gibco)
	0.2 % Gentamicin 50 mg/ml (Gibco)

6.2.1.2 Subcloning

The recovered hybridoma cultures were subcloned to eliminate cells mutated by freezing or storage; the stability of individual clones were very variable. For subcloning, 200 μ l growing culture was diluted in 10 ml HM20, the cell number was estimated and the

culture diluted in 20 ml HM20 + 10% HCF to 20-50 cells/ml. In a 96 well plate, 50 μ l culture per well was spread and incubated for 7-10 days. The supernatant from single growing clones were analyzed for anti-Mal3p specific IgG by ELISA. Positive monoclonal Ab-expressing cell lines were cultured further.

6.2.1.3 Maintenance and harvest

When cells were grown to a monolayer in the well they were split 1:2 or 1:4 into larger wells or culture flasks. For each passage the HCF was gradually decreased to 0 or 0.3% in the final culture. Harvested supernatant from every step was stored at 4°C and analyzed by ELISA, to verify the continuous Ab production. Finally, 30 ml hybridoma cell supernatant was harvested from a 75 cm² culture flask. All cell debris was removed by 15 minutes centrifugation at 2300x g and to inhibit bacterial growth during storage at 4°C 0.02% sodium azide was added. We found Abs still active after 4 years storage in culture media at 4°C.

6.2.1.4 Freezing cell culture

Well Ab-expressing hybridoma cell lines should be frozen as quick as possible (they seem to gradually and eventually withdraw the Ab expression and secretion). Cells from a 6 well plate were pelleted at 100 g for 5 minutes. The pellet were resuspended in 2 ml 90% FCS and 10% DMSO, splitted in to 1 ml aliquots, and frozen in -80°C. After more then 2 hours the storage aliquots were transferred to liquid nitrogen.

6.3.2 ELISA

A qualitative ELISA was used to detect the presence of α -Mal3p-Abs in the hybridoma cell culture supernatant. For this purpose 96 well Maxisorb plates (Nunc, Wiesbaden, Germany) were coated with 50 ng Mal3p full-length protein or fragments diluted in 50 μ l 0.1 M Sodium Carbonate buffer (pH 8.5) per well, overnight at room temperature. The plates were washed 3 x 5 minutes with PBS + 0.1% Tween. The remaining surface of the wells was blocked with 50 μ l 3% BSA in PBS for 1 hour and washed again, however the last wash was with only PBS. 50 μ l hybridoma cell culture supernatant or HM20 as a control, were added to each well, incubated for 1 hour and washed as for the first washing step. A secondary Ab, in the form of HRP-coupled anti-mouse-Ab was diluted 1:7500, 50 μ l were added to each well, incubated for 1 hour and washed as before. The detection reaction was induced by adding 50 μ l of an ABTS substrate mix (Zymed Laboratory, Invitrogen, Karlsruhe, Germany). The HRP-ABTS reaction was detected by GENios and

the Deltasoftware III version 2.248 software. The staining intensity is proportional to how well the Abs in the cell supernatant binds Mal3p.

6.3.3 α -Mal3p-Antibody epitope regions on Mal3p

We performed an ELISA using approximately 50 ng from all expressed Mal3p constructs (see section 4.1 and 4.6.2) per well and the supernatants from hybridoma cell cultures 18F8, 20D5, 1D1. Rabbit polyclonal α -Mal3p-Abs (Busch and Brunner, 2004) were used as a positive control (Figure 6.2). We also used Western blotting, where all Mal3p constructs were blotted together with *S. pombe* cell extract wild type (WT) and $\Delta mal3$ (Busch and Brunner, 2004) with all three monoclonal cell supernatants as primary antibody on three separate membranes (Figure 6.3). Both experiments displayed the same results. All three monoclonal Abs bound to the C-terminal region of Mal3p. 18F8 has affinity for full-length Mal3p (FL), -N-252, -163-252 and -163-308, which suggests a likely epitope in the EB1-domain in amino acids 163-252. 20D5 and 1D1 bind only Mal3p-FL and -163-308 in the Western blot and weakly to -N-252 and -163-252 by ELISA, which suggests that this epitope is in at the last 50 amino acids in the C-terminal acidic tail after the coiled-coil region, maybe overlapping with EB1-domain (Figure 6.3B). Puzzlingly, the signal is weaker for the C-terminal fragments than the full-length protein, even though the concentrations were estimated to be equal. This may indicate crosstalk between the acidic tail and the CH-domain, which could be possible in the ELISA but denatured in the Western blot. Also, the polyclonal α -Mal3p-Abs lack affinity for the CH-domain. We also noticed that the monoclonal Ab 1D1 has a high affinity for two of the protein markers, namely the 72 and 36 kDa bands (the marker content is a mix of prokaryotic proteins, though more specific information is not public). However, in *S. pombe* all three monoclonal Abs have no background and bind only Mal3p in the wild type strain and have no signal in the *mal3* deleted strain. These monoclonal α -Mal3p-Abs constitute important tools for further molecular studies.

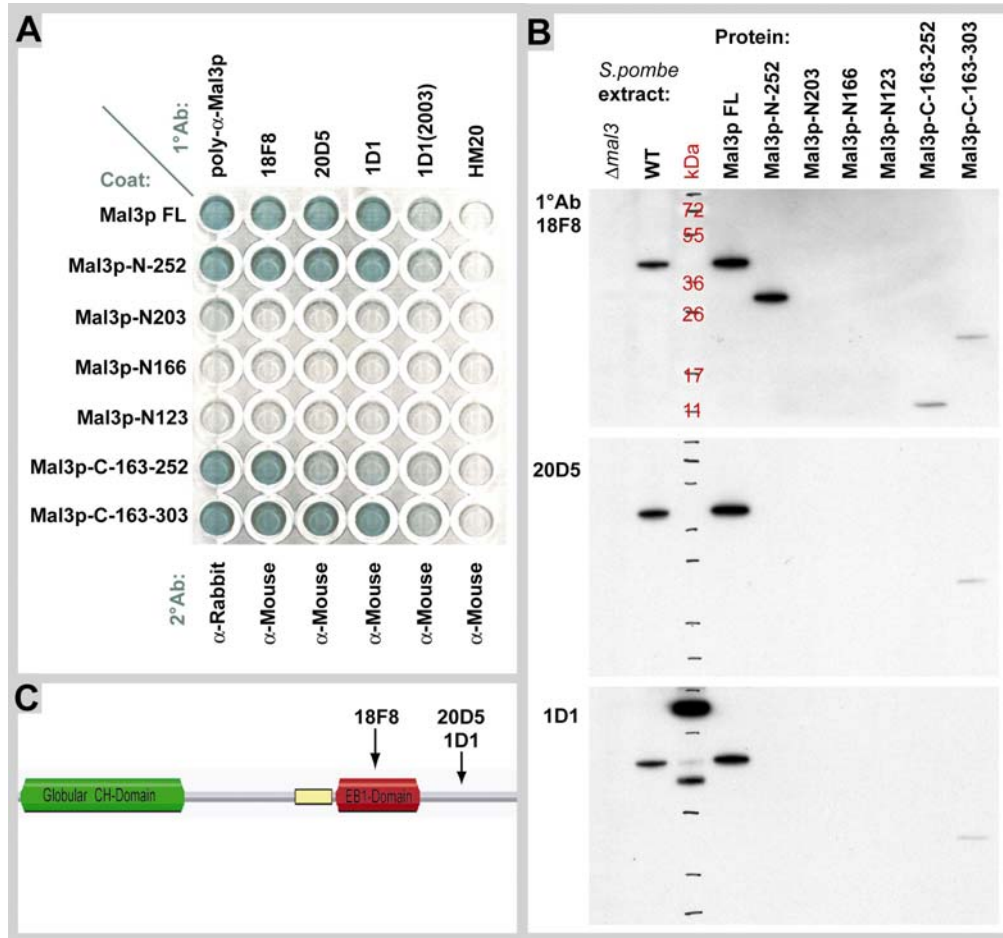


Figure 6.2: Partial epitope characterization for monoclonal α -Mal3p-antibodies (Ab). The Ab containing supernatant from three monoclonal hybridoma cell lines were analyzed by ELISA and Western blot concerning their affinity for the individual Mal3p domains. (A) In an ELISA all different Mal3p protein fragments including the full-length protein were coated onto the surface of a maxisorb 96 well plate. The cell supernatant from 18F8, 20D5 and 1D1 (and 4 year old supernatant from 1D1), were used as primary 1°Ab. As a control we added 1:5000 diluted polyclonal α -Mal3p-Ab, and one column with cell medium (HM20). (B) Western blot of three membranes loaded with the same samples and individually incubated with the same three monoclonal hybridoma cell supernatants as the ELISA experiment. (C) Summary of the results from the ELISA and Western blot experiments: 18F8 binds to the coiled-coil of the EB1-domain between residue 203 and 252; 20D5 and 1D1 also bind the C-terminal region. The ELISA results are slightly contradictory and the Western blot only confirms binding to the last 50 residues of the acidic tail. Although, 20D5 and 1D1 recognize the same region, they seem to have different epitopes, because the Ab 1D1 also recognizes a prokaryotic motive in the protein marker, which is unknown to us.

6.3 *S. pombe* endogenous concentrations of tubulin and Mal3p

The *S. pombe* endogenous concentrations of tubulin and Mal3p were determined by comparing the Western blot signals from cell extract with a concentration gradient of purified proteins. Bovine tubulin (purchased from Cytoskeleton) and recombinant Mal3p were diluted to concentration (C) gradients and 2.5 μl was mixed 1:2 with loading buffer respectively. The gradient together with two yeast cell extract concentrations or different volumes (V) were separated by SDS-PAGE and transferred onto the same membrane. The protein bands on the membrane were detected with primary anti α -tubulin/Mal3p monoclonal Ab and secondary anti-mouse HRP-Abs. Here we assume that the Ab affinity is the same for bovine and *S. pombe* α -tubulin and the same for recombinant and endogenous Mal3p. HRP luminescence was exposed to negative film, which was scanned and analyzed by ImageJ. The intensity is proportional to protein concentration. According to the concentration gradient constant (trendline equation, Figure 6.4) and the dilution or loading volume factor (Loading Factor, Table 6.1) the protein concentrations (C_e) in cell extract were calculated (Table 6.1). 340 μl cell extract was produced from 50 ml exponential growing cell culture (OD_{595} 0.5), accordingly the cell culture concentration (C_c) is $6.8 * 10^{-3}$ times the cell extract concentration (C_e). The cell culture contains 10^7 celles/ml and the average *S. pombe* cell volume in a growing cell culture was estimated to $78 \mu\text{m}^3$ (Loiodice and Tran, personal communication), which means that the cellular concentration (C_{pombe}) is 1300 times the cell culture concentration (C_c) (Table 6.1). However, the total cell volume used here does not exclude organelles or other cellular compartments where tubulin and Mal3p are thought to be excluded.

Table 6.1:

Band	Tubulin		Mal3p	
	a	b	a	b
Western blot intensity	5.7	8.1	1.6	4.1
Relative C (nM)	115	146	4.4	8.6
Loading V (μl)	0.15	0.3	2.5	5
Loading factor	16	8	1	0.5
Cell extract C_e (nM)	1800	1200	4.4	4.3
Average cell extract C_e (nM)	1500		4.4	
OD_{595} 0.5 Cell culture C_c (nM)	10		0.03	
<i>S. pombe</i> cell C_{pombe} (nM)	13000		38	

We found 300 times more tubulin than Mal3p monomers in this experiment and a final cellular concentration of 13 μM tubulin and 38 nM monomeric Mal3p (only here we use the monomeric concentration for Mal3, because a monoclonal Ab is likely to bind one monomer in the Western blot).

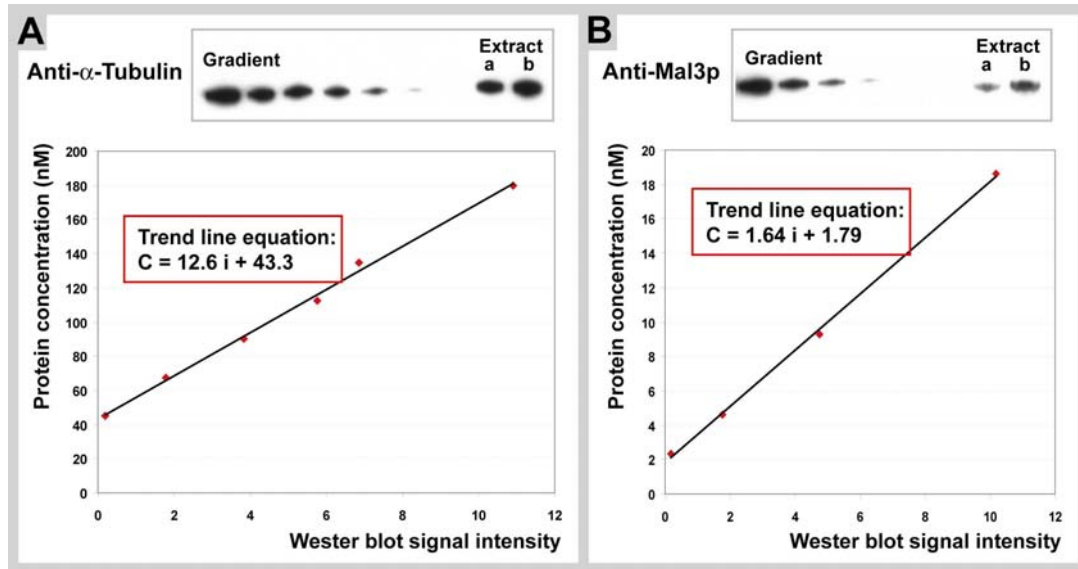


Figure 6.3: Western blot of tubulin and Mal3p concentration gradients together with *S. pombe* extract. Protein concentration is proportional to the Western blot signal intensity. (A) Western blot with monoclonal anti- α -tubulin and (B) with monoclonal anti-Mal3p from 1D1 cell supernatant. According to the standard curves of known concentration, the endogenous concentration on the cell extract could be estimated, a and b were two dilutions from same extracts.

This experiment suffers from several cellular and experimental inaccuracies. First, these proteins are likely to be regionally and cell cycle regulated. Second, the cell number in the cell culture was only estimated according to light scattering measurements. Third, *S. pombe* and bovine tubulin may have different affinities for the Ab even if though the proteins are extremely conserved (~75% identity). Fourth, HRP exposure to negative film was an indirect measurement and a direct fluorescent secondary Ab, which could be scanned directly from the membrane, might give better signal contrast. Nevertheless tubulin and Mal3p concentrations were estimated using the same approach and the endogenous concentration ratios were relevant.

7 Bibliography

- Afzelius, B.A., Bellon, P.L., and Lanzavecchia, S. (1990). Microtubules and their protofilaments in the flagellum of an insect spermatozoon. *J Cell Sci* 95 (Pt 2), 207-217.
- Akhmanova, A., and Hoogenraad, C.C. (2005). Microtubule plus-end-tracking proteins: mechanisms and functions. *Curr Opin Cell Biol* 17, 47-54.
- Akhmanova, A., Hoogenraad, C.C., Drabek, K., Stepanova, T., Dortland, B., Verkerk, T., Vermeulen, W., Burgering, B.M., De Zeeuw, C.I., Grosveld, F., and Galjart, N. (2001). Clasps are CLIP-115 and -170 associating proteins involved in the regional regulation of microtubule dynamics in motile fibroblasts. *Cell* 104, 923-935.
- Al-Bassam, J., Ozer, R.S., Safer, D., Halpain, S., and Milligan, R.A. (2002). MAP2 and tau bind longitudinally along the outer ridges of microtubule protofilaments. *J Cell Biol* 157, 1187-1196.
- Amos, L., and Klug, A. (1974). Arrangement of subunits in flagellar microtubules. *J Cell Sci* 14, 523-549.
- Amos, L.A., and Lowe, J. (1999). How Taxol stabilises microtubule structure. *Chem Biol* 6, R65-69.
- Amos, L.A., and Schlieper, D. (2005). Microtubules and maps. *Adv Protein Chem* 71, 257-298.
- Amos, L.A., van den Ent, F., and Lowe, J. (2004). Structural/functional homology between the bacterial and eukaryotic cytoskeletons. *Curr Opin Cell Biol* 16, 24-31.
- Andreu, J.M., Diaz, J.F., Gil, R., de Pereda, J.M., Garcia de Lacoba, M., Peyrot, V., Briand, C., Towns-Andrews, E., and Bordas, J. (1994). Solution structure of Taxotere-induced microtubules to 3-nm resolution. The change in protofilament number is linked to the binding of the taxol side chain. *J Biol Chem* 269, 31785-31792.
- Arnal, I., Heichette, C., Diamantopoulos, G.S., and Chretien, D. (2004). CLIP-170/tubulin-curved oligomers coassemble at microtubule ends and promote rescues. *Curr Biol* 14, 2086-2095.
- Arnal, I., Karsenti, E., and Hyman, A.A. (2000). Structural transitions at microtubule ends correlate with their dynamic properties in *Xenopus* egg extracts. *J Cell Biol* 149, 767-774.

- Arnal, I., Metoz, F., DeBonis, S., and Wade, R.H. (1996). Three-dimensional structure of functional motor proteins on microtubules. *Curr Biol* 6, 1265-1270.
- Asakawa, K., Kume, K., Kanai, M., Goshima, T., Miyahara, K., Dhut, S., Tee, W.W., Hirata, D., and Toda, T. (2006). The V260I mutation in fission yeast alpha-tubulin Atb2 affects microtubule dynamics and EB1-Mal3 localization and activates the Bub1 branch of the spindle checkpoint. *Mol Biol Cell* 17, 1421-1435.
- Asakawa, K., and Toda, T. (2006). Cooperation of EB1-Mal3 and the Bub1 spindle checkpoint. *Cell Cycle* 5, 27-30.
- Asakawa, K., Toya, M., Sato, M., Kanai, M., Kume, K., Goshima, T., Garcia, M.A., Hirata, D., and Toda, T. (2005). Mal3, the fission yeast EB1 homologue, cooperates with Bub1 spindle checkpoint to prevent monopolar attachment. *EMBO Rep* 6, 1194-1200.
- Askham, J.M., Moncur, P., Markham, A.F., and Morrison, E.E. (2000). Regulation and function of the interaction between the APC tumour suppressor protein and EB1. *Oncogene* 19, 1950-1958.
- Askham, J.M., Vaughan, K.T., Goodson, H.V., and Morrison, E.E. (2002). Evidence that an interaction between EB1 and p150(Glued) is required for the formation and maintenance of a radial microtubule array anchored at the centrosome. *Mol Biol Cell* 13, 3627-3645.
- Ausmees, N., Kuhn, J.R., and Jacobs-Wagner, C. (2003). The bacterial cytoskeleton: an intermediate filament-like function in cell shape. *Cell* 115, 705-713.
- Austin, J.R., 2nd, Segui-Simarro, J.M., and Staehelin, L.A. (2005). Quantitative analysis of changes in spatial distribution and plus-end geometry of microtubules involved in plant-cell cytokinesis. *J Cell Sci* 118, 3895-3903.
- Baas, P.W., Deitch, J.S., Black, M.M., and Banker, G.A. (1988). Polarity orientation of microtubules in hippocampal neurons: uniformity in the axon and nonuniformity in the dendrite. *Proc Natl Acad Sci U S A* 85, 8335-8339.
- Bartolini, F., and Gundersen, G.G. (2006). Generation of noncentrosomal microtubule arrays. *J Cell Sci* 119, 4155-4163.
- Basto, R., Lau, J., Vinogradova, T., Gardiol, A., Woods, C.G., Khodjakov, A., and Raff, J.W. (2006). Flies without centrioles. *Cell* 125, 1375-1386.
- Behrens, R., and Nurse, P. (2002). Roles of fission yeast tealp in the localization of polarity factors and in organizing the microtubular cytoskeleton. *J Cell Biol* 157, 783-793.

- Beinhauer, J.D., Hagan, I.M., Hegemann, J.H., and Fleig, U. (1997). Mal3, the fission yeast homologue of the human APC-interacting protein EB-1 is required for microtubule integrity and the maintenance of cell form. *J Cell Biol* 139, 717-728.
- Berrueta, L., Kraeft, S.K., Tirnauer, J.S., Schuyler, S.C., Chen, L.B., Hill, D.E., Pellman, D., and Bierer, B.E. (1998). The adenomatous polyposis coli-binding protein EB1 is associated with cytoplasmic and spindle microtubules. *Proc Natl Acad Sci U S A* 95, 10596-10601.
- Beuron, F., and Hoenger, A. (2001). Structural analysis of the microtubule-kinesin complex by cryo-electron microscopy. *Methods Mol Biol* 164, 235-254.
- Bi, E.F., and Lutkenhaus, J. (1991). FtsZ ring structure associated with division in *Escherichia coli*. *Nature* 354, 161-164.
- Bornens, M. (2002). Centrosome composition and microtubule anchoring mechanisms. *Curr Opin Cell Biol* 14, 25-34.
- Bouchet-Marquis, C., Zuber, B., Glynn, A.M., Eltsov, M., Grabenbauer, M., Goldie, K.N., Thomas, D., Frangakis, A.S., Dubochet, J., and Chretien, D. (2007). Visualization of cell microtubules in their native state. *Biol Cell* 99, 45-53.
- Bradford, M.M. (1976). A rapid and sensitive method for the quantitation of microgram quantities of protein utilizing the principle of protein-dye binding. *Anal Biochem* 72, 248-254.
- Bre, M.H., Kreis, T.E., and Karsenti, E. (1987). Control of microtubule nucleation and stability in Madin-Darby canine kidney cells: the occurrence of noncentrosomal, stable deetyrosinated microtubules. *J Cell Biol* 105, 1283-1296.
- Browning, H., and Hackney, D.D. (2005). The EB1 homolog Mal3 stimulates the ATPase of the kinesin Tea2 by recruiting it to the microtubule. *J Biol Chem* 280, 12299-12304.
- Browning, H., Hackney, D.D., and Nurse, P. (2003). Targeted movement of cell end factors in fission yeast. *Nat Cell Biol* 5, 812-818.
- Brunner, D., and Nurse, P. (2000). CLIP170-like tip1p spatially organizes microtubular dynamics in fission yeast. *Cell* 102, 695-704.
- Bu, W., and Su, L.K. (2003). Characterization of functional domains of human EB1 family proteins. *J Biol Chem* 278, 49721-49731.
- Burgess, S.A., Walker, M.L., Sakakibara, H., Knight, P.J., and Oiwa, K. (2003). Dynein structure and power stroke. *Nature* 421, 715-718.

- Busch, K.E., and Brunner, D. (2004). The microtubule plus end-tracking proteins mal3p and tip1p cooperate for cell-end targeting of interphase microtubules. *Curr Biol* *14*, 548-559.
- Busch, K.E., Hayles, J., Nurse, P., and Brunner, D. (2004). Tea2p kinesin is involved in spatial microtubule organization by transporting tip1p on microtubules. *Dev Cell* *6*, 831-843.
- Carrier, M.F. (1992). Nucleotide hydrolysis regulates the dynamics of actin filaments and microtubules. *Philos Trans R Soc Lond B Biol Sci* *336*, 93-97.
- Carvalho, P., Gupta, M.L., Jr., Hoyt, M.A., and Pellman, D. (2004). Cell cycle control of kinesin-mediated transport of Bik1 (CLIP-170) regulates microtubule stability and dynein activation. *Dev Cell* *6*, 815-829.
- Carvalho, P., Tirnauer, J.S., and Pellman, D. (2003). Surfing on microtubule ends. *Trends Cell Biol* *13*, 229-237.
- Cassimeris, L. (1999). Accessory protein regulation of microtubule dynamics throughout the cell cycle. *Curr Opin Cell Biol* *11*, 134-141.
- Cassimeris, L. (2002). The oncoprotein 18/stathmin family of microtubule destabilizers. *Curr Opin Cell Biol* *14*, 18-24.
- Cassimeris, L., Gard, D., Tran, P.T., and Erickson, H.P. (2001). XMAP215 is a long thin molecule that does not increase microtubule stiffness. *J Cell Sci* *114*, 3025-3033.
- Caudron, N., Arnal, I., Buhler, E., Job, D., and Valiron, O. (2002). Microtubule nucleation from stable tubulin oligomers. *J Biol Chem* *277*, 50973-50979.
- Caudron, N., Valiron, O., Usson, Y., Valiron, P., and Job, D. (2000). A reassessment of the factors affecting microtubule assembly and disassembly in vitro. *J Mol Biol* *297*, 211-220.
- Chen, C.R., Chen, J., and Chang, E.C. (2000). A conserved interaction between Moel1 and Mal3 is important for proper spindle formation in *Schizosaccharomyces pombe*. *Mol Biol Cell* *11*, 4067-4077.
- Chen, J., Kanai, Y., Cowan, N.J., and Hirokawa, N. (1992). Projection domains of MAP2 and tau determine spacings between microtubules in dendrites and axons. *Nature* *360*, 674-677.
- Choi, J.H., Bertram, P.G., Drenan, R., Carvalho, J., Zhou, H.H., and Zheng, X.F. (2002). The FKBP12-rapamycin-associated protein (FRAP) is a CLIP-170 kinase. *EMBO Rep* *3*, 988-994.

- Chretien, D., Flyvbjerg, H., and Fuller, S.D. (1998). Limited flexibility of the interprotofilament bonds in microtubules assembled from pure tubulin. *Eur Biophys J* 27, 490-500.
- Chretien, D., Fuller, S.D., and Karsenti, E. (1995). Structure of growing microtubule ends: two-dimensional sheets close into tubes at variable rates. *J Cell Biol* 129, 1311-1328.
- Chretien, D., Jainosi, I., Taveau, J.C., and Flyvbjerg, H. (1999). Microtubule's conformational cap. *Cell Struct Funct* 24, 299-303.
- Chretien, D., Kenney, J.M., Fuller, S.D., and Wade, R.H. (1996). Determination of microtubule polarity by cryo-electron microscopy. *Structure* 4, 1031-1040.
- Chretien, D., Metoz, F., Verde, F., Karsenti, E., and Wade, R.H. (1992). Lattice defects in microtubules: protofilament numbers vary within individual microtubules. *J Cell Biol* 117, 1031-1040.
- Chretien, D., and Wade, R.H. (1991). New data on the microtubule surface lattice. *Biol Cell* 71, 161-174.
- Craig, R., and Woodhead, J.L. (2006). Structure and function of myosin filaments. *Curr Opin Struct Biol* 16, 204-212.
- Crowther, R.A., and Goedert, M. (2000). Abnormal tau-containing filaments in neurodegenerative diseases. *J Struct Biol* 130, 271-279.
- Dantzig, J.A., Liu, T.Y., and Goldman, Y.E. (2006). Functional studies of individual myosin molecules. *Ann N Y Acad Sci* 1080, 1-18.
- Dawe, H.R., Farr, H., and Gull, K. (2007). Centriole/basal body morphogenesis and migration during ciliogenesis in animal cells. *J Cell Sci* 120, 7-15.
- DeRosier, D.J., and Moore, P.B. (1970). Reconstruction of three-dimensional images from electron micrographs of structures with helical symmetry. *J Mol Biol* 52, 355-369.
- Desai, A., Verma, S., Mitchison, T.J., and Walczak, C.E. (1999). Kin I kinesins are microtubule-destabilizing enzymes. *Cell* 96, 69-78.
- Diamantopoulos, G.S., Perez, F., Goodson, H.V., Batelier, G., Melki, R., Kreis, T.E., and Rickard, J.E. (1999). Dynamic localization of CLIP-170 to microtubule plus ends is coupled to microtubule assembly. *J Cell Biol* 144, 99-112.

- Dias, D.P., and Milligan, R.A. (1999). Motor protein decoration of microtubules grown in high salt conditions reveals the presence of mixed lattices. *J Mol Biol* 287, 287-292.
- dos Remedios, C.G., Chhabra, D., Kekic, M., Dedova, I.V., Tsubakihara, M., Berry, D.A., and Nosworthy, N.J. (2003). Actin binding proteins: regulation of cytoskeletal microfilaments. *Physiol Rev* 83, 433-473.
- Downing, K.H., and Nogales, E. (1998). Tubulin and microtubule structure. *Curr Opin Cell Biol* 10, 16-22.
- Drabik, P., Gusarov, S., and Kovalenko, A. (2007). Microtubule stability studied by three-dimensional molecular theory of solvation. *Biophys J* 92, 394-403.
- Drewes, G., Ebneith, A., and Mandelkow, E.M. (1998). MAPs, MARKs and microtubule dynamics. *Trends Biochem Sci* 23, 307-311.
- Drummond, D.R., and Cross, R.A. (2000). Dynamics of interphase microtubules in *Schizosaccharomyces pombe*. *Curr Biol* 10, 766-775.
- Dubochet, J., Adrian, M., Chang, J.J., Homo, J.C., Lepault, J., McDowell, A.W., and Schultz, P. (1988). Cryo-electron microscopy of vitrified specimens. *Q Rev Biophys* 21, 129-228.
- Dujardin, D., Wacker, U.I., Moreau, A., Schroer, T.A., Rickard, J.E., and De Mey, J.R. (1998). Evidence for a role of CLIP-170 in the establishment of metaphase chromosome alignment. *J Cell Biol* 141, 849-862.
- Ebneith, A., Drewes, G., Mandelkow, E.M., and Mandelkow, E. (1999). Phosphorylation of MAP2c and MAP4 by MARK kinases leads to the destabilization of microtubules in cells. *Cell Motil Cytoskeleton* 44, 209-224.
- Ebneith, A., Godemann, R., Stamer, K., Illenberger, S., Trinczek, B., and Mandelkow, E. (1998). Overexpression of tau protein inhibits kinesin-dependent trafficking of vesicles, mitochondria, and endoplasmic reticulum: implications for Alzheimer's disease. *J Cell Biol* 143, 777-794.
- Esue, O., Cordero, M., Wirtz, D., and Tseng, Y. (2005). The assembly of MreB, a prokaryotic homolog of actin. *J Biol Chem* 280, 2628-2635.
- Fleig, U., Salus, S.S., Karig, I., and Sazer, S. (2000). The fission yeast ran GTPase is required for microtubule integrity. *J Cell Biol* 151, 1101-1111.
- Flyvbjerg, H., Jobs, E., and Leibler, S. (1996). Kinetics of self-assembling microtubules: an "inverse problem" in biochemistry. *Proc Natl Acad Sci U S A* 93, 5975-5979.

- Foeger, N., Wiesel, N., Lotsch, D., Mucke, N., Kreplak, L., Aebi, U., Gruenbaum, Y., and Herrmann, H. (2006). Solubility properties and specific assembly pathways of the B-type lamin from *Caenorhabditis elegans*. *J Struct Biol* *155*, 340-350.
- Gache, V., Louwagie, M., Garin, J., Caudron, N., Lafanechere, L., and Valiron, O. (2005). Identification of proteins binding the native tubulin dimer. *Biochem Biophys Res Commun* *327*, 35-42.
- Galjart, N. (2005). CLIPs and CLASPs and cellular dynamics. *Nat Rev Mol Cell Biol* *6*, 487-498.
- Galjart, N., and Perez, F. (2003). A plus-end raft to control microtubule dynamics and function. *Curr Opin Cell Biol* *15*, 48-53.
- Garcia, M.L., and Cleveland, D.W. (2001). Going new places using an old MAP: tau, microtubules and human neurodegenerative disease. *Curr Opin Cell Biol* *13*, 41-48.
- Garner, E.C., Campbell, C.S., and Mullins, R.D. (2004). Dynamic instability in a DNA-segregating prokaryotic actin homolog. *Science* *306*, 1021-1025.
- Garvalov, B.K., Zuber, B., Bouchet-Marquis, C., Kudryashev, M., Gruska, M., Beck, M., Leis, A., Frischknecht, F., Bradke, F., Baumeister, W., Dubochet, J., and Cyrklaff, M. (2006). Luminal particles within cellular microtubules. *J Cell Biol* *174*, 759-765.
- Gaskin, F., Cantor, C.R., and Shelanski, M.L. (1974). Turbidimetric studies of the in vitro assembly and disassembly of porcine neurotubules. *J Mol Biol* *89*, 737-755.
- Gibbons, I.R. (1981). Cilia and flagella of eukaryotes. *J Cell Biol* *91*, 107s-124s.
- Gigant, B., Curmi, P.A., Martin-Barbey, C., Charbaut, E., Lachkar, S., Lebeau, L., Siavoshian, S., Sobel, A., and Knossow, M. (2000). The 4 Å X-ray structure of a tubulin:stathmin-like domain complex. *Cell* *102*, 809-816.
- Gigant, B., Wang, C., Ravelli, R.B., Roussi, F., Steinmetz, M.O., Curmi, P.A., Sobel, A., and Knossow, M. (2005). Structural basis for the regulation of tubulin by vinblastine. *Nature* *435*, 519-522.
- Gilbert, S.P., Webb, M.R., Brune, M., and Johnson, K.A. (1995). Pathway of processive ATP hydrolysis by kinesin. *Nature* *373*, 671-676.
- Gimona, M., Djinovic-Carugo, K., Kranewitter, W.J., and Winder, S.J. (2002). Functional plasticity of CH domains. *FEBS Lett* *513*, 98-106.

- Goldie, K.N., Wedig, T., Mitra, A.K., Aebi, U., Herrmann, H., and Hoenger, A. (2006). Dissecting the 3-D structure of vimentin intermediate filaments by cryo-electron tomography. *J Struct Biol*.
- Green, R.A., and Kaplan, K.B. (2003). Chromosome instability in colorectal tumor cells is associated with defects in microtubule plus-end attachments caused by a dominant mutation in APC. *J Cell Biol* *163*, 949-961.
- Gross, H. (1987). High resolution metal replication of freeze-dried specimens. In: *Cryotechniques in Biological Electron Microscopy*, eds. E.R.A. Steinbrecht and K. Zierold: Springer Verlag, 205-215.
- Gross, H., Krusche, K., and Tittmann, P. (1990). Recent progress in high resolutionschadowing for biological samples. XIIth International Congress for Electron Microscopy.
- Hayashi, I., and Ikura, M. (2003). Crystal structure of the amino-terminal microtubule-binding domain of end-binding protein 1 (EB1). *J Biol Chem* *278*, 36430-36434.
- Hayashi, I., Wilde, A., Mal, T.K., and Ikura, M. (2005). Structural basis for the activation of microtubule assembly by the EB1 and p150Glued complex. *Mol Cell* *19*, 449-460.
- Heald, R., Tournebize, R., Blank, T., Sandaltzopoulos, R., Becker, P., Hyman, A., and Karsenti, E. (1996). Self-organization of microtubules into bipolar spindles around artificial chromosomes in *Xenopus* egg extracts. *Nature* *382*, 420-425.
- Helenius, J., Brouhard, G., Kalaidzidis, Y., Diez, S., and Howard, J. (2006). The depolymerizing kinesin MCAK uses lattice diffusion to rapidly target microtubule ends. *Nature* *441*, 115-119.
- Helfand, B.T., Chang, L., and Goldman, R.D. (2004). Intermediate filaments are dynamic and motile elements of cellular architecture. *J Cell Sci* *117*, 133-141.
- Herrmann, H., and Aebi, U. (2004). Intermediate filaments: molecular structure, assembly mechanism, and integration into functionally distinct intracellular Scaffolds. *Annu Rev Biochem* *73*, 749-789.
- Hirose, K., Henningsen, U., Schliwa, M., Toyoshima, C., Shimizu, T., Alonso, M., Cross, R.A., and Amos, L.A. (2000). Structural comparison of dimeric Eg5, *Neurospora* kinesin (Nkin) and Ncd head-Nkin neck chimera with conventional kinesin. *Embo J* *19*, 5308-5314.
- Hizlan, D., Mishima, M., Tittmann, P., Gross, H., Glotzer, M., and Hoenger, A. (2006). Structural analysis of the ZEN-4/CeMKLP1 motor domain and its interaction with microtubules. *J Struct Biol* *153*, 73-84.

- Hoenger, A., Doerhoefer, M., Woehlke, G., Tittmann, P., Gross, H., Song, Y.H., and Mandelkow, E. (2000a). Surface topography of microtubule walls decorated with monomeric and dimeric kinesin constructs. *Biol Chem* 381, 1001-1011.
- Hoenger, A., Sablin, E.P., Vale, R.D., Fletterick, R.J., and Milligan, R.A. (1995). Three-dimensional structure of a tubulin-motor-protein complex. *Nature* 376, 271-274.
- Hoenger, A., Sack, S., Thormahlen, M., Marx, A., Muller, J., Gross, H., and Mandelkow, E. (1998). Image reconstructions of microtubules decorated with monomeric and dimeric kinesins: comparison with x-ray structure and implications for motility. *J Cell Biol* 141, 419-430.
- Hoenger, A., Thormahlen, M., Diaz-Avalos, R., Doerhoefer, M., Goldie, K.N., Muller, J., and Mandelkow, E. (2000b). A new look at the microtubule binding patterns of dimeric kinesins. *J Mol Biol* 297, 1087-1103.
- Honnappa, S., John, C.M., Kostrewa, D., Winkler, F.K., and Steinmetz, M.O. (2005). Structural insights into the EB1-APC interaction. *Embo J* 24, 261-269.
- Honnappa, S., Okhrimenko, O., Jaussi, R., Jawhari, H., Jelesarov, I., Winkler, F.K., and Steinmetz, M.O. (2006). Key interaction modes of dynamic +TIP networks. *Mol Cell* 23, 663-671.
- Hoog, J.L., Schwartz, C., Noon, A.T., O'Toole E, T., Mastronarde, D.N., McIntosh, J.R., and Antony, C. (2007). Organization of interphase microtubules in fission yeast analyzed by electron tomography. *Dev Cell* 12, 349-361.
- Horesh, D., Sapir, T., Francis, F., Wolf, S.G., Caspi, M., Elbaum, M., Chelly, J., and Reiner, O. (1999). Doublecortin, a stabilizer of microtubules. *Hum Mol Genet* 8, 1599-1610.
- Howard, J., and Hyman, A.A. (2007). Microtubule polymerases and depolymerases. *Curr Opin Cell Biol* 19, 31-35.
- Hyman, A.A., Salser, S., Drechsel, D.N., Unwin, N., and Mitchison, T.J. (1992). Role of GTP hydrolysis in microtubule dynamics: information from a slowly hydrolyzable analogue, GMPCPP. *Mol Biol Cell* 3, 1155-1167.
- Janson, M.E., Setty, T.G., Paoletti, A., and Tran, P.T. (2005). Efficient formation of bipolar microtubule bundles requires microtubule-bound gamma-tubulin complexes. *J Cell Biol* 169, 297-308.
- Jimbo, T., Kawasaki, Y., Koyama, R., Sato, R., Takada, S., Haraguchi, K., and Akiyama, T. (2002). Identification of a link between the tumour suppressor APC and the kinesin superfamily. *Nat Cell Biol* 4, 323-327.

- Job, D., Valiron, O., and Oakley, B. (2003). Microtubule nucleation. *Curr Opin Cell Biol* *15*, 111-117.
- Juwana, J.P., Henderikx, P., Mischo, A., Wadle, A., Fadle, N., Gerlach, K., Arends, J.W., Hoogenboom, H., Pfreundschuh, M., and Renner, C. (1999). EB/RP gene family encodes tubulin binding proteins. *Int J Cancer* *81*, 275-284.
- Kapitein, L.C., Peterman, E.J., Kwok, B.H., Kim, J.H., Kapoor, T.M., and Schmidt, C.F. (2005). The bipolar mitotic kinesin Eg5 moves on both microtubules that it crosslinks. *Nature* *435*, 114-118.
- Kerssemakers, J.W., Munteanu, E.L., Laan, L., Noetzel, T.L., Janson, M.E., and Dogterom, M. (2006). Assembly dynamics of microtubules at molecular resolution. *Nature* *442*, 709-712.
- Kikkawa, M., Ishikawa, T., Nakata, T., Wakabayashi, T., and Hirokawa, N. (1994). Direct visualization of the microtubule lattice seam both in vitro and in vivo. *J Cell Biol* *127*, 1965-1971.
- Kim, M.H., Cierpicki, T., Derewenda, U., Krowarsch, D., Feng, Y., Devedjiev, Y., Dauter, Z., Walsh, C.A., Otlewski, J., Bushweller, J.H., and Derewenda, Z.S. (2003). The DCX-domain tandems of doublecortin and doublecortin-like kinase. *Nat Struct Biol* *10*, 324-333.
- Kinoshita, K., Arnal, I., Desai, A., Drechsel, D.N., and Hyman, A.A. (2001). Reconstitution of physiological microtubule dynamics using purified components. *Science* *294*, 1340-1343.
- Kirschner, M., and Mitchison, T. (1986). Beyond self-assembly: from microtubules to morphogenesis. *Cell* *45*, 329-342.
- Komarova, Y.A., Akhmanova, A.S., Kojima, S., Galjart, N., and Borisy, G.G. (2002a). Cytoplasmic linker proteins promote microtubule rescue in vivo. *J Cell Biol* *159*, 589-599.
- Komarova, Y.A., Vorobjev, I.A., and Borisy, G.G. (2002b). Life cycle of MTs: persistent growth in the cell interior, asymmetric transition frequencies and effects of the cell boundary. *J Cell Sci* *115*, 3527-3539.
- Krebs, A., Goldie, K.N., and Hoenger, A. (2004). Complex formation with kinesin motor domains affects the structure of microtubules. *J Mol Biol* *335*, 139-153.
- Krebs, A., Goldie, K.N., and Hoenger, A. (2005). Structural rearrangements in tubulin following microtubule formation. *EMBO Rep* *6*, 227-232.

- Krzysiak, T.C., Wendt, T., Sproul, L.R., Tittmann, P., Gross, H., Gilbert, S.P., and Hoenger, A. (2006). A structural model for monastrol inhibition of dimeric kinesin Eg5. *Embo J* 25, 2263-2273.
- La Carbona, S., Le Goff, C., and Le Goff, X. (2006). Fission yeast cytoskeletons and cell polarity factors: connecting at the cortex. *Biol Cell* 98, 619-631.
- Laemmli, U.K. (1970). Cleavage of structural proteins during the assembly of the head of bacteriophage T4. In: *Nature*, vol. 227, 680-685.
- Langford, K.J., Askham, J.M., Lee, T., Adams, M., and Morrison, E.E. (2006). Examination of actin and microtubule dependent APC localisations in living mammalian cells. *BMC Cell Biol* 7, 3.
- Lansbergen, G., Komarova, Y., Modesti, M., Wyman, C., Hoogenraad, C.C., Goodson, H.V., Lemaitre, R.P., Drechsel, D.N., van Munster, E., Gadella, T.W., Jr., Grosveld, F., Galjart, N., Borisy, G.G., and Akhmanova, A. (2004). Conformational changes in CLIP-170 regulate its binding to microtubules and dynactin localization. *J Cell Biol* 166, 1003-1014.
- Lawrence, C.J., Dawe, R.K., Christie, K.R., Cleveland, D.W., Dawson, S.C., Endow, S.A., Goldstein, L.S., Goodson, H.V., Hirokawa, N., Howard, J., Malmberg, R.L., McIntosh, J.R., Miki, H., Mitchison, T.J., Okada, Y., Reddy, A.S., Saxton, W.M., Schliwa, M., Scholey, J.M., Vale, R.D., Walczak, C.E., and Wordeman, L. (2004). A standardized kinesin nomenclature. *J Cell Biol* 167, 19-22.
- Lee, H., Engel, U., Rusch, J., Scherrer, S., Sheard, K., and Van Vactor, D. (2004). The microtubule plus end tracking protein Orbit/MAST/CLASP acts downstream of the tyrosine kinase Abl in mediating axon guidance. *Neuron* 42, 913-926.
- Li, H., DeRosier, D.J., Nicholson, W.V., Nogales, E., and Downing, K.H. (2002a). Microtubule structure at 8 Å resolution. *Structure* 10, 1317-1328.
- Li, S., Finley, J., Liu, Z.J., Qiu, S.H., Chen, H., Luan, C.H., Carson, M., Tsao, J., Johnson, D., Lin, G., Zhao, J., Thomas, W., Nagy, L.A., Sha, B., DeLucas, L.J., Wang, B.C., and Luo, M. (2002b). Crystal structure of the cytoskeleton-associated protein glycine-rich (CAP-Gly) domain. *J Biol Chem* 277, 48596-48601.
- Ligon, L.A., Shelly, S.S., Tokito, M., and Holzbaur, E.L. (2003). The microtubule plus-end proteins EB1 and dynactin have differential effects on microtubule polymerization. *Mol Biol Cell* 14, 1405-1417.
- Ligon, L.A., Shelly, S.S., Tokito, M.K., and Holzbaur, E.L. (2006). Microtubule binding proteins CLIP-170, EB1, and p150Glued form distinct plus-end complexes. *FEBS Lett* 580, 1327-1332.

- Littauer, U.Z., Givon, D., Thierauf, M., Ginzburg, I., and Ponstingl, H. (1986). Common and distinct tubulin binding sites for microtubule-associated proteins. *Proc Natl Acad Sci U S A* 83, 7162-7166.
- Louie, R.K., Bahmanyar, S., Siemers, K.A., Votin, V., Chang, P., Stearns, T., Nelson, W.J., and Barth, A.I. (2004). Adenomatous polyposis coli and EB1 localize in close proximity of the mother centriole and EB1 is a functional component of centrosomes. *J Cell Sci* 117, 1117-1128.
- Lowe, J., and Amos, L.A. (1999). Tubulin-like protofilaments in Ca²⁺-induced FtsZ sheets. *Embo J* 18, 2364-2371.
- Lowe, J., Li, H., Downing, K.H., and Nogales, E. (2001). Refined structure of alpha beta-tubulin at 3.5 Å resolution. *J Mol Biol* 313, 1045-1057.
- Lu, C., Srayko, M., and Mains, P.E. (2004). The *Caenorhabditis elegans* microtubule-severing complex MEI-1/MEI-2 katanin interacts differently with two superficially redundant beta-tubulin isoforms. *Mol Biol Cell* 15, 142-150.
- Luders, J., and Stearns, T. (2007). Microtubule-organizing centres: a re-evaluation. *Nat Rev Mol Cell Biol* 8, 161-167.
- Lupas, A., Van Dyke, M., and Stock, J. (1991). Predicting coiled coils from protein sequences. *Science* 252, 1162-1164.
- Mandelkow, E., Schultheiss, R., and Mandelkow, E.M. (1984). Assembly and three-dimensional image reconstruction of tubulin hoops. *J Mol Biol* 177, 507-529.
- Mandelkow, E.M., and Mandelkow, E. (1985). Unstained microtubules studied by cryo-electron microscopy. Substructure, supertwist and disassembly. *J Mol Biol* 181, 123-135.
- Mandelkow, E.M., Mandelkow, E., and Milligan, R.A. (1991). Microtubule dynamics and microtubule caps: a time-resolved cryo-electron microscopy study. *J Cell Biol* 114, 977-991.
- Mandelkow, E.M., Rapp, R., and Mandelkow, E. (1986a). Microtubule structure studied by quick freezing: cryo-electron microscopy and freeze fracture. *J Microsc* 141, 361-373.
- Mandelkow, E.M., Schultheiss, R., Rapp, R., Muller, M., and Mandelkow, E. (1986b). On the surface lattice of microtubules: helix starts, protofilament number, seam, and handedness. *J Cell Biol* 102, 1067-1073.

- Marklund, U., Larsson, N., Gradin, H.M., Brattsand, G., and Gullberg, M. (1996). Oncoprotein 18 is a phosphorylation-responsive regulator of microtubule dynamics. *Embo J* 15, 5290-5298.
- Martin, S.G., and Chang, F. (2006). Dynamics of the formin for3p in actin cable assembly. *Curr Biol* 16, 1161-1170.
- Martin, S.G., McDonald, W.H., Yates, J.R., 3rd, and Chang, F. (2005). Tea4p links microtubule plus ends with the formin for3p in the establishment of cell polarity. *Dev Cell* 8, 479-491.
- Marx, A., Muller, J., and Mandelkow, E. (2005). The structure of microtubule motor proteins. *Adv Protein Chem* 71, 299-344.
- Mata, J., and Nurse, P. (1997). tea1 and the microtubular cytoskeleton are important for generating global spatial order within the fission yeast cell. *Cell* 89, 939-949.
- McConnell, S.J., and Yaffe, M.P. (1993). Intermediate filament formation by a yeast protein essential for organelle inheritance. *Science* 260, 687-689.
- Mennella, V., Rogers, G.C., Rogers, S.L., Buster, D.W., Vale, R.D., and Sharp, D.J. (2005). Functionally distinct kinesin-13 family members cooperate to regulate microtubule dynamics during interphase. *Nat Cell Biol* 7, 235-245.
- Meurer-Grob, P., Kasparian, J., and Wade, R.H. (2001). Microtubule structure at improved resolution. *Biochemistry* 40, 8000-8008.
- Miki, H., Okada, Y., and Hirokawa, N. (2005). Analysis of the kinesin superfamily: insights into structure and function. *Trends Cell Biol* 15, 467-476.
- Milligan, R.A., and Flicker, P.F. (1987). Structural relationships of actin, myosin, and tropomyosin revealed by cryo-electron microscopy. *J Cell Biol* 105, 29-39.
- Mimori-Kiyosue, Y., Shiina, N., and Tsukita, S. (2000). The dynamic behavior of the APC-binding protein EB1 on the distal ends of microtubules. *Curr Biol* 10, 865-868.
- Mimori-Kiyosue, Y., and Tsukita, S. (2003). "Search-and-capture" of microtubules through plus-end-binding proteins (+TIPs). *J Biochem (Tokyo)* 134, 321-326.
- Mitchison, T., and Kirschner, M. (1984). Dynamic instability of microtubule growth. *Nature* 312, 237-242.
- Mizuno, N., Toba, S., Edamatsu, M., Watai-Nishii, J., Hirokawa, N., Toyoshima, Y.Y., and Kikkawa, M. (2004). Dynein and kinesin share an overlapping microtubule-binding site. *Embo J* 23, 2459-2467.

- Moore, P.B., Huxley, H.E., and DeRosier, D.J. (1970). Three-dimensional reconstruction of F-actin, thin filaments and decorated thin filaments. *J Mol Biol* 50, 279-295.
- Moore, C.A., Cooper, J., Wagenbach, M., Ovechkina, Y., Wordeman, L., and Milligan, R.A. (2006). The role of the kinesin-13 neck in microtubule depolymerization. *Cell Cycle* 5, 1812-1815.
- Moore, C.A., Hekmat-Nejad, M., Sakowicz, R., and Milligan, R.A. (2003). Regulation of KinI kinesin ATPase activity by binding to the microtubule lattice. *J Cell Biol* 163, 963-971.
- Moore, C.A., and Milligan, R.A. (2006). Lucky 13-microtubule depolymerisation by kinesin-13 motors. *J Cell Sci* 119, 3905-3913.
- Moore, C.A., Perderiset, M., Francis, F., Chelly, J., Houdusse, A., and Milligan, R.A. (2004). Mechanism of microtubule stabilization by doublecortin. *Mol Cell* 14, 833-839.
- Moore, C.A., Yu, M., Guo, J., Beraud, C., Sakowicz, R., and Milligan, R.A. (2002). A mechanism for microtubule depolymerization by KinI kinesins. *Mol Cell* 9, 903-909.
- Moreno, S., Klar, A., and Nurse, P. (1991). Molecular genetic analysis of fission yeast *Schizosaccharomyces pombe*. *Methods Enzymol* 194, 795-823.
- Moritz, M., Braunfeld, M.B., Guenebaut, V., Heuser, J., and Agard, D.A. (2000). Structure of the gamma-tubulin ring complex: a template for microtubule nucleation. *Nat Cell Biol* 2, 365-370.
- Morrison, E.E. (2007). Action and interactions at microtubule ends. *Cell Mol Life Sci* 64, 307-317.
- Morrison, E.E., Wardleworth, B.N., Askham, J.M., Markham, A.F., and Meredith, D.M. (1998). EB1, a protein which interacts with the APC tumour suppressor, is associated with the microtubule cytoskeleton throughout the cell cycle. *Oncogene* 17, 3471-3477.
- Mukrasch, M.D., von Bergen, M., Biernat, J., Fischer, D., Griesinger, C., Mandelkow, E., and Zweckstetter, M. (2007). The "jaws" of the tau-microtubule interaction. *J Biol Chem* 282, 12230-12239.
- Muller-Reichert, T., Chrétien, D., Severin, F., and Hyman, A.A. (1998). Structural changes at microtubule ends accompanying GTP hydrolysis: information from a slowly hydrolyzable analogue of GTP, guanylyl (alpha,beta)methylenediphosphonate. *Proc Natl Acad Sci U S A* 95, 3661-3666.

- Musch, A. (2004). Microtubule organization and function in epithelial cells. *Traffic* 5, 1-9.
- Nakamura, M., Zhou, X.Z., and Lu, K.P. (2001). Critical role for the EB1 and APC interaction in the regulation of microtubule polymerization. *Curr Biol* 11, 1062-1067.
- Nicastro, D., McIntosh, J.R., and Baumeister, W. (2005). 3D structure of eukaryotic flagella in a quiescent state revealed by cryo-electron tomography. *Proc Natl Acad Sci U S A* 102, 15889-15894.
- Niederstrasser, H., Salehi-Had, H., Gan, E.C., Walczak, C., and Nogales, E. (2002). XKCM1 acts on a single protofilament and requires the C terminus of tubulin. *J Mol Biol* 316, 817-828.
- Nogales, E. (2001). Structural insight into microtubule function. *Annu Rev Biophys Biomol Struct* 30, 397-420.
- Nogales, E., Whittaker, M., Milligan, R.A., and Downing, K.H. (1999). High-resolution model of the microtubule. *Cell* 96, 79-88.
- Nogales, E., Wolf, S.G., and Downing, K.H. (1998). Structure of the alpha beta tubulin dimer by electron crystallography. *Nature* 391, 199-203.
- O'Toole, E.T., McDonald, K.L., Mantler, J., McIntosh, J.R., Hyman, A.A., and Muller-Reichert, T. (2003). Morphologically distinct microtubule ends in the mitotic centrosome of *Caenorhabditis elegans*. *J Cell Biol* 163, 451-456.
- O'Toole, E.T., Winey, M., and McIntosh, J.R. (1999). High-voltage electron tomography of spindle pole bodies and early mitotic spindles in the yeast *Saccharomyces cerevisiae*. *Mol Biol Cell* 10, 2017-2031.
- Ogawa, T., Nitta, R., Okada, Y., and Hirokawa, N. (2004). A common mechanism for microtubule destabilizers-M type kinesins stabilize curling of the protofilament using the class-specific neck and loops. *Cell* 116, 591-602.
- Oliva, M.A., Cordell, S.C., and Lowe, J. (2004). Structural insights into FtsZ protofilament formation. *Nat Struct Mol Biol* 11, 1243-1250.
- Pampaloni, F., Lattanzi, G., Jonas, A., Surrey, T., Frey, E., and Florin, E.L. (2006). Thermal fluctuations of grafted microtubules provide evidence of a length-dependent persistence length. *Proc Natl Acad Sci U S A* 103, 10248-10253.
- Percipalle, P., and Visa, N. (2006). Molecular functions of nuclear actin in transcription. *J Cell Biol* 172, 967-971.

- Perez, F., Diamantopoulos, G.S., Stalder, R., and Kreis, T.E. (1999). CLIP-170 highlights growing microtubule ends in vivo. *Cell* *96*, 517-527.
- Peth, A., Boettcher, J.P., and Dubiel, W. (2007). Ubiquitin-dependent Proteolysis of the Microtubule End-binding Protein 1, EB1, Is Controlled by the COP9 Signalosome: Possible Consequences for Microtubule Filament Stability. *J Mol Biol* *368*, 550-563.
- Pfister, K.K., Fisher, E.M., Gibbons, I.R., Hays, T.S., Holzbaur, E.L., McIntosh, J.R., Porter, M.E., Schroer, T.A., Vaughan, K.T., Witman, G.B., King, S.M., and Vallee, R.B. (2005). Cytoplasmic dynein nomenclature. *J Cell Biol* *171*, 411-413.
- Pierre, P., Pepperkok, R., and Kreis, T.E. (1994). Molecular characterization of two functional domains of CLIP-170 in vivo. *J Cell Sci* *107* (Pt 7), 1909-1920.
- Pierre, P., Scheel, J., Rickard, J.E., and Kreis, T.E. (1992). CLIP-170 links endocytic vesicles to microtubules. *Cell* *70*, 887-900.
- Pollard, T.D., and Borisy, G.G. (2003). Cellular motility driven by assembly and disassembly of actin filaments. *Cell* *112*, 453-465.
- Ravelli, R.B., Gigant, B., Curmi, P.A., Jourdain, I., Lachkar, S., Sobel, A., and Knossow, M. (2004). Insight into tubulin regulation from a complex with colchicine and a stathmin-like domain. *Nature* *428*, 198-202.
- Raynaud-Messina, B., and Merdes, A. (2007). Gamma-tubulin complexes and microtubule organization. *Curr Opin Cell Biol* *19*, 24-30.
- Reck-Peterson, S.L., Yildiz, A., Carter, A.P., Gennerich, A., Zhang, N., and Vale, R.D. (2006). Single-molecule analysis of dynein processivity and stepping behavior. *Cell* *126*, 335-348.
- Rehberg, M., and Graf, R. (2002). Dictyostelium EB1 is a genuine centrosomal component required for proper spindle formation. *Mol Biol Cell* *13*, 2301-2310.
- Rickard, J.E., and Kreis, T.E. (1990). Identification of a novel nucleotide-sensitive microtubule-binding protein in HeLa cells. *J Cell Biol* *110*, 1623-1633.
- Rogers, S.L., Rogers, G.C., Sharp, D.J., and Vale, R.D. (2002). Drosophila EB1 is important for proper assembly, dynamics, and positioning of the mitotic spindle. *J Cell Biol* *158*, 873-884.
- Samejima, I., Lourenco, P.C., Snaith, H.A., and Sawin, K.E. (2005). Fission yeast mto2p regulates microtubule nucleation by the centrosomin-related protein mto1p. *Mol Biol Cell* *16*, 3040-3051.

- Samso, M., Radermacher, M., Frank, J., and Koonce, M.P. (1998). Structural characterization of a dynein motor domain. *J Mol Biol* 276, 927-937.
- Sandblad, L., Busch, K.E., Tittmann, P., Gross, H., Brunner, D., and Hoenger, A. (2006). The *Schizosaccharomyces pombe* EB1 homolog Mal3p binds and stabilizes the microtubule lattice seam. *Cell* 127, 1415-1424.
- Santarella, R.A., Skiniotis, G., Goldie, K.N., Tittmann, P., Gross, H., Mandelkow, E.M., Mandelkow, E., and Hoenger, A. (2004). Surface-decoration of microtubules by human tau. *J Mol Biol* 339, 539-553.
- Savage, C., Hamelin, M., Culotti, J.G., Coulson, A., Albertson, D.G., and Chalfie, M. (1989). *mec-7* is a beta-tubulin gene required for the production of 15-prot filament microtubules in *Caenorhabditis elegans*. *Genes Dev* 3, 870-881.
- Sawin, K.E., LeGuellec, K., Philippe, M., and Mitchison, T.J. (1992). Mitotic spindle organization by a plus-end-directed microtubule motor. *Nature* 359, 540-543.
- Sawin, K.E., and Tran, P.T. (2006). Cytoplasmic microtubule organization in fission yeast. *Yeast* 23, 1001-1014.
- Schiff, P.B., Fant, J., and Horwitz, S.B. (1979). Promotion of microtubule assembly in vitro by taxol. *Nature* 277, 665-667.
- Schroeter, J.P., and Breaudiere, J.P. (1996). SUPRIM: easily modified image processing software. *J Struct Biol* 116, 131-137.
- Schuyler, S.C., and Pellman, D. (2001). Microtubule "plus-end-tracking proteins": The end is just the beginning. *Cell* 105, 421-424.
- Schwartz, K., Richards, K., and Botstein, D. (1997). BIM1 encodes a microtubule-binding protein in yeast. *Mol Biol Cell* 8, 2677-2691.
- Seitz, A., Kojima, H., Oiwa, K., Mandelkow, E.M., Song, Y.H., and Mandelkow, E. (2002). Single-molecule investigation of the interference between kinesin, tau and MAP2c. *Embo J* 21, 4896-4905.
- Sept, D., Baker, N.A., and McCammon, J.A. (2003). The physical basis of microtubule structure and stability. *Protein Sci* 12, 2257-2261.
- Serrano, L., Avila, J., and Maccioni, R.B. (1984). Controlled proteolysis of tubulin by subtilisin: localization of the site for MAP2 interaction. *Biochemistry* 23, 4675-4681.

- Severin, F.F., Sorger, P.K., and Hyman, A.A. (1997). Kinetochores distinguish GTP from GDP forms of the microtubule lattice. *Nature* *388*, 888-891.
- Sharp, D.J., Brown, H.M., Kwon, M., Rogers, G.C., Holland, G., and Scholey, J.M. (2000). Functional coordination of three mitotic motors in *Drosophila* embryos. *Mol Biol Cell* *11*, 241-253.
- Shaw, R.M., Fay, A.J., Puthenveedu, M.A., von Zastrow, M., Jan, Y.N., and Jan, L.Y. (2007). Microtubule plus-end-tracking proteins target gap junctions directly from the cell interior to adherens junctions. *Cell* *128*, 547-560.
- Shih, Y.L., Le, T., and Rothfield, L. (2003). Division site selection in *Escherichia coli* involves dynamic redistribution of Min proteins within coiled structures that extend between the two cell poles. *Proc Natl Acad Sci U S A* *100*, 7865-7870.
- Shih, Y.L., and Rothfield, L. (2006). The bacterial cytoskeleton. *Microbiol Mol Biol Rev* *70*, 729-754.
- Sindelar, C.V., and Downing, K.H. (2007). The beginning of kinesin's force-generating cycle visualized at 9-A resolution. *J Cell Biol*.
- Skiniotis, G., Cochran, J.C., Muller, J., Mandelkow, E., Gilbert, S.P., and Hoenger, A. (2004). Modulation of kinesin binding by the C-termini of tubulin. *Embo J* *23*, 989-999.
- Skiniotis, G., Surrey, T., Altmann, S., Gross, H., Song, Y.H., Mandelkow, E., and Hoenger, A. (2003). Nucleotide-induced conformations in the neck region of dimeric kinesin. *Embo J* *22*, 1518-1528.
- Slep, K.C., Rogers, S.L., Elliott, S.L., Ohkura, H., Kolodziej, P.A., and Vale, R.D. (2005). Structural determinants for EB1-mediated recruitment of APC and spectraplakins to the microtubule plus end. *J Cell Biol* *168*, 587-598.
- Smith, P.R., and Kistler, J. (1977). Surface reliefs computed from micrographs of heavy metal-shadowed specimens. *J Ultrastruct Res* *61*, 124-133.
- Smits, R., Kielman, M.F., Breukel, C., Zurcher, C., Neufeld, K., Jagmohan-Changur, S., Hofland, N., van Dijk, J., White, R., Edelmann, W., Kucherlapati, R., Khan, P.M., and Fodde, R. (1999). Apc1638T: a mouse model delineating critical domains of the adenomatous polyposis coli protein involved in tumorigenesis and development. *Genes Dev* *13*, 1309-1321.
- Song, Y.H., and Mandelkow, E. (1993). Recombinant kinesin motor domain binds to beta-tubulin and decorates microtubules with a B surface lattice. *Proc Natl Acad Sci U S A* *90*, 1671-1675.

- Song, Y.H., and Mandelkow, E. (1995). The anatomy of flagellar microtubules: polarity, seam, junctions, and lattice. *J Cell Biol* 128, 81-94.
- Song, Y.H., Marx, A., Muller, J., Woehlke, G., Schliwa, M., Krebs, A., Hoenger, A., and Mandelkow, E. (2001). Structure of a fast kinesin: implications for ATPase mechanism and interactions with microtubules. *Embo J* 20, 6213-6225.
- Sosa, H., and Chretien, D. (1998). Relationship between moire patterns, tubulin shape, and microtubule polarity. *Cell Motil Cytoskeleton* 40, 38-43.
- Sosa, H., Dias, D.P., Hoenger, A., Whittaker, M., Wilson-Kubalek, E., Sablin, E., Fletterick, R.J., Vale, R.D., and Milligan, R.A. (1997). A model for the microtubule-Ncd motor protein complex obtained by cryo-electron microscopy and image analysis. *Cell* 90, 217-224.
- Sosa, H., and Milligan, R.A. (1996). Three-dimensional structure of ncd-decorated microtubules obtained by a back-projection method. *J Mol Biol* 260, 743-755.
- Squire, J.M. (1997). Architecture and function in the muscle sarcomere. *Curr Opin Struct Biol* 7, 247-257.
- Steinmetz, M.O., Stoffler, D., Hoenger, A., Bremer, A., and Aebi, U. (1997). Actin: from cell biology to atomic detail. *J Struct Biol* 119, 295-320.
- Stewart, M. (1988). Computer image processing of electron micrographs of biological structures with helical symmetry. *J Electron Microscop Tech* 9, 325-358.
- Strelkov, S.V., Herrmann, H., and Aebi, U. (2003). Molecular architecture of intermediate filaments. *Bioessays* 25, 243-251.
- Su, L.K., Burrell, M., Hill, D.E., Gyuris, J., Brent, R., Wiltshire, R., Trent, J., Vogelstein, B., and Kinzler, K.W. (1995). APC binds to the novel protein EB1. *Cancer Res* 55, 2972-2977.
- Su, L.K., and Qi, Y. (2001). Characterization of human MAPRE genes and their proteins. *Genomics* 71, 142-149.
- Sui, H., and Downing, K.H. (2006). Molecular architecture of axonemal microtubule doublets revealed by cryo-electron tomography. *Nature* 442, 475-478.
- Tan, D., Asenjo, A.B., Mennella, V., Sharp, D.J., and Sosa, H. (2006). Kinesin-13s form rings around microtubules. *J Cell Biol* 175, 25-31.
- Thormahlen, M., Marx, A., Muller, S.A., Song, Y., Mandelkow, E.M., Aebi, U., and Mandelkow, E. (1998). Interaction of monomeric and dimeric kinesin with microtubules. *J Mol Biol* 275, 795-809.

- Tilney, L.G., Bryan, J., Bush, D.J., Fujiwara, K., Mooseker, M.S., Murphy, D.B., and Snyder, D.H. (1973). Microtubules: evidence for 13 protofilaments. *J Cell Biol* *59*, 267-275.
- Tirnauer, J.S., Canman, J.C., Salmon, E.D., and Mitchison, T.J. (2002a). EB1 targets to kinetochores with attached, polymerizing microtubules. *Mol Biol Cell* *13*, 4308-4316.
- Tirnauer, J.S., Grego, S., Salmon, E.D., and Mitchison, T.J. (2002b). EB1-microtubule interactions in *Xenopus* egg extracts: role of EB1 in microtubule stabilization and mechanisms of targeting to microtubules. *Mol Biol Cell* *13*, 3614-3626.
- Tirnauer, J.S., O'Toole, E., Berrueta, L., Bierer, B.E., and Pellman, D. (1999). Yeast Bim1p promotes the G1-specific dynamics of microtubules. *J Cell Biol* *145*, 993-1007.
- Tran, P.T., Walker, R.A., and Salmon, E.D. (1997). A metastable intermediate state of microtubule dynamic instability that differs significantly between plus and minus ends. *J Cell Biol* *138*, 105-117.
- Tuszynski, J.A., Brown, J.A., Crawford, E., Carpenter, E.J., Nip, M.L.A., Dixon, J.M., and Sataric, M.V. (2005). Molecular dynamics simulations of tubulin structure and calculations of electrostatic properties of microtubules. *Mat Comp Mod*.
- Tuszynski, J.A., Carpenter, E.J., Huzil, J.T., Malinski, W., Luchko, T., and Luduena, R.F. (2006). The evolution of the structure of tubulin and its potential consequences for the role and function of microtubules in cells and embryos. *Int J Dev Biol* *50*, 341-358.
- Vale, R.D. (2003). The molecular motor toolbox for intracellular transport. *Cell* *112*, 467-480.
- Varmark, H. (2004). Functional role of centrosomes in spindle assembly and organization. *J Cell Biochem* *91*, 904-914.
- Vaughan, K.T. (2005). TIP maker and TIP marker; EB1 as a master controller of microtubule plus ends. *J Cell Biol* *171*, 197-200.
- Vaughan, K.T., Tynan, S.H., Faulkner, N.E., Echeverri, C.J., and Vallee, R.B. (1999). Colocalization of cytoplasmic dynein with dynactin and CLIP-170 at microtubule distal ends. *J Cell Sci* *112* (Pt 10), 1437-1447.
- Vaughan, P.S., Miura, P., Henderson, M., Byrne, B., and Vaughan, K.T. (2002). A role for regulated binding of p150(Glued) to microtubule plus ends in organelle transport. *J Cell Biol* *158*, 305-319.

- Vilfan, A., Frey, E., Schwabl, F., Thormahlen, M., Song, Y.H., and Mandelkow, E. (2001). Dynamics and cooperativity of microtubule decoration by the motor protein kinesin. *J Mol Biol* 312, 1011-1026.
- Vogel, J., Drapkin, B., Oomen, J., Beach, D., Bloom, K., and Snyder, M. (2001). Phosphorylation of gamma-tubulin regulates microtubule organization in budding yeast. *Dev Cell* 1, 621-631.
- Volkman, N., Liu, H., Hazelwood, L., Krementsova, E.B., Lowey, S., Trybus, K.M., and Hanein, D. (2005). The structural basis of myosin V processive movement as revealed by electron cryomicroscopy. *Mol Cell* 19, 595-605.
- von Bergen, M., Barghorn, S., Muller, S.A., Pickhardt, M., Biernat, J., Mandelkow, E.M., Davies, P., Aebi, U., and Mandelkow, E. (2006). The core of tau-paired helical filaments studied by scanning transmission electron microscopy and limited proteolysis. *Biochemistry* 45, 6446-6457.
- Wade, R.H., Chretien, D., and Job, D. (1990). Characterization of microtubule protofilament numbers. How does the surface lattice accommodate? *J Mol Biol* 212, 775-786.
- Walz, T., Tittmann, P., Fuchs, K.H., Muller, D.J., Smith, B.L., Agre, P., Gross, H., and Engel, A. (1996). Surface topographies at subnanometer-resolution reveal asymmetry and sidedness of aquaporin-1. *J Mol Biol* 264, 907-918.
- Wang, H.W., Long, S., Finley, K.R., and Nogales, E. (2005). Assembly of GMPCPP-bound tubulin into helical ribbons and tubes and effect of colchicine. *Cell Cycle* 4, 1157-1160.
- Wang, H.W., and Nogales, E. (2005). Nucleotide-dependent bending flexibility of tubulin regulates microtubule assembly. *Nature* 435, 911-915.
- Wani, M.C., Taylor, H.L., Wall, M.E., Coggon, P., and McPhail, A.T. (1971). Plant antitumor agents. VI. The isolation and structure of taxol, a novel antileukemic and antitumor agent from *Taxus brevifolia*. *J Am Chem Soc* 93, 2325-2327.
- Wegner, A., and Isenberg, G. (1983). 12-fold difference between the critical monomer concentrations of the two ends of actin filaments in physiological salt conditions. *Proc Natl Acad Sci U S A* 80, 4922-4925.
- Wendt, T.G., Volkman, N., Skiniotis, G., Goldie, K.N., Muller, J., Mandelkow, E., and Hoenger, A. (2002). Microscopic evidence for a minus-end-directed power stroke in the kinesin motor ncd. *Embo J* 21, 5969-5978.

- Westermann, S., Wang, H.W., Avila-Sakar, A., Drubin, D.G., Nogales, E., and Barnes, G. (2006). The Dam1 kinetochore ring complex moves processively on depolymerizing microtubule ends. *Nature* *440*, 565-569.
- White, S.R., Evans, K.J., Lary, J., Cole, J.L., and Lauring, B. (2007). Recognition of C-terminal amino acids in tubulin by pore loops in Spastin is important for microtubule severing. *J Cell Biol* *176*, 995-1005.
- Whittaker, M., Carragher, B.O., and Milligan, R.A. (1995). PHOELIX: a package for semi-automated helical reconstruction. *Ultramicroscopy* *58*, 245-259.
- Wittmann, T., Bokoch, G.M., and Waterman-Storer, C.M. (2004). Regulation of microtubule destabilizing activity of Op18/stathmin downstream of Rac1. *J Biol Chem* *279*, 6196-6203.
- Wittmann, T., and Desai, A. (2005). Microtubule cytoskeleton: a new twist at the end. *Curr Biol* *15*, R126-129.
- Woehlke, G., Ruby, A.K., Hart, C.L., Ly, B., Hom-Booher, N., and Vale, R.D. (1997). Microtubule interaction site of the kinesin motor. *Cell* *90*, 207-216.
- Wolf, E., Kim, P.S., and Berger, B. (1997). MultiCoil: a program for predicting two- and three-stranded coiled coils. *Protein Sci* *6*, 1179-1189.
- Wood, V., Gwilliam, R., Rajandream, M.A., Lyne, M., Lyne, R., Stewart, A., Sgouros, J., Peat, N., Hayles, J., Baker, S., Basham, D., Bowman, S., Brooks, K., Brown, D., Brown, S., Chillingworth, T., Churcher, C., Collins, M., Connor, R., Cronin, A., Davis, P., Feltwell, T., Fraser, A., Gentles, S., Goble, A., Hamlin, N., Harris, D., Hidalgo, J., Hodgson, G., Holroyd, S., Hornsby, T., Howarth, S., Huckle, E.J., Hunt, S., Jagels, K., James, K., Jones, L., Jones, M., Leather, S., McDonald, S., McLean, J., Mooney, P., Moule, S., Mungall, K., Murphy, L., Niblett, D., Odell, C., Oliver, K., O'Neil, S., Pearson, D., Quail, M.A., Rabbinowitsch, E., Rutherford, K., Rutter, S., Saunders, D., Seeger, K., Sharp, S., Skelton, J., Simmonds, M., Squares, R., Squares, S., Stevens, K., Taylor, K., Taylor, R.G., Tivey, A., Walsh, S., Warren, T., Whitehead, S., Woodward, J., Volckaert, G., Aert, R., Robben, J., Grymonprez, B., Weltjens, I., Vanstreels, E., Rieger, M., Schafer, M., Muller-Auer, S., Gabel, C., Fuchs, M., Dusterhoft, A., Fritz, C., Holzer, E., Moestl, D., Hilbert, H., Borzym, K., Langer, I., Beck, A., Lehrach, H., Reinhardt, R., Pohl, T.M., Eger, P., Zimmermann, W., Wedler, H., Wambutt, R., Purnelle, B., Goffeau, A., Cadieu, E., Dreano, S., Gloux, S., Lelaure, V., Mottier, S., Galibert, F., Aves, S.J., Xiang, Z., Hunt, C., Moore, K., Hurst, S.M., Lucas, M., Rochet, M., Gaillardin, C., Tallada, V.A., Garzon, A., Thode, G., Daga, R.R., Cruzado, L., Jimenez, J., Sanchez, M., del Rey, F., Benito, J., Dominguez, A., Revuelta, J.L., Moreno, S., Armstrong, J., Forsburg, S.L., Cerutti, L., Lowe, T., McCombie, W.R., Paulsen, I., Potashkin, J., Shpakovski, G.V., Ussery, D.,

- Barrell, B.G., and Nurse, P. (2002). The genome sequence of *Schizosaccharomyces pombe*. *Nature* *415*, 871-880.
- Xiao, H., Verdier-Pinard, P., Fernandez-Fuentes, N., Burd, B., Angeletti, R., Fiser, A., Horwitz, S.B., and Orr, G.A. (2006). Insights into the mechanism of microtubule stabilization by Taxol. *Proc Natl Acad Sci U S A* *103*, 10166-10173.
- Yeh, E., Yang, C., Chin, E., Maddox, P., Salmon, E.D., Lew, D.J., and Bloom, K. (2000). Dynamic positioning of mitotic spindles in yeast: role of microtubule motors and cortical determinants. *Mol Biol Cell* *11*, 3949-3961.
- Yildiz, A., and Selvin, P.R. (2005). Kinesin: walking, crawling or sliding along? *Trends Cell Biol* *15*, 112-120.

8 Abbreviations

+TIP	Microtubule plus end binding protein
2-D	Two-dimensional
3-D	Three-dimensional
A	Ampere
Å	Ångström
Ab	Antibody
ADP	Adenosine diphosphate
AMPPNP	Adenosine 5'-(β,γ -imido)triphosphate
APC	Adenomatous polyposis coli
ATP	Adenosine triphosphate
BSA	Bovine serum albumin
CLIP	Cytoplasmic linker protein
DMSO	Dimethylsulphoxide
EB1	End-binding protein 1
EGTA	Ethyleneglycol-bis(β -aminoethyl)-N,N,N',N'-tetraacetic acid
EM	Electron Microscopy
FCS	Fetal calf serum
GDP	Guanosine triphosphate
GTP	Guanosine diphosphate
HEPES	N-(2-hydroxyethyl)piperazine-N'-(2-ethanolsulphonic acid)
HRP	Horseradish peroxidase
IPTG	Isoporyl- β -thiogalactoside
kDa	Kilo Dalton
M	Molar
mA	Milli Ampere
MAP	Microtubule associated protein
mm	Millimeter
mM	Millimolar
MTOC	Microtubule organizing center
MW	Molecular weight
nm	Nanometer
nM	Nanomolar
OD	Optical density
PAGE	Polyacrylamide gel electrophoresis
PIPES	2-[4-(2sulfoethyl)piperazin-1-yl]ethanesulfonic acid
SDS	Sodium dodecyl sulphate
TEM	Transmission electron microscope
TEV	Tobacco etch virus
Tris	Tris-(hydroxymethyl)-aminomethane
V	Volt
γ -TuRC	Gamma-tubulin ring complex
μ l	Microliter
μ m	Micrometer

9 Curriculum vitae

Name: Linda Maria Sandblad
Address: Römerstrasse 62, 69 115 Heidelberg, Germany
E-mail address: sandblad@embl.de
Date of birth: May 8th, 1975
Place of birth: Uppsala, Sweden
Nationality: Swedish
Family status: Married, one daughter

Education and experience:

2003-2007 PhD project work at the European Molecular Biology Laboratory (EMBL) in Heidelberg (EMBL Internal PhD program fellowship), under the supervision of Dr. Andreas Hoenger and Dr. Damian Brunner

29th of Sept. 2003 Diploma in Biology, University of Würzburg. Overall mark: excellent (sehr gut).

2002-2003 Biology studies at the University of Würzburg. Final exams in cell and developmental biology, biochemistry, immunology and virology, December 2002.

2001 Chef and organizer of the restaurant at the Student Association Västmanlands-Dala Nation in Uppsala. (Klubbmästarinna)

2000-2001 Diploma thesis, carried out at Karolinska Institutet, Stockholm, Sweden, in the Department of Cell and Molecular Biology, under the supervision of Dr. Volker Cordes.

1999-2000 Biology studies at the University of Uppsala. Advanced courses in immunology, biochemistry and molecular virology, and medical genetics.

1996-1999 Biology studies at the University of Würzburg, Germany. Intermediate exam in botany, zoology, chemistry and physics, October 1998.

1995-1996 One year photographic education at Forsa folkhögskola, Sweden. (Foto och videolinjen)

1994-1995 Au pair in Heidelberg, Germany.

1991-1994 High school exam in science, Katedralskolan in Uppsala, Sweden, June 1994. (Naturvetenskapliga linjen)

10 Acknowledgments

The way, to finally write this PhD thesis, has been very long. From Uppsala to Heidelberg, some years in Würzburg and back to Uppsala, some more years in Würzburg and then back to Heidelberg again. I would like to thank all of you, and there are very many of you, who have helped me on the way. It would not have been possible without you. I mean, I never had a final goal, and I had to test all opportunities on the way, open every possible door. Good decisions come by chance, by time or by good friends, thank you all, to help me to get here. I just do what I enjoy to do, and it is just getting better and better!

Most of all, thanks to my two EMBL PhD supervisors, Andreas Hoenger and Damian Brunner. It is really great to work with both of you. As supervisors you complement each other perfectly. Thanks Andy for believing in me and introducing me to the world of microtubule structure and EM. I learned to work independently and to believe what we see. I am very happy you have the right eyes and feeling for picking out and promote the good stuff from all the crap I tried out during the past years. With great priority and extremely effective work you make things move in time. Even if Boulder is far away, I really appreciated your instant feedback and help. Especially to the end of writing, you were enormously helpful to me. Thanks Damian, for the chocolate! You are a great resource of good ideas, new experimental suggestions and possible explanations to all kind of problems. Discussing with you is always inspiring, thanks for all that motivation.

A person who has followed me all the way from my first year of biology studies is Professor Krohne in Würzburg. I'm very thankful you cared for my all this time. I'm especially happy that you are my external "Doktorvater". It is great that you are so interested in my PhD topic and that you took the time to visit the seminars at EMBL, your participation is most appreciated.

Greetings to our collaborators at ETH in Zurich, Heinz Gross and Peter Tittmann. Thanks Peter, for your friendly help and shadowing.

Thanks to all former members of the Hoenger lab who are now spread out all over the world. You gave me a good start at EMBL, an introduction to EM, protein purification and EMBL gossips. Dilem for sharing the frustration of all non-functional experiments. Rachel for the super, super technician help, you are great! Angelica, who patiently tried to teach me the helical reconstruction mysteries. Thousands of thanks to Kenny, you have the patience of an angle and the right hands for every high vacuum pump. Thanks for making every thing work, and all I learned about microscopy. Gook luck to all of you! Additionally, not to forget are the other heroes from Structure, the protein purification expertise from David and extraordinary computing service by Chris.

Thanks for every day of fun in the Brunner lab; with such a great atmosphere and colleagues I managed to get out of bed and up to work every morning. Manolo, who told me every thing about Mal3p. Tanja and Imo for the perfect organization and the lab services. The postdocs: Ference, Katarina, Paulo, Jerome and Stephen. The girls, I mean

the predocs: Andrea, Lindsay, Aynur and Tatyana, all so talented and good looking, I can not express my gratefulness in words, I give you this: ☺ . And Lindsay, I would not have survived this without you!

Big acknowledgements to the Pompom club, not only for yeast, coffee and cake, but for being the best expertise panel on “how to survive a PhD”.

I have been very lucky. All my family supported us to live in Heidelberg. It is very nice of you all to come and see us so often. Lea, Dan and I are also very lucky because Anna, Johan, Agnes and Julia moved to Heidelberg. We love your friendship, food, home, Christmas and Knut, discussions and some more coffee? A special thanks from me, for taking care of Lea and Dan all the times I had to travel and work. Maybe you also helped them tolerate their scientist mother and wife a bit better. The biggest thanks goes to Dan and Lea, who took care of me every day. Even if you both had a really hard time, you gave me the necessary distance and a more objective relation to work. Thanks for loving me, you are the best I have!

I like the darkness of the EM rooms, there is something peaceful and timeless about it. Experimental work suits me very good, as stubborn and patient as I am. For me this was a very enjoyable project. Writing, though is not my strength, as you all might have noticed. It is not because English is a very unlogical language or the German grammar is impossible to remember or Swedish sounds can be spelled in hundred different ways. These are all excuses I tell you just because I do not like to admit I have some kind of dyslexia. All special teachers failed to teach me writing, and maybe suffered hearing me reading. Does it matter? A language is a tool of communication. When I tell you something and you can understand me, the language we use is perfect. A language lives and changes with the people who use it. Is it then suitable to have rules? Some people use a language as art, others see it as a science in itself. Some people have perfect pitch for music, other a feeling for correct use of languages. However, I learned to survive. I learned that I'm dependent on you who have a good command of languages. To write this thesis, I consulted the excellent proofreaders: Lindsay Murrells and Ellen Dearden and Jamie Riches, who entered this task even if the time was short. Thanks for every correct word and comma, your help was absolutely essential. If the readers find mistakes, blame only me, I must have put them in afterwards.

Thanks again, to you all, from your Linda

I'm not going to thank the little devil sitting on my shoulders giving me bad conscious every day, for not taking care of my family when I'm working another late night and for not working hard enough when I spent a weekend with my family. That little devil is not going to become a PhD, it can go directly to hell, because I'm not going to carry it around anymore!